NASA Contractor Report 170405

NASA-CR-170405
19840005129

Flight Test and Analyses of the B-1 Structural Mode Control System at Supersonic Flight Conditions

John H. Wykes, Martin J. Klepl, and Michael J. Brosnan

Contract NAS4-2932
December 1983

NASA
National Aeronautics and
Space Administration

NASA Contractor Report 170405

Flight Test and Analyses of the B-1 Structural Mode Control System at Supersonic Flight Conditions

John H. Wykes, Martin J. Klepl, and Michael J. Brosnan
Rockwell International Corporation, Los Angeles, California 90009

Prepared for
Ames Research Center
Dryden Flight Research Facility
Edwards, California
under Contract NAS4-2932

1983

National Aeronautics and
Space Administration
Ames Research Center
Dryden Flight Research Facility
Edwards, California 93523

This Page Intentionally Left Blank

TABLE OF CONTENTS

LIST OF ILLUSTRATIONS

LIST OF TABLES

This Page Intentionally Left Blank

FLIGHT TEST AND ANALYSES OF THE B-1 STRUCTURAL MODE CONTROL SYSTEM AT SUPERSONIC FLIGHT CONDITIONS

John H. Wykes, Martin J. Klepl, and Michael J. Brosnan
Rockwell International
North American Aircraft Operations

INTRODUCTION AND SUMMARY

NASA has conducted an evaluation of the Air Force B-1 Development Program with a view toward obtaining research data suitable for advanced vehicles. One particular area of interest is in the evaluation of the active structural mode control system installed on the B-1 aircraft. Any aircraft flying through turbulence has dynamic loads problems, which are especially severe for a flexible aircraft because of the induced structural motions. Previous analytical studies and limited flight tests have shown that active control techniques can be used to damp the structural motions of large flexible vehicles. The B-1 offers an excellent opportunity for much needed further evaluation of such a system to insure the optimum use of these systems for future applications. The B-1 is the first aircraft to have a structural mode control system integrated into the complete design cycle.

The overall objectives of this research are to compile and document information about the conceptual design, development, and flight tests of the B-1 structural mode control system (SMCS) and its impact on ride quality. Since the B-1 is the first aircraft to have a system such as the SMCS designed for production and long service use, it is expected that the reports prepared will add to the technology base for the design of future large military or civil aircraft. The specific objectives are to accomplish the following:

(1) Investigate the improvements in total dynamic response of a flexible aircraft and the potential benefits to ride and handling quality, crew efficiency, and reduced loads on the primary structure.

(2) Evaluate the effectiveness and performance of the SMCS, which uses small aerodynamic surfaces at the vehicle nose to provide damping to the structural modes.

The first phase of this study, which covered the design and development of the SMCS, has been completed and reported in reference 1. The second phase, which encompassed summaries of analyses and flight tests of the SMCS, has been completed and reported in reference 2.

The B-1 SMCS was a point design system where the design point flight condition was M = 0.85 at sea level. The logic was that ride quality needed to be addressed only during the long-time low-altitude penetration phases of the mission and would be turned off at all other times. However, NASA recognized the potential of the SMCS for ride quality benefits to large flexible aircraft flying at supersonic speeds and the desirability of demonstrating the possibility of designing an SMCS that could be turned on at takeoff and be left on for the whole flight without further attention (as is the case for all conventional control augmentation systems). Such a system then would be able to automatically attenuate structural motion due to low-altitude subsonic turbulence and high-altitude supersonic clear air turbulence. In addition, it was determined to be valuable to perform analyses matching the SMCS test performance data obtained at supersonic speeds in order to evaluate existing analyses techniques.

Thus it was that a third phase of study was initiated in the spring of 1981 involving flight tests of the B-1 SMCS at two supersonic flight conditions. There are two parts of this third phase. The first involves the reduction of both vertical and lateral response test data and analyses matching the vertical response data as well as demonstrating analytically the impact of the SMCS on vertical ride quality. The second part involves matching the lateral flight test dynamic responses at one supersonic flight condition and demonstrating analytically the impact of the SMCS on lateral ride quality. Both parts of the third phase are reported herein.

The authors wish to acknowledge the significant contributions to this study of the following people. Roy P. Hill assembled the aircraft mass characteristics required. Kenneth F. Anderson assisted in correlating the Mach Box aerodynamics with the B-1 System Design Manual Data. Kenneth W. Williston is responsible for the computer graphics form of presentation of the flight test data included herein.

B-1 AIRCRAFT

The aircraft used in the reported tests and studies is the Rockwell International B-1 Strategic Aircraft. Figure 1 shows three views of the basic configuration. The wing has variable sweep capability and is shown in its most aft sweep position of 67.5°, which was the position used in the tests and analyses of this study. The structural mode control system (SMCS) vanes located at the forward end of the fuselage are also of particular note relative to this study. B-1 A/C-3 was the particular aircraft employed in the reported tests and analyses.

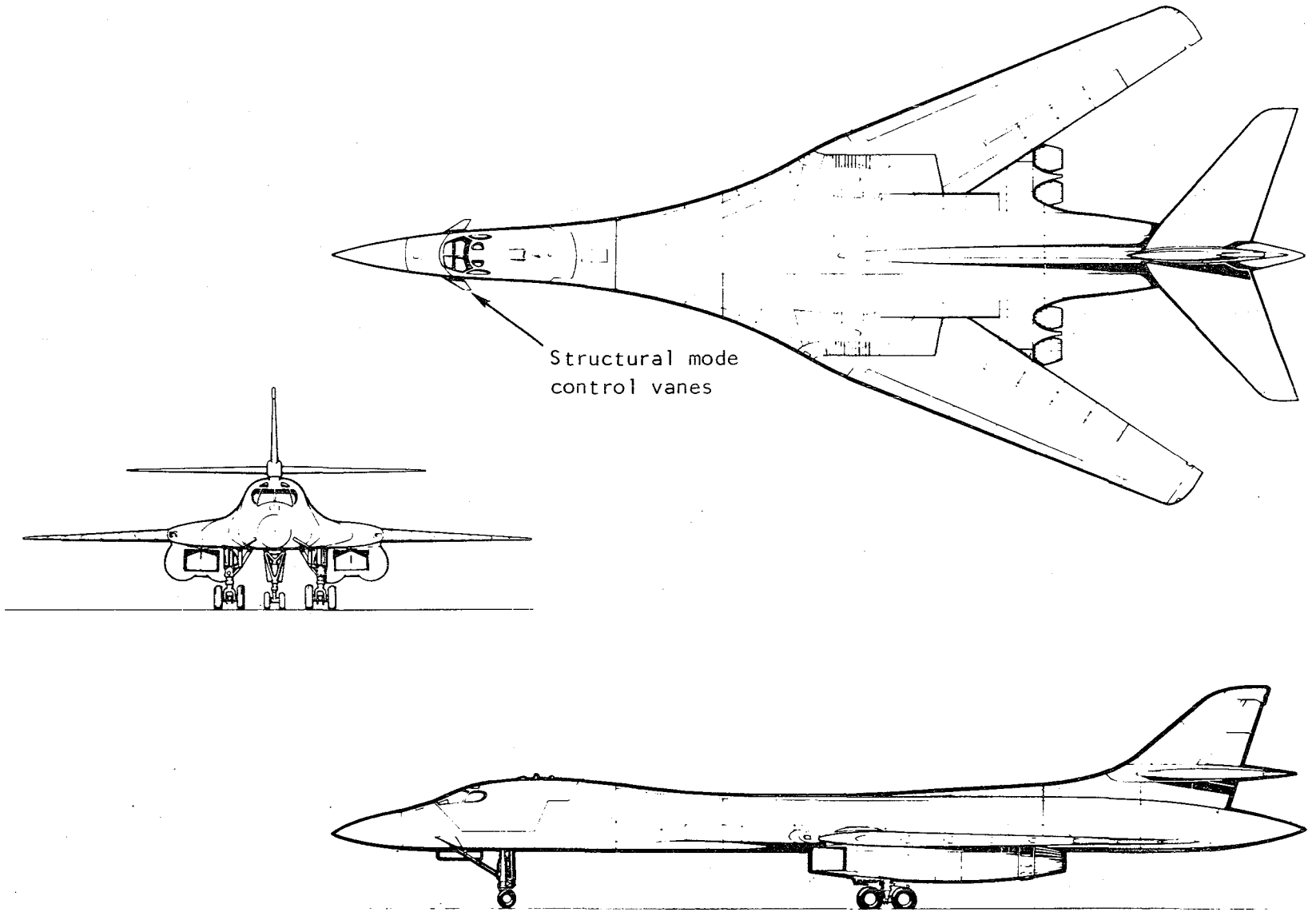

Figure 1. - B-1 aircraft.

TEST DESCRIPTION

Flight Conditions

To form a basis for relative performance evaluations of the SMCS between subsonic and supersonic flight conditions, it was decided to fly at supersonic speeds at the same dynamic pressure as at M = 0.85 at sea level (the SMCS design condition). Figure 2 shows this constant (q_o = 51423 N/m^2 (1,074 psf)) line on a mach-altitude plot. Flying along this constant q_o line permits the SMCS gains to remain unchanged from those for the design condition of M = 0.85 at sea level. As shown, the two supersonic conditions chosen for the tests were M = 1.6 at 9,449 meters (31,000 feet) altitude and M = 1.25 at 5,791 meters (19,000 feet) altitude.

Test Equipment and Techniques

The most appropriate test environment for the SMCS would have been a turbulent atmosphere. However, to find a turbulent atmosphere at altitude on cue in a tight test schedule was highly unlikely. It was decided to provide a reliable dynamic test environment by using the SMCS vanes to excite the aircraft structure across a range of frequencies up to 10 Hz. This technique had the advantages of being the one used to obtain excellent frequency responses of the flexible B-1 during the SMCS development phase (see reference 2) and having the necessary equipment available.

The required excitation equipment was removed from B-1 A/C-2 and installed in A/C-3. The control panel, as shown in figure 3, was installed on the left-hand console. All operations on the panel were manual including the frequency sweep. As indicated, the rate limit and vane trim capability were not needed for the planned tests and were made inoperative. The panel switches and dials performed two basic functions: (1) turned the basic SMCS off or on and set the operating gains; and (2) operated the SMCS vanes as exciters at set amplitudes and frequencies. These functions could be performed concurrently.

The top toggle switch activated the SMCS vane actuator hydraulics whether the system was used as a damper or an exciter. If the system was to be used in the exciter mode, then the lower toggle switch was set to excite either the vertical or lateral axis. When set for the vertical axis, the vanes would deflect symmetrically; and when set in the lateral axis, the vanes would deflect anti-symmetrically. The amplitude would be set next by turning the dial shown. The maximum setting was 999, representing approximately 20° maximum deflection of the vanes. Figure 4 shows a calibration curve for an amplitude setting of 100 versus frequency. Once the amplitude was set, the frequency was manually swept from a setting of 000 to 999 (which represented the maximum frequency of 10 Hz).

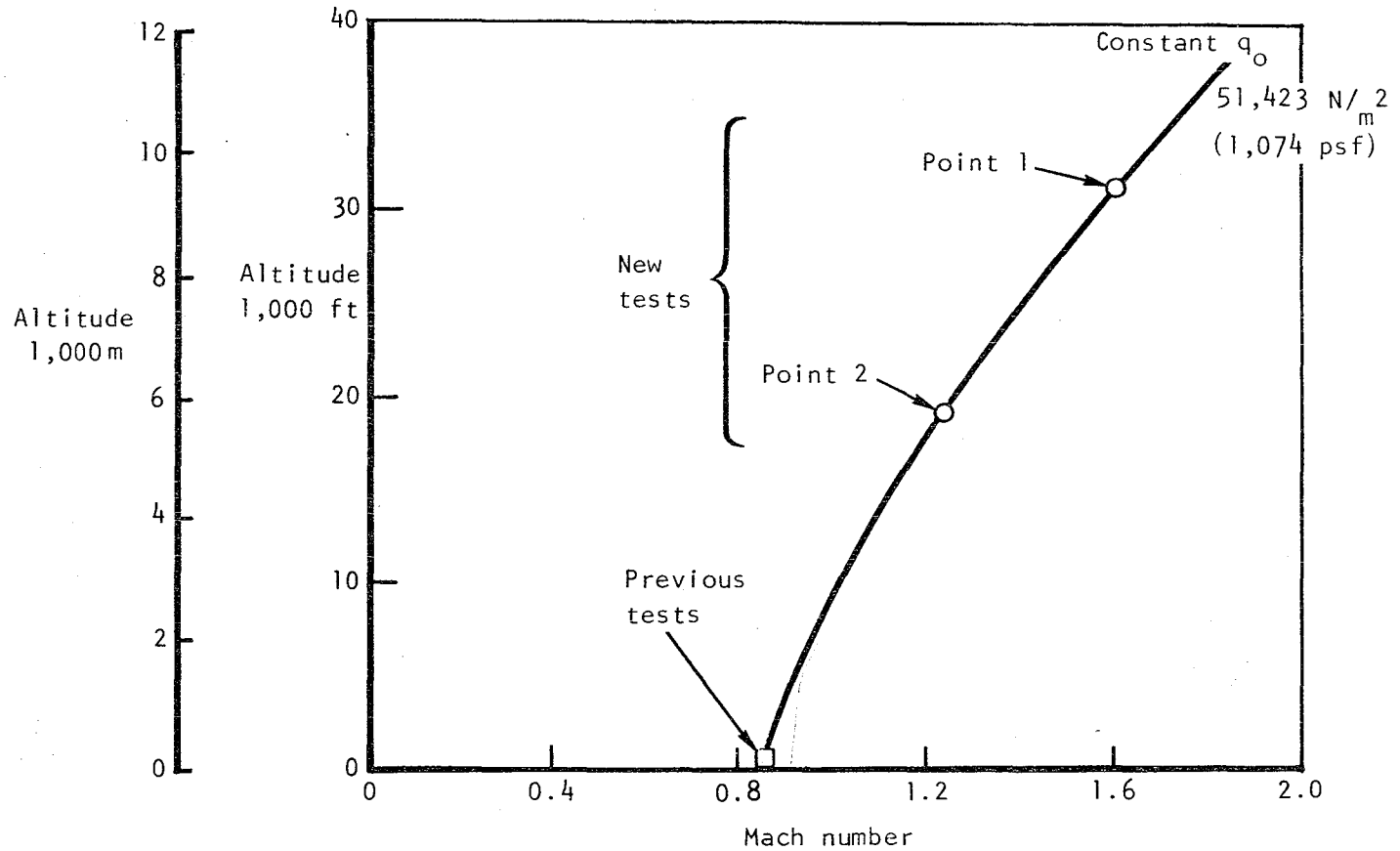

Figure 2. - Test flight conditions.

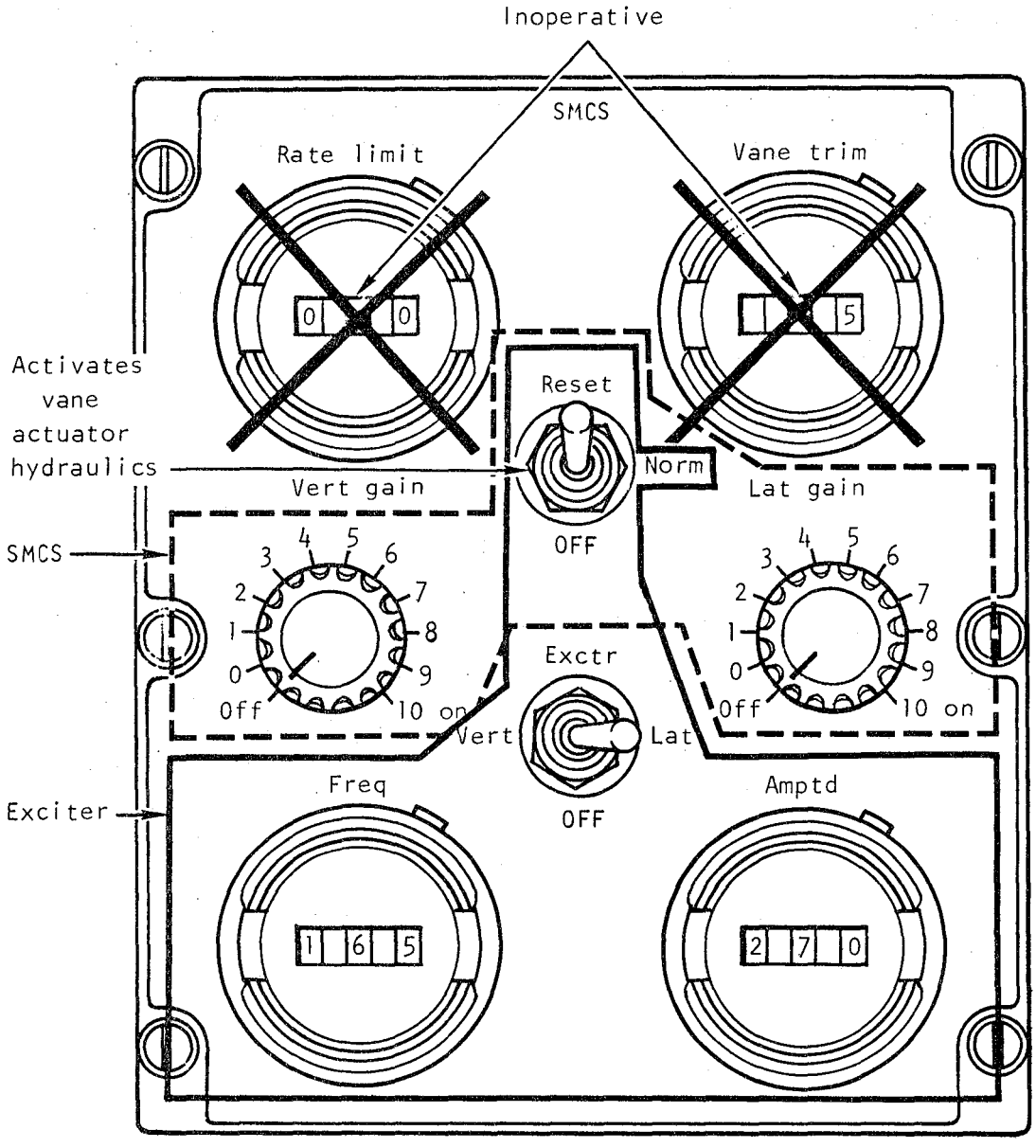

Figure 3. - SMCS exciter panel.

Vertical mode: Read as right and left vane panels deflected symmetrically

Lateral mode: Read as deflection of one panel; each panel is deflected opposite to other

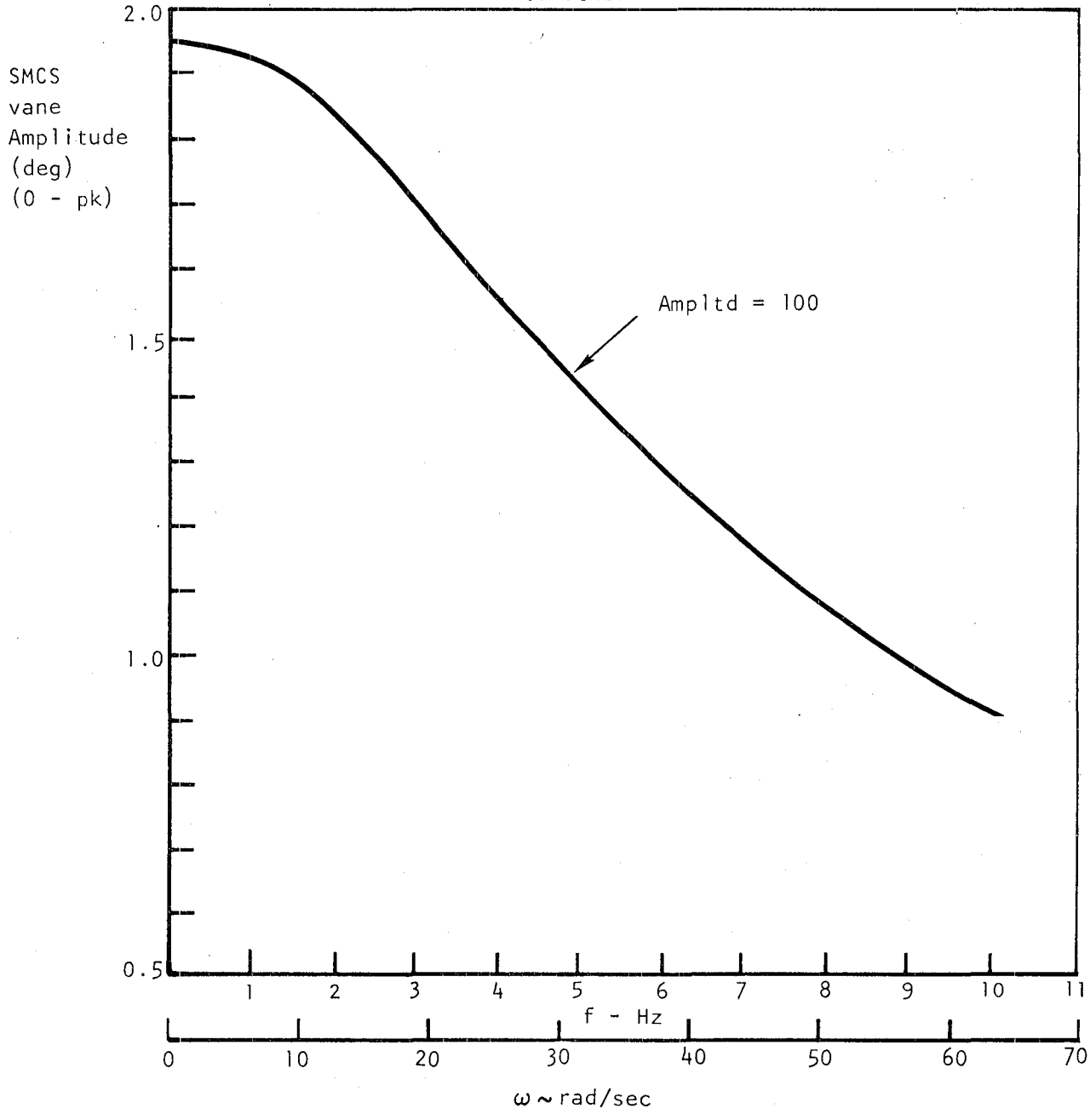

Figure 4. - Deflection of SMCS vanes as driven from SMCS exciter panel frequency generator with amplitude = 100.

The SMCS was operated in its normal mode of structural damper by setting the vertical or lateral gain (or both) at the indicated maximum setting of 10. This maximum gain setting allowed the SMCS to operate at its nominal setting built into the controller.

While preliminary analyses and development flutter testing showed little adverse impact of the SMCS on flutter structural modes or any other modes, an additional safety precaution was taken to prevent inadvertent difficulties. The SMCS (both as a structural damper and as an exciter) was rigged to be shut off by normal load factor increments over +1.0 g of $\pm$0.6 g and by lateral load factor increments of $\pm$0.3 g. The SMCS accelerometer signals at the vane station were used for this purpose.

While the SMCS exciter system was checked out on the ground, it was decided to check it out further in flight. So on the way to the test range, functional checks were made at low amplitudes through the frequency range to 10 Hz. As part of these tests, the vertical load factor cutoff setting was checked by activating it with appropriate maneuvers. The installation performed as designed on both supersonic test flights.

Preliminary analyses of the stability characteristics of the basic aircraft (no active systems), SCAS on, and SCAS + SMCS on configurations at the two supersonic flight conditions, indicated no difficulties. However, it was decided that prior to running the basic frequency sweeps, a series of stability checks would be run. These tests consisted of horizontal tail pitch pulses to excite vertical modes and rudder pulses to excite antisymmetric modes for the above indicated configurations. When these tests were performed, no adverse stability or damping was noted.

Because of the rapid consumption of fuel at supersonic speeds, it became essential to carefully plan the tests performed to minimize time at the test points and yet obtain data adequate to define the frequency responses desired. The following is a description of some of the key test design factors.

The SMCS was designed to damp structural bending modes occurring in the frequency range up to 10 Hz. This, then, set the requirement for the bandwidth of the test. A signal with 5 to 6 samples per cycle was required for adequate definition. This requirement, applied at 10 Hz, set the data sampling rate of 50 to 60 samples per second. This requirement was met by the standard available rate of 64 samples per second.

An input signal of a frequency sweep, instead of discrete frequency dwells, was chosen so that all frequencies would be tested rather than specific frequencies. This precluded making inadequate guesses as to the frequency points required.

Experience from similar supersonic tests of the SMCS provided a basis for making judgments on other test factors. For one, the duration of the calculated covariance function had to be estimated. This was determined from the plotting requirement of the frequency responses. If calculated points are too far apart in frequency, the gain and phase are not adequately shown. Experience had demonstrated that plotting the points at an interval of about 0.5 radians/second is adequate. This requirement established the duration of the covariance function through the frequency resolution formula:

$$\Delta\omega = \pi/\tau_M$$

$$\therefore \tau_M = 2\pi \text{ seconds}$$

This is the value that was used.

The above time consideration was part of the determination of one of the key test elements to be estimated, that of the frequency sweep duration. From statistical estimation theory it is known that the accuracy bounds on the data of a power spectral density curve are a function of a Chi-squared distribution. A proper accuracy evaluation of the data points of a frequency response (which is determined from the division of one power spectral density curve by another) requires an application of an F-distribution. However, an understanding can be obtained from the Chi-squared distribution. In looking at a standard Chi-squared curve, one sees that the quality of the data improves with increased degrees of freedom. It can be shown that degrees of freedom in this case are proportional to T_M/τ_M, the maximum time history duration divided by the maximum duration of the covariance function. In the range of 500 to 1,000 degrees of freedom, very little improvement is obtained with increased degrees of freedom; whereas in the low range of degrees of freedom, a large error can be greatly decreased by a small increase in degrees of freedom. For the present tests, an estimation of $T_M/\tau_M > 20$ was used to obtain reasonable statistical accuracy. This, then established the frequency sweep duration to be $T_M > (2\pi)(20) = 125$ seconds. An actual duration of 150 seconds was chosen to accommodate an easy manual frequency sweep rate of 15 sec/Hz.

Data Reduction Techniques

Figure 5 identifies those parameters measured during these tests: the pilot seat acceleration, the vane station acceleration, nominal CG acceleration, vane deflections, vane actuator command, and the frequency generator signal.

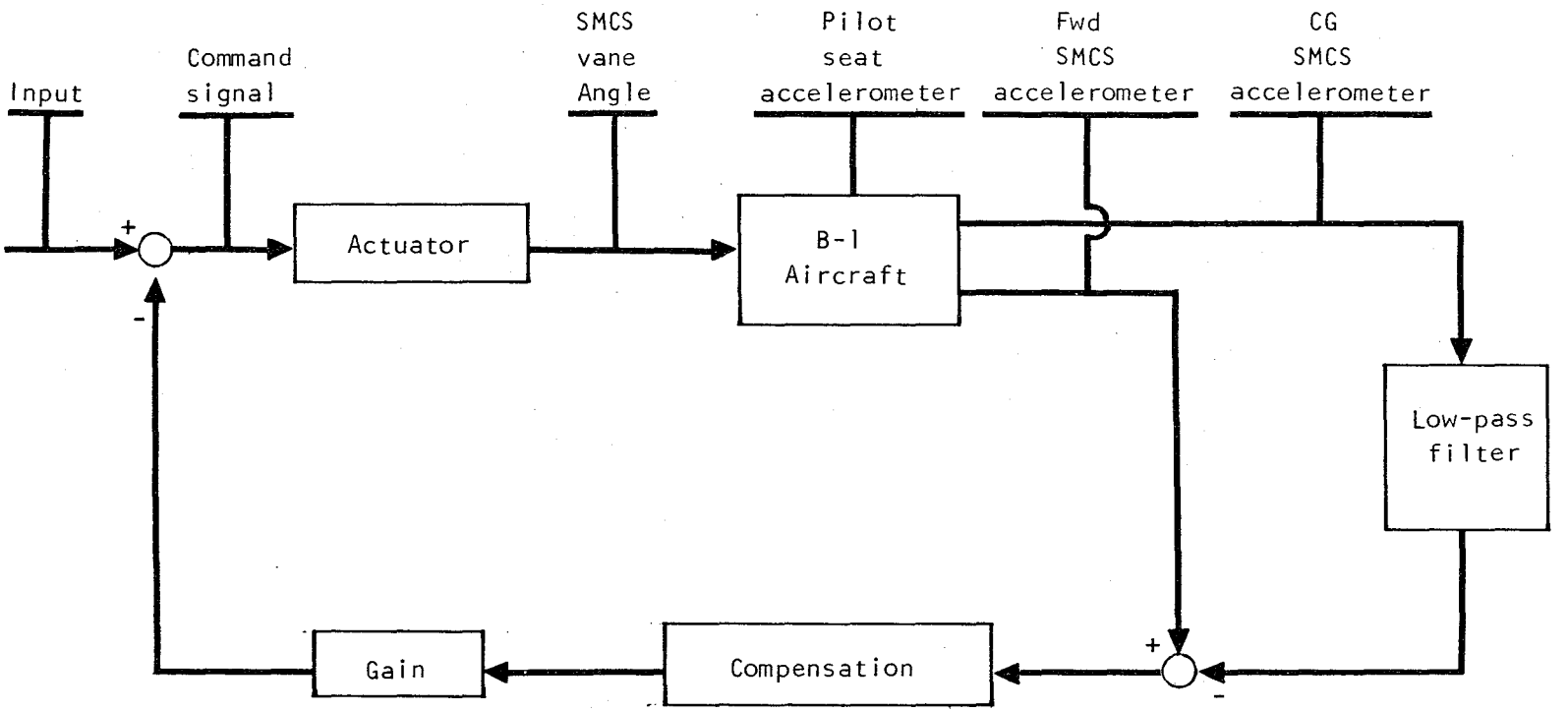

Diagram is representative of vertical and lateral systems

Figure 5. - B-1 structural mode control system data measurement points.

Digital time history data were obtained at each of these measurement points during all test runs. All of these parameter instrumentations were checked out and calibrated prior to the tests.

In brief, the data processing approach was as follows. First, the recorded time histories were processed to calculate the average reading of each parameter, which was then subtracted from the data to obtain zero mean time history data required for subsequent statistical analyses. The autocorrelation and the crosscorrelation functions were calculated from these zero mean time histories of an input and response pair. By using the zero mean time histories, these calculations result in the autocovariance and the cross-covariance functions. These functions look like the transient response of a single-degree-of-freedom spring-mass-damper system response to an initial position input. These four covariance functions are converted to power spectral density functions by the discrete Fourier transform. This approach has been found to give better results than the popular fast Fourier transform. These autospectra calculations are checked by using the identity that the area under the power spectral density function (calculated from the autocovariance) is just the autocovariance at zero lag.

From these power spectral density functions, the desired frequency response data are obtained as well as an evaluation of the quality of these data, the coherence. First, the co-spectra and quad-spectra are calculated and then, from these data, the gain and phase of the frequency response. The coherence is also calculated and is a measure of the validity of the frequency response for an assumed model of noise added to the response, but with the input noise-free. The final frequency response presents every point calculated except for those frequencies in which the coherence either exceeds 1.0 or was less than 0.5 (an arbitrary selection) for the vertical load factor data and 0.3 (again, an arbitrary selection) for the lateral load factor data.

All reduced data are presented herein without filtering other than that associated with antialiasing and coherence rejection.

ANALYSES DESCRIPTION

Flexible Aircraft Dynamic Analyses Summary

Figure 6 summarizes the steps taken in performing the analyses conducted during this study in matching the dynamic response flight test data.

The stiffness characteristics were those previously obtained from analyses correlated with ground vibration tests and further verified in a flight test (Reference 2). The mass characteristics were determined for the midtest time point. These mass characteristics were processed to the format required by the

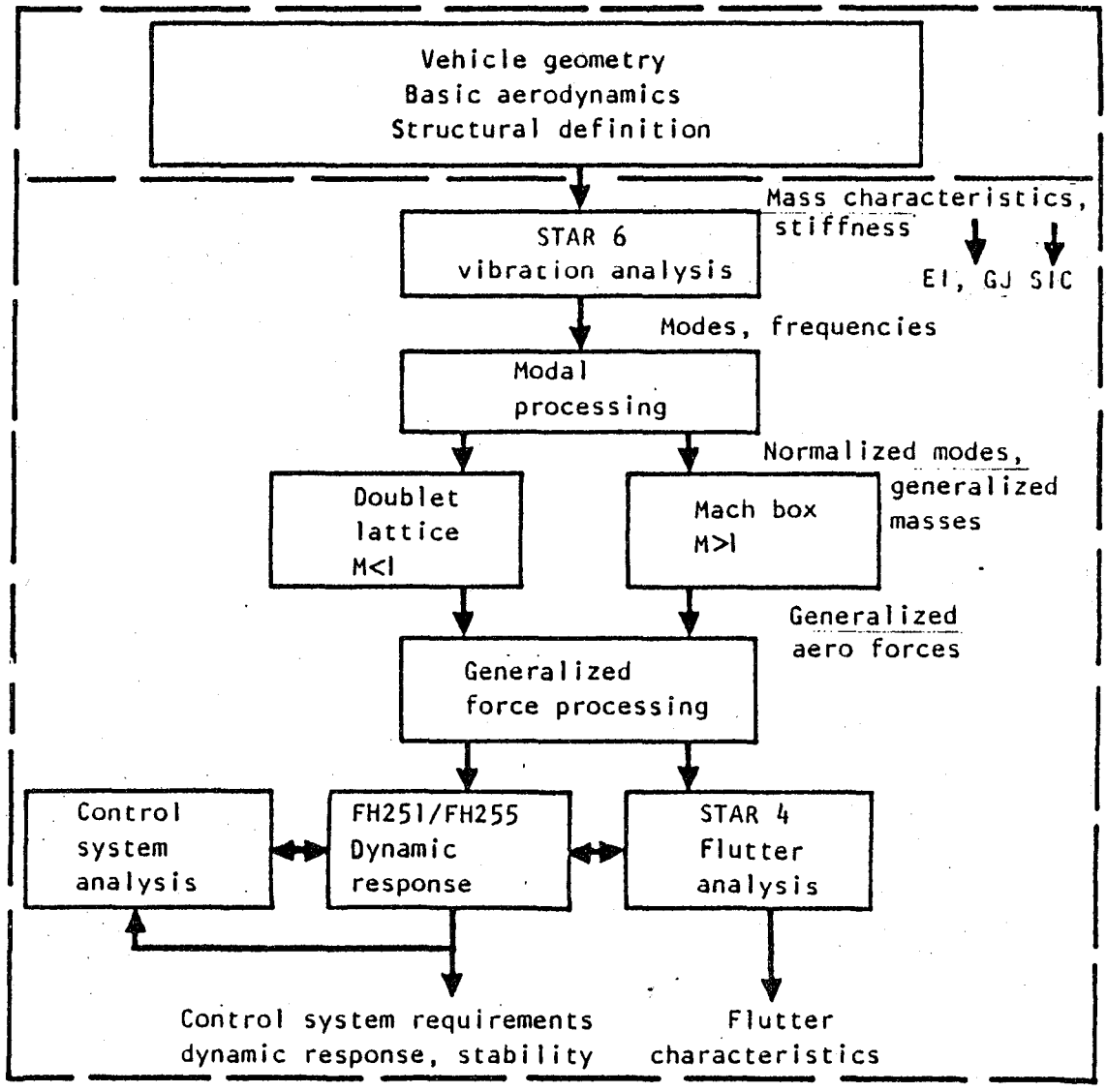

Figure 6. - Flexible aircraft dynamic analysis flow.

STAR6 Vibration Analyses Program. Once the mode shapes and frequencies were obtained, the mode shapes were processed to the form required by the aerodynamics program; in this case, the Mach Box Program. Given the mode shape characteristics, the Mach Box Aerodynamic Program produced dimensional generalized aerodynamic derivatives at low frequencies. These low-frequency derivatives and airload distributions were then compared to wind tunnel test results, and corrections were made to the Mach Box produced data as required. At this point, flexible-to-rigid ratio data were obtained and employed in selecting the structural modes to be used in analyses to match the flight test data. The unsteady aerodynamics for the modes selected were then run for the full frequency range. The dynamic analyses were performed using longitudinal-symmetric analysis program FH-251, and the lateral-directional-antisymmetric program FH-255. These analyses were frequency responses of the vertical and lateral load factor at the vane station and at the pilot station.

Vertical and lateral ride quality analyses were also conducted using the same data as were used in the flight-test data matching. These analyses demonstrate the relative ride quality ($\bar{H}$ criterion form) improvement possible with the SMCS at supersonic flight conditions.

With this overview in mind, the following discussions will elaborate each of these steps in some detail.

Flexible Aircraft Equations of Motion

The equations of motion of the flexible aircraft used in these studies have been treated extensively in reference 2, which deals with the analyses techniques used in the design development of the SMCS. Except for the specific numbers associated with the mass and aerodynamic characteristics, the equations of motions of the present study are identical to those of reference 2.

The equations of motion are written in the body axes system where the X-axis passes through the center of gravity and is parallel to the vehicle fuselage reference line (FRL). In the present study, longitudinal-symmetric degrees of freedom have been treated as uncoupled from the lateral-directional-antisymmetric degrees of freedom. The longitudinal-symmetric degrees of freedom consist of whole vehicle vertical plunge and pitch modes and 10 symmetric structural vibration modes. The lateral-directional-antisymmetric degrees of freedom consist of vehicle lateral plunge, yaw, and roll modes and 12 antisymmetric structural vibration modes.

Control surfaces employed in the longitudinal-symmetric case included the all-movable horizontal tail deflected symmetrically and the SMCS vanes deflected symmetrically. Control surfaces employed in the lateral-directional-antisymmetric case included the lower rudder panel, the horizontal tail deflected

antisymmetrically, and the SMCS vanes deflected antisymmetrically. The yaw and roll axis SCAS drove the rudder and horizontal tail, respectively, and the lateral SMCS drove the SMCS vanes.

The aerodynamics employed were a mix of unsteady and quasi-steady data; what was used, and where, will become apparent as discussions expand. Unsteady one-dimensional gust models were used to develop aerodynamic inputs which simulated flying in a continuous turbulence patch with many frequency components. The von Karman model of the turbulence power spectral density curve with the characteristic length, L, equal to 762 meters (2,500 feet) was used in dynamic-response-in-turbulence analyses.

Control surface inertia reaction forces were included in the subject analyses. Again, reference 2 contains detailed elaboration on how this is accomplished.

An extensive list of symbols is included in reference 2. Appendix A of the present report reproduces part of this list of symbols for ready reference in understanding the material presented.

Mass Characteristics

It was a goal for the tests to hold a fixed CG location and to minimize the weight variation during a particular test in order not to confuse the comparison data evaluating the SMCS. Furthermore, in order to have a mass characteristics accounting as accurate as possible, it was a goal not to use wing fuel (the installed wing fuel instrumentation could not define fuel distribution in the wing,-only quantity). The technique was to refuel, accelerate to a test condition, conduct vertical axis tests, refuel again, and then conduct lateral axis tests.

Table I summarizes data against which to judge the success of the test approaches. First, it was relatively easy to hold the desired M = 1.6 at 9,449 meters (31,000 feet) compared to the M = 1.25 at 5,791 meters (19,000 feet); it was difficult to hold M = 1.25, and the actual average for this series of tests was closer to 1.2, at a slightly lower altitude than planned. The impact on the flight dynamic pressure was 8 percent or less than the test goal. During the first run on flight 3-137 (M = 1.6), it was not possible to hold the wing fuel at the full level and still maintain total CG location. In subsequent runs, the attempt to hold wing fuel at the full level was abandoned in favor of maintaining a fixed CG.

The weight variations during a series of tests (i.e., vertical or lateral) were fairly significant (but unavoidable), as table I indicates. However, to minimize the impact on the analytical data matches to be undertaken, the

TABLE I. - SUMMARY OF CONFIGURATIONS AND FLIGHT CONDITIONS FOR FREQUENCY RESPONSE RUNS

Flt	Run No.	Config	Weight, Kg (lb)	CG $\%\bar{C}_w$	Excitation mode	Mach No.	hp, m (ft)	q_o, N/m^2 (psf)
M = 1.6 at 9,449 m (31,000 ft)								
3-137	4.4	Basic	134,191 (295,840)	41.62	Vertical	1.605	9,506 (31,189)	51,423 (1,074)
3-137	4.5	SCAS	128,893 (284,160)	44.36	Vertical	1.603	9,514 (31,213)	51,280[a] (1,071)
3-137	4.6	SCAS + SMCS	124,211 (273,840)	45.61	Vertical	1.607	9,542 (31,307)	51,328 (1,072)
3-137	6.4	Basic	119,903 (264,340)	45.11	Lateral	1.614	9,523 (31,244)	51,854 (1,083
3-137	6.5	SCAS	108,173 (238,480)	45.11	Lateral	1.606	9,451 (31,008)	51,711 (1,080)
3-137	6.6	SCAS + SMCS	114,156 (251,670)	45.49	Lateral	1.597	9,496 (31,154)	50,993[a] (1,065)
M = 1.2 at 5,791 m (19,000 ft)								
3-138	4.6	Basic	127,487 (281,060)	46.99	Vertical	1.176	5,658 (18,564)	47,880 (1,000)
3-138	4.4	SCAS	141,308 (311,530)	46.36	Vertical	1.183	5,689 (18,664)	48,216 (1,007)
3-138	4.5	SCAS + SMCS	134,690 (296,940)	46.49	Vertical	1.188	5,684 (18,649)	48,742[a] (1,018)
3-138	6.6	Basic	129,161 (284,750)	46.74	Lateral	1.189	5,682 (18,643)	48,790 (1,019)
3-138	6.4]	SCAS	143,263 (315,840)	46.61	Lateral	1.173	5,671 (18,604)	47,593 (994)
3-138	6.5	SCAS + SMCS	136,377 (300,660)	46.74	Lateral	1.186	5,703 (18,710)	48,407 (1,011)

[a] Indicates configuration selected as base for analyses.

superscript a's indicate the midtest flight conditions for which detailed mass accounting was accomplished to support vibration analyses and, subsequently, analyses attempting to match flight test data.

The mass accounting to support analyses was a two-step operation. First, a detailed accounting was done of the aircraft weight items minus the fuel. Secondly, in-flight fuel measurement at specific points in test time (table I) provided the remaining mass items required to determine vehicle total mass, inertias, CG location, and support vibration analyses.

Free-Free Vibration Modal Data

The flexible aspects of the aircraft have been treated in the modal format as opposed to the direct-influence-coefficient approach. The structural stiffness has been described in the EI-GJ form. The details of this approach are discussed in reference 2. It is sufficient here to say that the B-1 aircraft stiffnesses utilized in this study have been correlated with ground vibration test (GVT) with good results. The correctness of these stiffness data was further verified by virtue of the good matches of analytical-to-flight test data discussed in reference 2.

Table II summarizes the symmetric vibration characteristics of the modes selected for use in the flight-test-data matching analyses. As shown, the 10 modes employed were not the first 10 sequential modes. The logic in picking these modes was as follows. First, past experience indicated that modes with primary fore and aft motion contributed little to the aerodynamics of the flexing or to response dynamics. This logic eliminated sequential modes 4, 8, and 19 from the 20 calculated. See Appendix B for a graphical description of modes 4 and 8 as well as modes retained. Next, flexible-to-rigid aerodynamic data were calculated for all significant whole-vehicle motion aerodynamic derivatives for the 17 remaining modes. This was for the flight condition of M = 1.6 and h_p = 9,449 meters (31,000 feet). As an example of the technique, figure 7 shows the flexible-to-rigid data for two of the key derivatives, C_{N_α} and C_{M_α} for successive number of modes up to 17. The criterion for selecting a mode for retention (up to 10 desired) was to note jumps in the contribution to the flexible-to-rigid ratio data of any of the derivatives as successive modes were added to the calculation. Using this technique on the first 20 modes, modes 1, 2, 3, 5, 6, 7, 9, 12, 15, and 20 were selected for the frequency response and ride quality analyses. Figure 8 shows the flexible-to-rigid ratio data for C_{N_α} and C_{M_α} for the modes selected for M = 1.2 and h_p = 5,791 meters (19,000 feet).

Table II summarizes the frequencies and structural damping and identifies the main modal components for the cases at M = 1.6 and 1.2 for the 10 symmetric

TABLE II. - SUMMARY OF SYMMETRIC VIBRATION CHARACTERISTICS

M = 1.2, Flt 3-138, 134,690 kg (296,940 lb)				M = 1.6, Flt 3-137, 128,893 kg (284,160 lb)			
Mode No.(a)	Freq (Hz)	Damping (g_{s_i})	Ident(b)	Mode No.(a)	Freq (Hz)	Damping (g_{s_i})	Ident(b)
1	2.06	0.062	W1B	1	2.00	0.062	W1B
2	2.75	0.094	F1B	2	2.77	0.094	F1B
3	3.01	0.024	F1B+NAC1 +H1B	3	3.06	0.024	F1B+NAC1 +H1B
5	5.21	0.028	H1B	5	5.27	0.028	H1B
6	6.19	0.022	W2B	6	6.22	0.022	W2B
7	7.85	0.016	F2B +W2B	7	8.35	0.016	F2B +W2B
9	10.66	0.025	F3B	9	10.80	0.025	F3B
12	14.11	0.020	W1T	12	14.09	0.020	W1T
15	19.32	0.020	-	15	19.91	0.020	-
20	26.98	0.042	H1T	20	27.66	0.042	H1T

a Refer to appendix B.

b Refer to list of symbols in appendix A.

Participating modes:
1,2,3,5,6,7,9,10,11,12,13,14,15,16,17,18,20

Selected modes for analysis:
1,2,3,5,6,7,9,12,15,20 (See Appendix B)

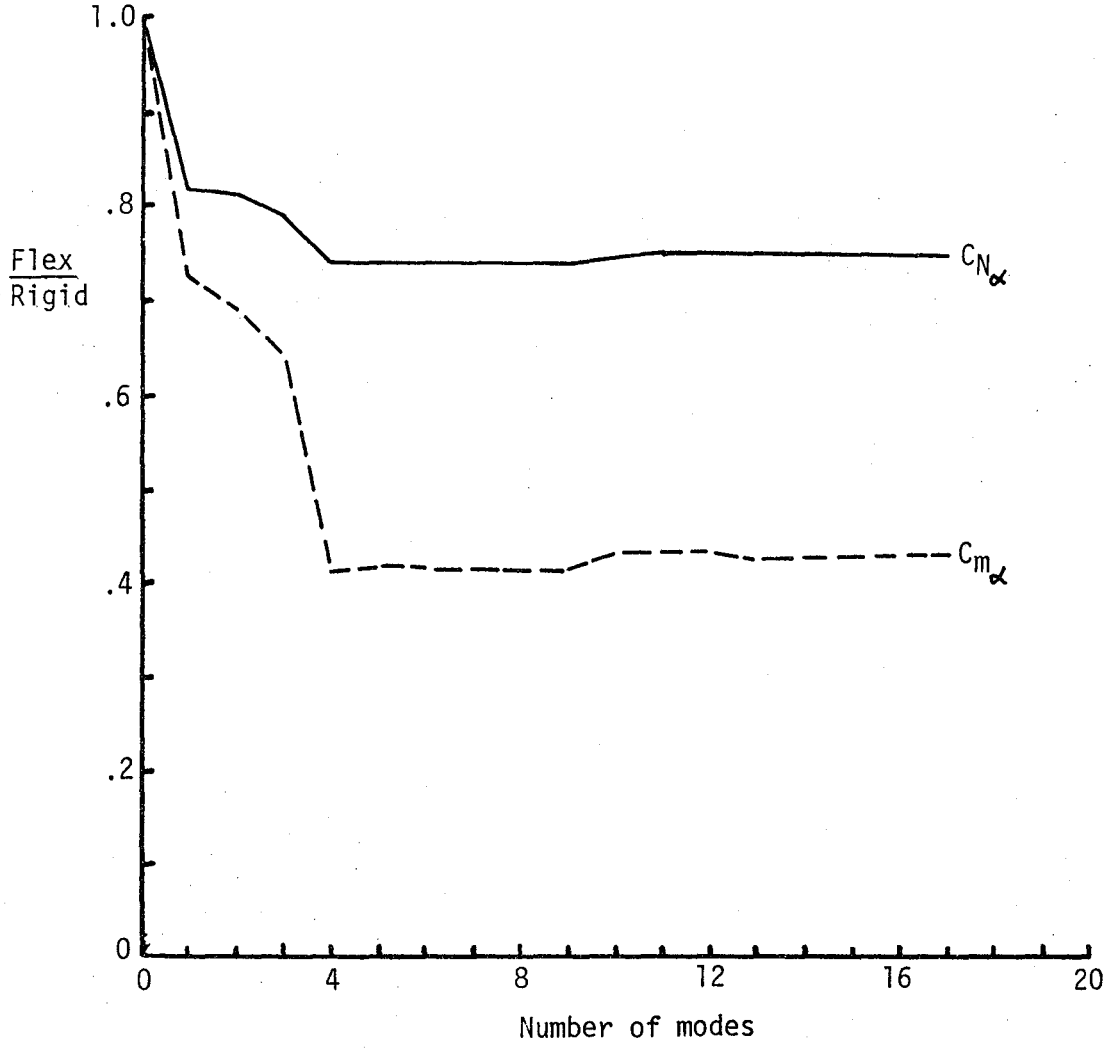

Figure 7. - Typical aeroelastic flexible-to-rigid ratio data for aerodynamic coefficients as a function of participating structural modes, M = 1.6, h_p = 9,449 m (31,000 ft), Λ = 67.5°.

Selected modes for analysis:
1,2,3,5,6,7,9,12,15,20 (See Appendix B)

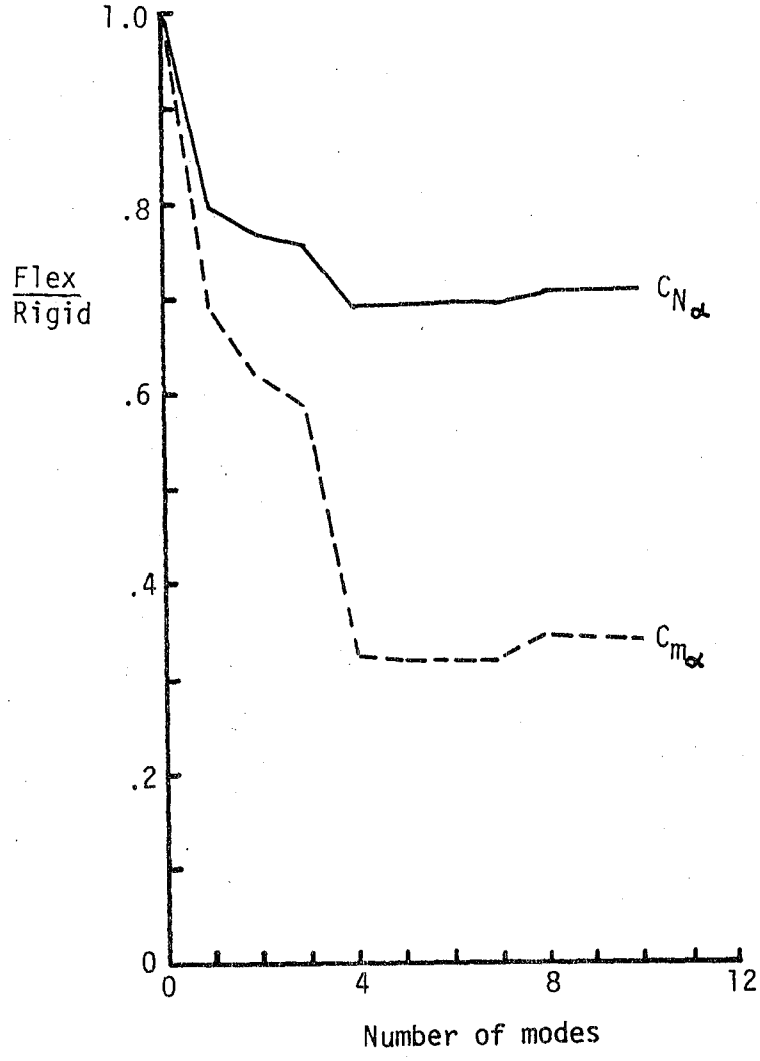

Figure 8. - Typical aeroelastic flexible-to-rigid ratio data for aerodynamic coefficients as a function of participating structural modes, M = 1.2, h_p = 5,791 m (19,000 ft), Λ = 67.5°.

modes selected. The structural damping was assigned to the modes indicated by similarity with those of reference 2 which had their source in GVT data.

Table III summarizes the frequencies and structural damping and identifies the main modal components for the 12 antisymmetric modes selected for lateral analyses at M = 1.6. The structural damping was assigned to the modes indicated by similarity with those of reference 2 which had their source in GVT data.

The mode shape data at the points indicated in figures 52 through 54 were processed to points required by the aerodynamic Mach Box Program.

All mode shapes were normalized for a generalized mass of 0.4536 kg (1 pound) for a half aircraft, or 0.9072 kg (2 pounds) for the whole vehicle.

Aerodynamics

Two sources of supersonic aerodynamics were utilized in this study. One was the B-1 System Definition Manual (SDM), which contains the correlated results of theory and wind tunnel tests for load distributions as well as for aerodynamic stability and control derivatives. The second was a digital computer program based on Mach Box theory as described in reference 3, which provided the structural mode aerodynamics, SMCS vane aerodynamics, and gust mode aerodynamics. All data generated were frequency dependent except for the SMCS vane data. These two sources of aerodynamic data were coordinated as follows:

First, most rigid body mode aerodynamics and their companion load distributions were taken from the B-1 SDM. The Mach Box program also produced aerodynamics for the rigid body modes which provided comparisons for loading distributions which gave a feel for the reliability of the Mach Box configuration modeling. Figure 9 shows the Mach Box pattern developed for the M = 1.2 flight condition for the wing and horizontal tail, and figure 10 shows the similar data for M = 1.6. Figures 11 and 12 display a separate modeling of the forebody and SMCS vanes to obtain vane normal force effectiveness data at M = 1.2 and 1.6, respectively. Figure 13 shows the fuselage and vertical tail modeling at M = 1.6 for the lateral-directional-antisymmetric component data.

The comparisons of the normalized spanload distributions on the wing-body and horizontal tail for the Mach Box theory and B-1 SDM data are shown in figures 14 and 15 for M = 1.2. The similar data for M = 1.6 are shown in figures 16 and 17. The comparisons are not outstanding, but do show similar gross characteristics. Some improvement of the comparisons could have been expected from using the program option which subdivides the edge boxes for area on and off the surface and adjusts the loads accordingly. This is an expensive option and was not utilized for that reason.

TABLE III. - SUMMARY OF ANTISYMMETRIC VIBRATION CHARACTERISTICS

M = 1.6, flt 3-137 114,156 Kg (251,670 lb)			
Mode No.[a]	Frequency Hz	Damping g_{s_i}	Ident [b]
1	1.68	0.145	NACI
2	2.47	0.054	WIB
3	3.81	0.049	FIT
4	4.31	0.031	WF&A
5	4.77	0.043	HIB
6	4.89	0.025	HF&A
7	6.10	0.032	FIB
8	7.13	0.031	W2B
9	9.27	0.019	V1B
10	10.59	0.020	-
11	12.03	0.022	F2B
32	34.44	0.020	VIT

[a] = Refer to appendix B.

[b] = Refer to list of symbols in appendix A.

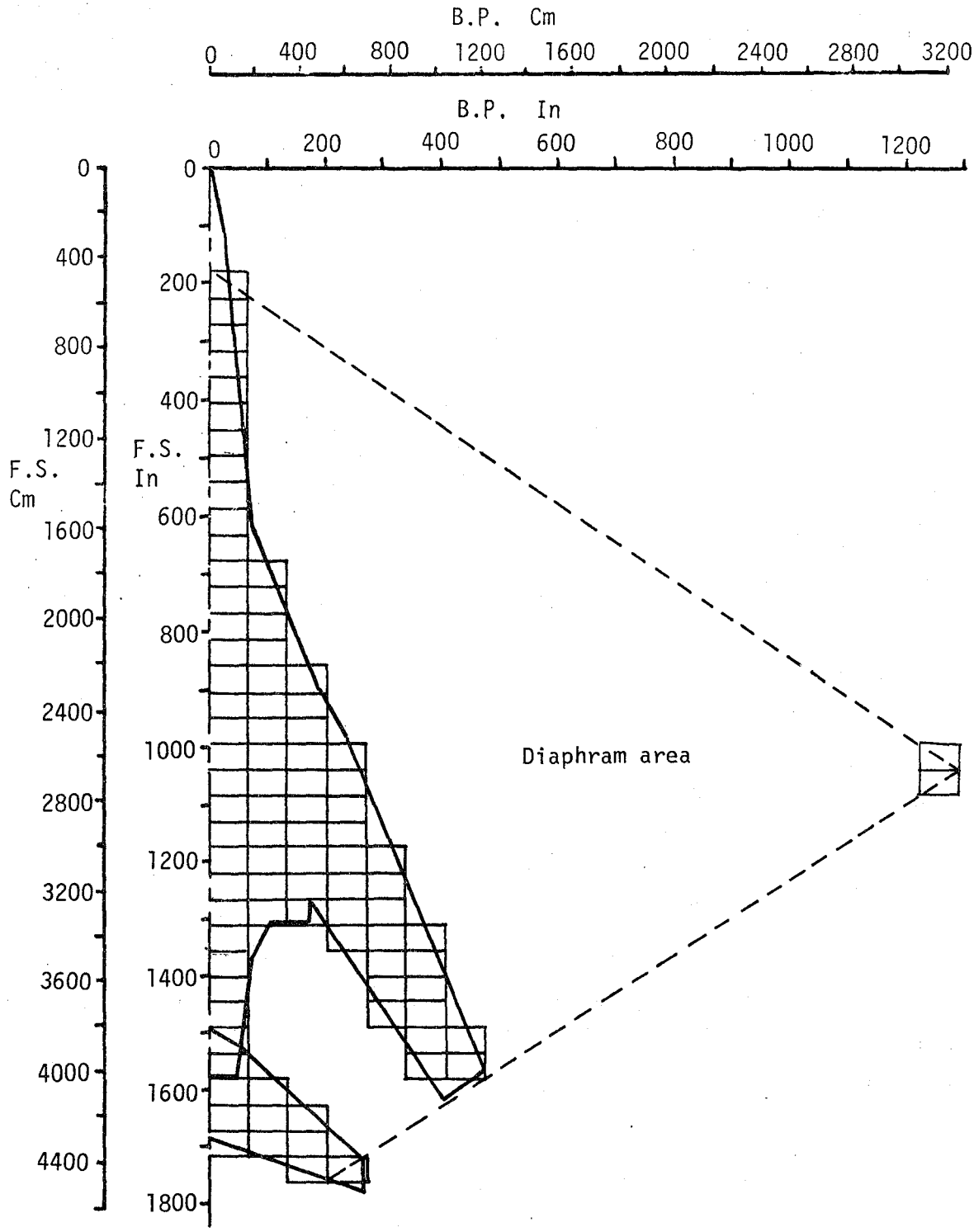

Figure 9. - Planform and box pattern for Mach Box program for whole vehicle aerodynamics, M = 1.2.

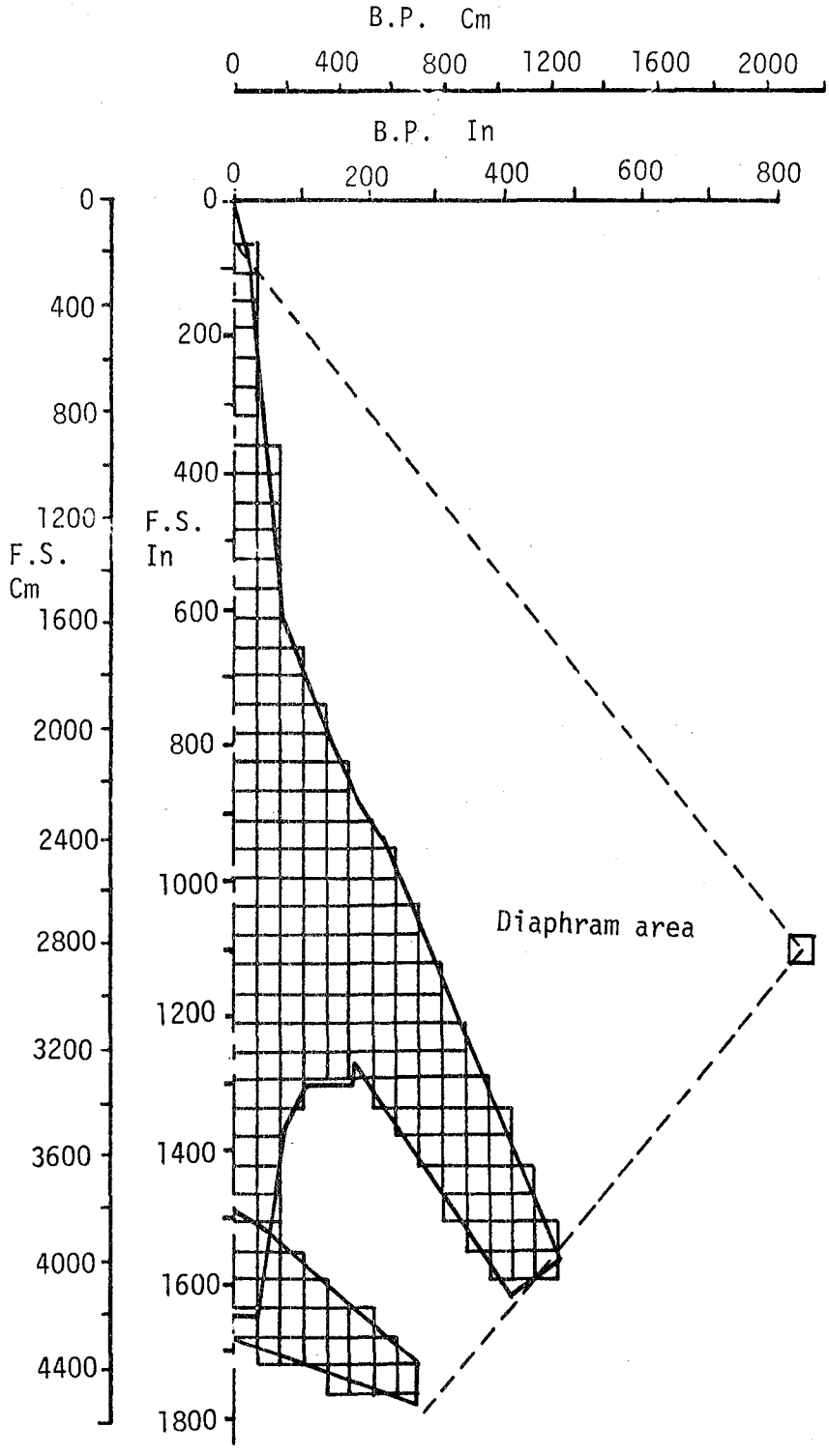

Figure 10. - Planform and box pattern for Mach Box program for whole vehicle aerodynamics, M = 1.6.

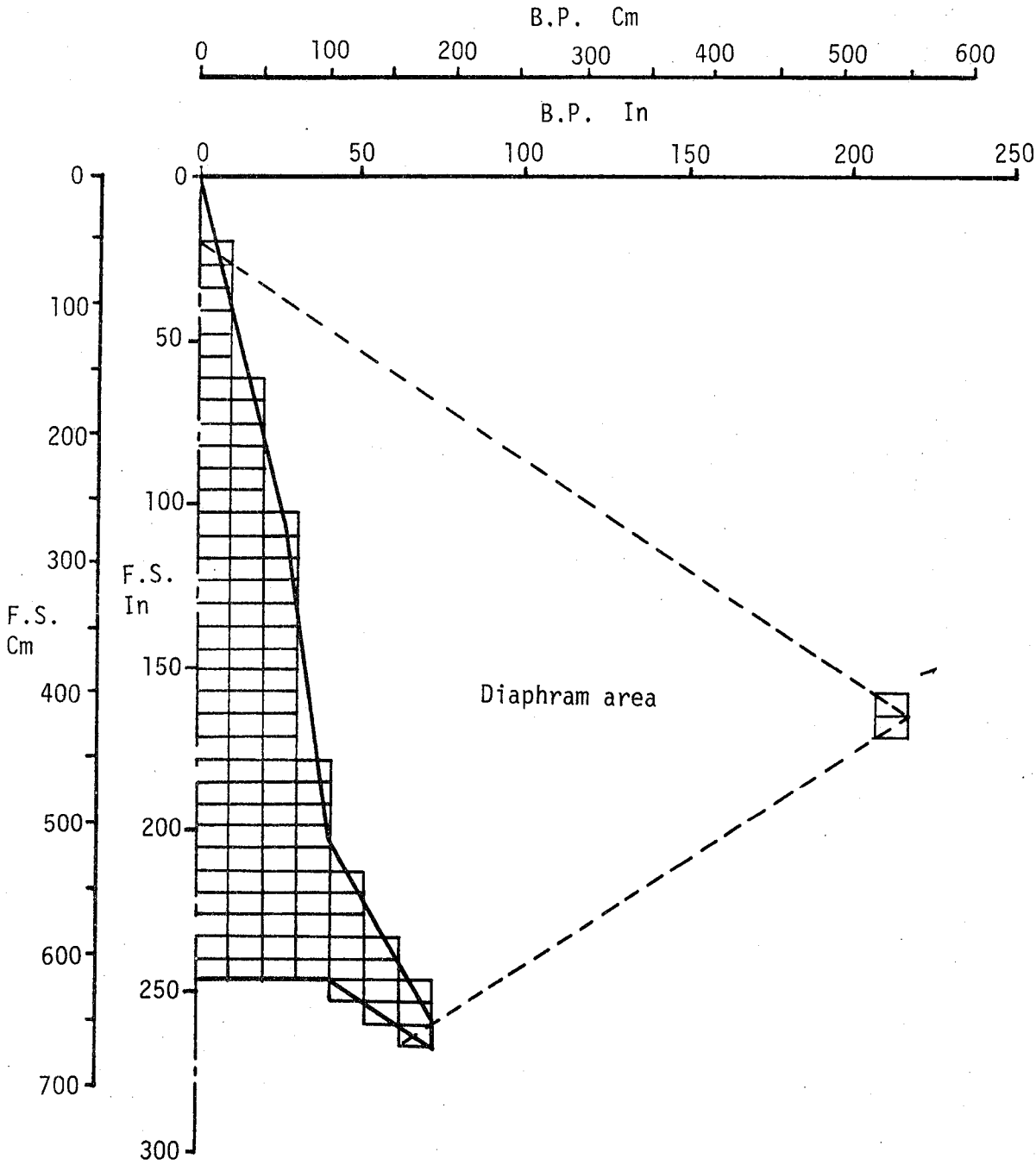

Figure 11. - Planform and box pattern for Mach Box Program for SMCS vane normal force effectiveness aerodynamics, M = 1.2.

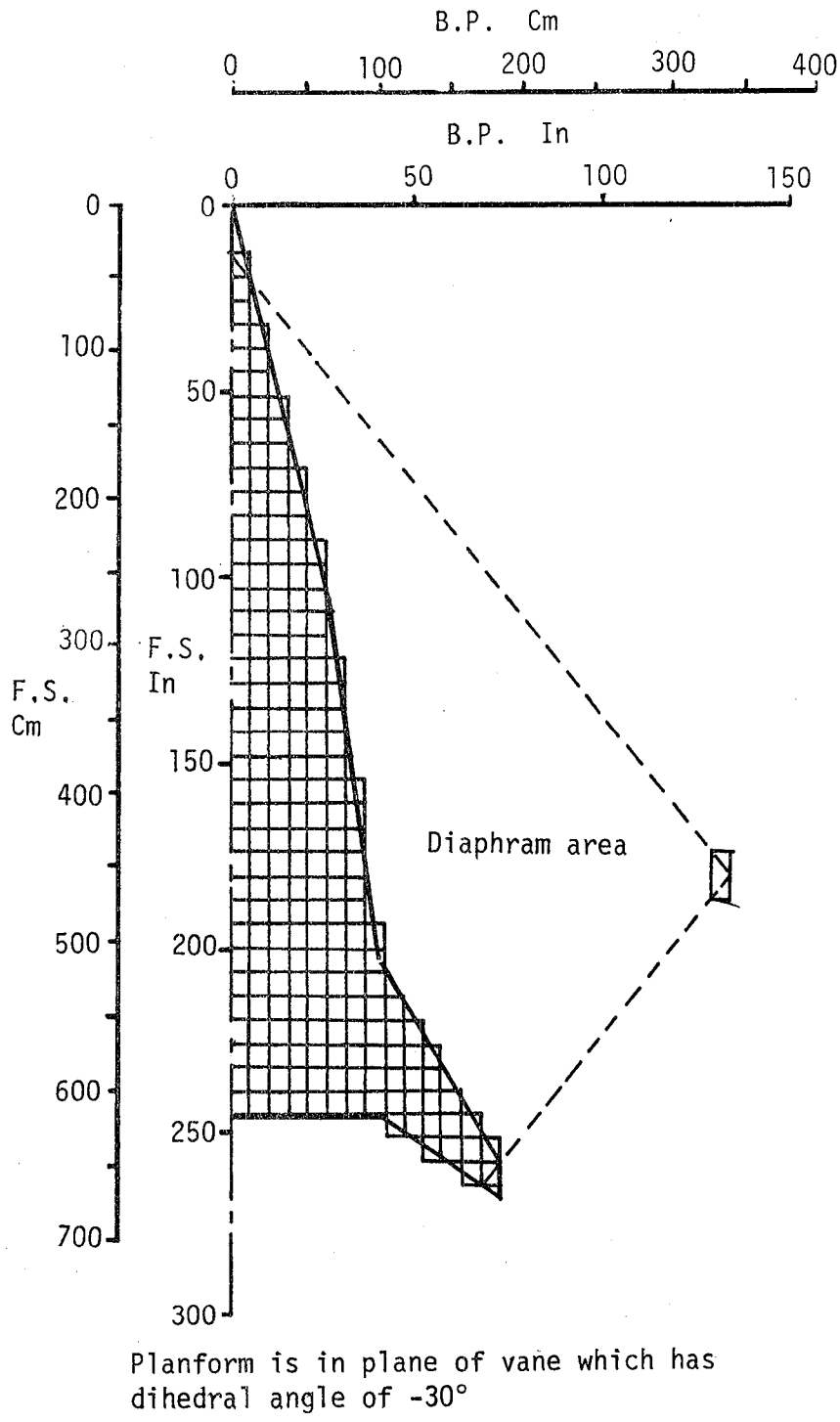

Figure 12. - Planform and box pattern for Mach Box program for SMCS vane normal force effectiveness aerodynamics, M = 1.6.

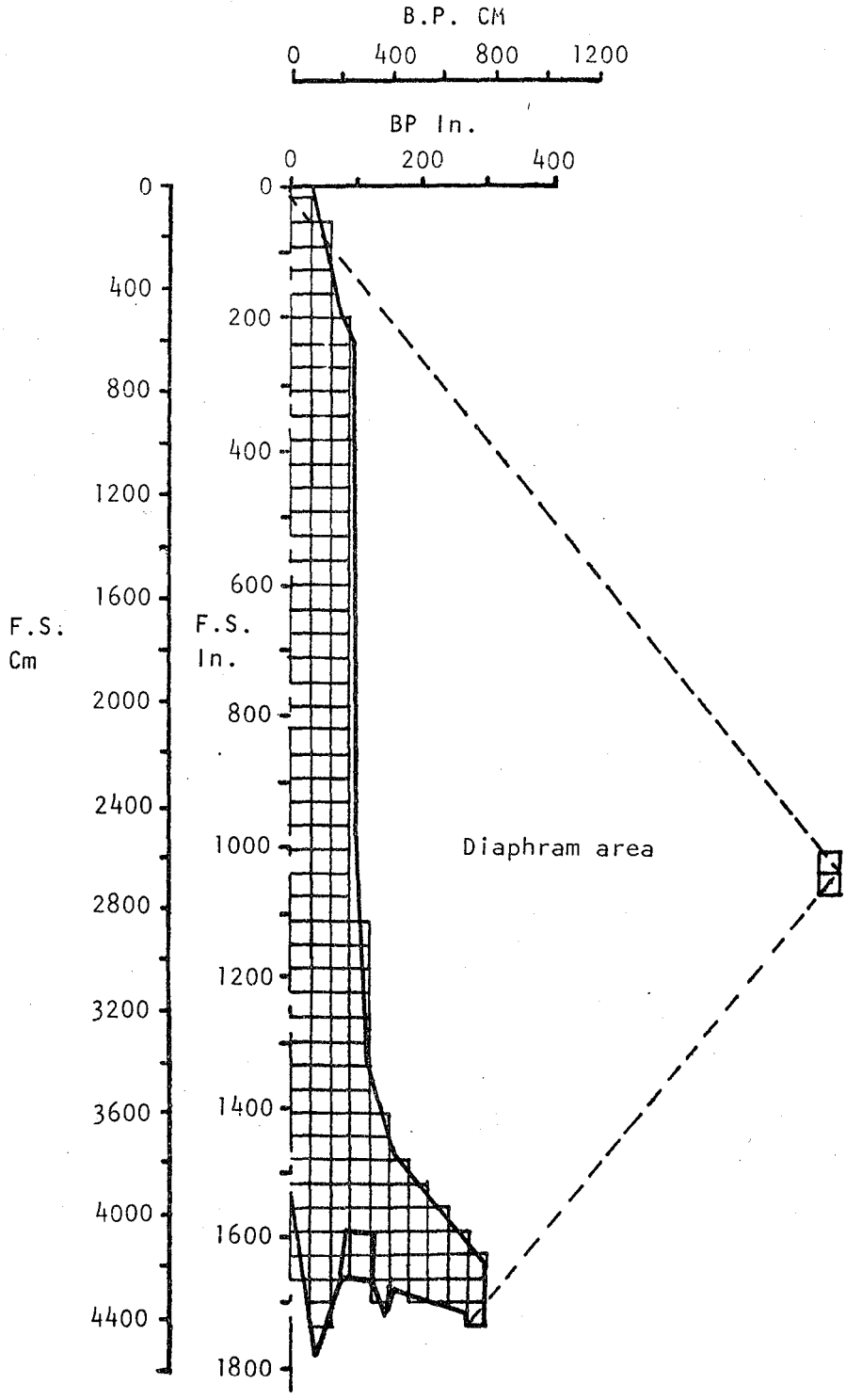

Figure 13. - Side view and box pattern for Mach Box program for fuselage and vertical tail aerodynamics, M = 1.6.

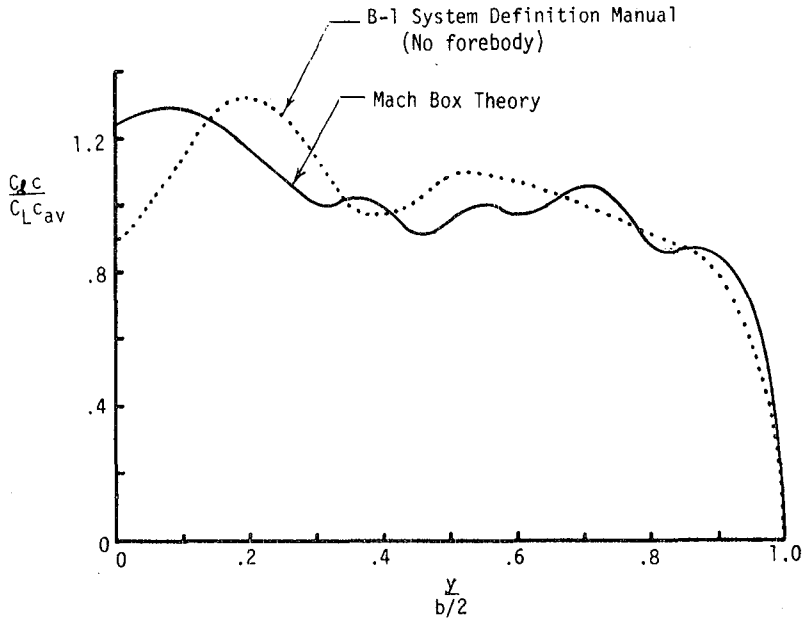

Figure 14. - Comparison of spanload distribution for wing-body for Mach Box theory and B-1 System Definition Manual data, M = 1.6, Λ = 67.5°.

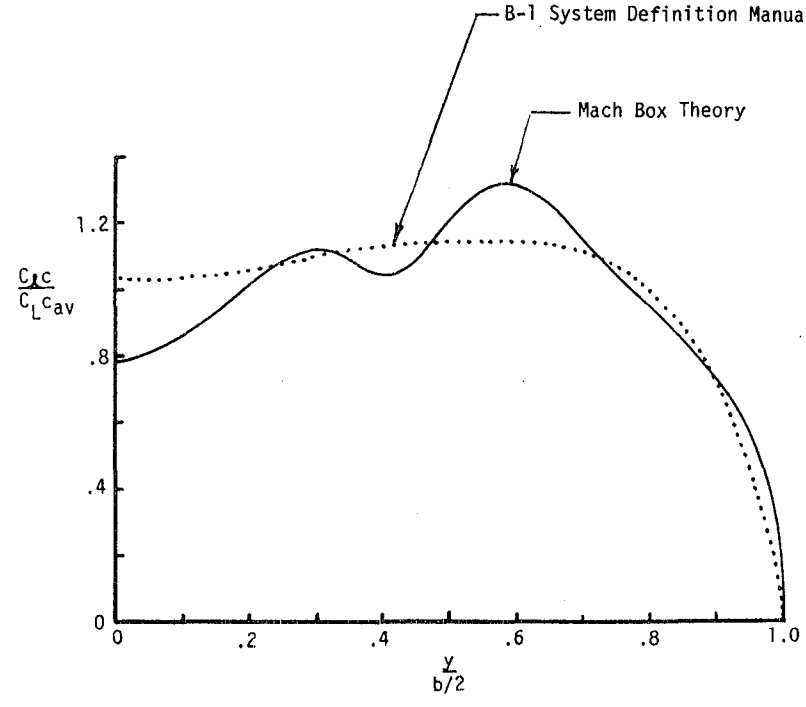

Figure 15. - Comparison of spanload distribution for horizontal tail for Mach Box theory and B-1 System Definition Manual data, M = 1.6, Λ = 67.5°.

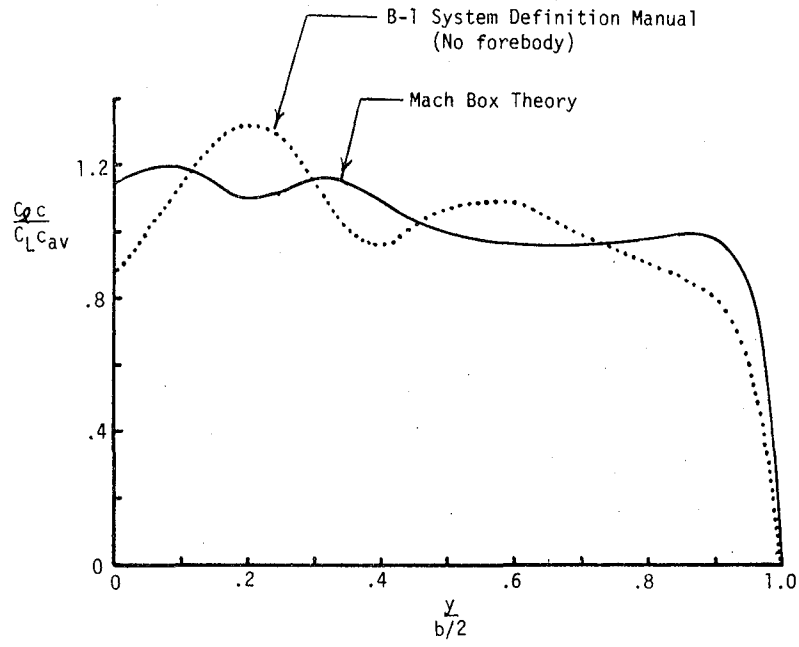

Figure 16. - Comparison of spanload distribution for wing-body for Mach Box theory and B-1 System Definition Manual data, M = 1.2, = 67.5°.

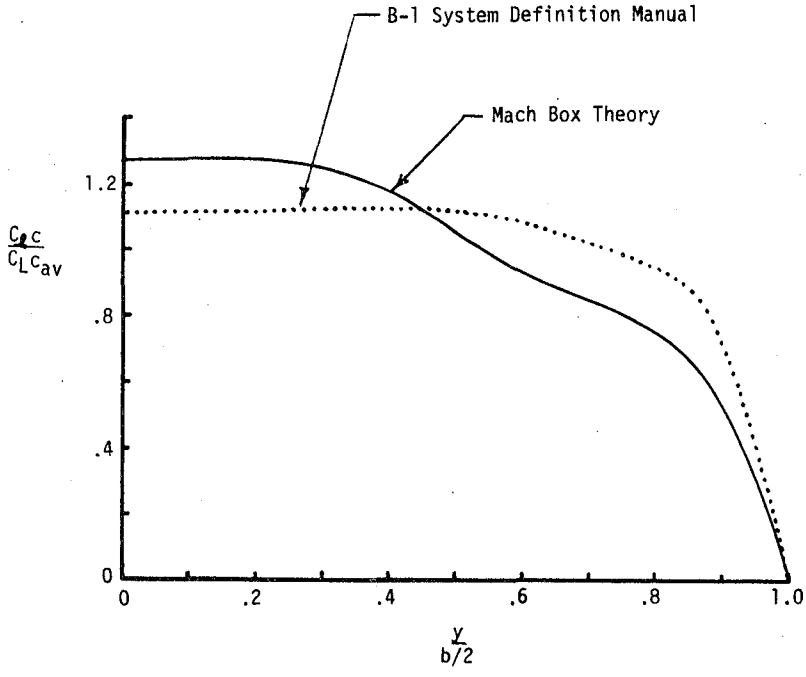

Figure 17. - Comparison of spanload distribution for horizontal tail for Mach Box theory and B-1 System Definition Manual data, M = 1.2, Λ = 67.5°.

A correction factor was developed by ratioing SDM C_{N_α} to Mach Box C_{N_α}, which was applied to all Mach Box symmetric structural mode aerodynamics. Similarly, a correction was applied to the antisymmetric structural mode aerodynamics for the fuselage-vertical tail component by a ratio of C_{Y_β} from the SDM to C_{Y_β} from the Mach Box data. The wing-horizontal antisymmetric structural mode data used the same factor as for the symmetric case.

The subject of SMCS vane normal force effectiveness is deserving of special attention. Pretest estimates of normal load factor frequency responses due to SMCS vane inputs predicted low responses and caused the normal load factor limiter to trip off several times during the first supersonic flight 3-137. Having this fact in mind, it was decided to use Mach Box theory to estimate the SMCS vane normal force effectiveness data. Because of the relatively small surface of the SMCS vane compared to the wing, these aerodynamics were not frequency dependent. The analyses results are compared in figure 18 to the earlier SDM estimate. In defense of the earlier estimate, it must be remembered that the original SMCS was designed to operate at subsonic speeds only. The curve was extended to the supersonic range using a typical mach number trend for completeness only.

The vane lateral force characteristics used in the analyses were obtained by first defining the force characteristics normal to the vane surface and then taking the lateral component of that force vector.

Active Control Systems

Two types of active control systems were included in the analyses pertaining to this study. One type, the stability and control augmentation system (SCAS), is associated with control of whole vehicle (short period and Dutch roll) modes of motion. The second type, the structural mode control system (SMCS), has the function of controlling fuselage structural motion to improve ride quality.

The block diagrams and analytical modeling of the SCAS are given in figures 19 through 21 and of the SMCS in figures 22 and 23. Flight condition-dependent gains are shown for M = 1.6 at 9,449 meters (31,000 feet) and M = 1.2 at 5,791 meters (19,000 feet). These figures indicate the type of sensors, compensations, gains, and actuator modeling assumed for each of the indicated systems. The control-surface deflection equations are cast in a form directly usable by the Rockwell response analyses programs. That is to say, the overall gain is indicated, system dynamics are represented by numerator and denominator roots of polynomials, and vehicle motions are defined as measured by the appropriate sensors.

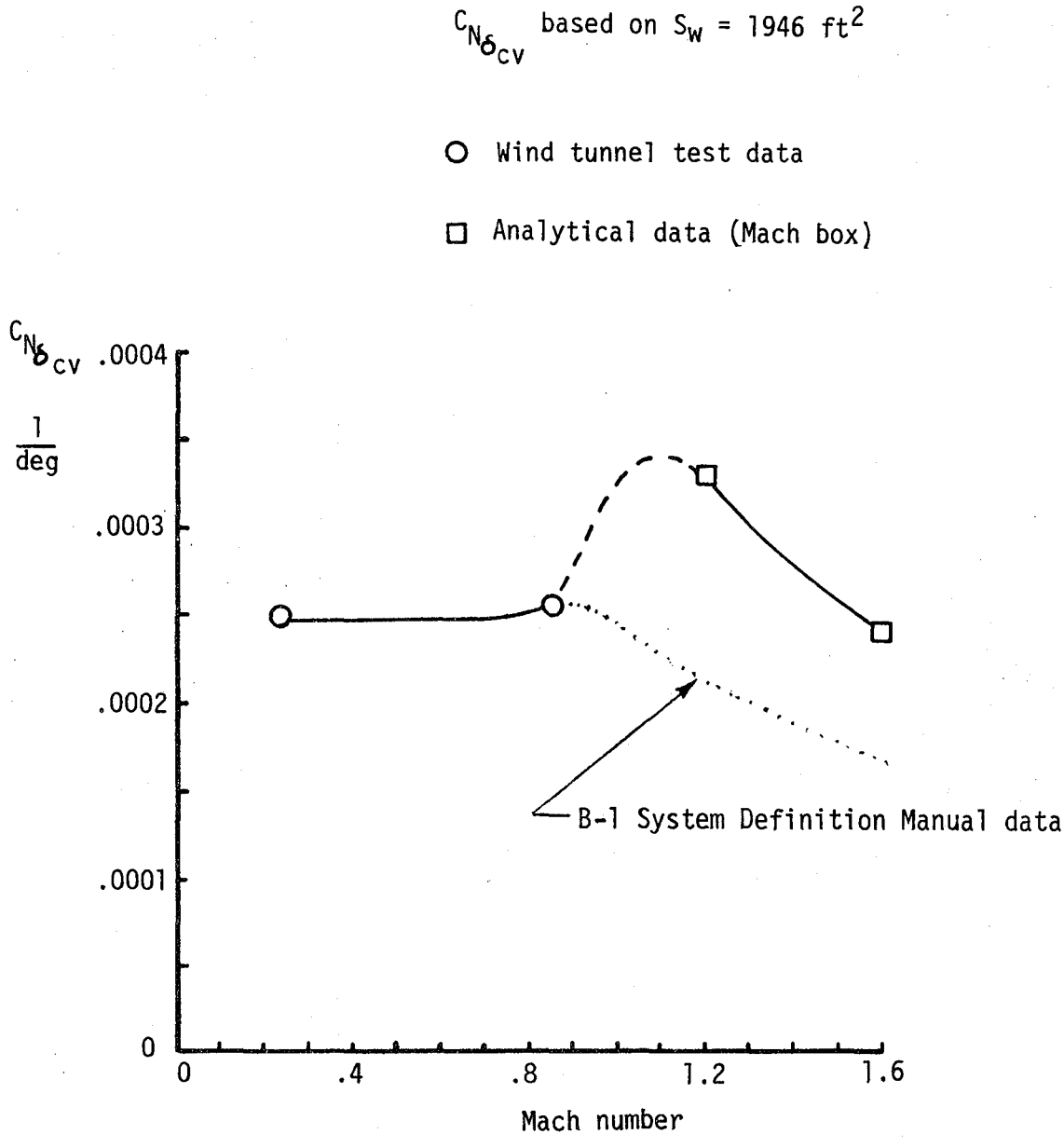

Figure 18. - SMCS vane normal force effectiveness.

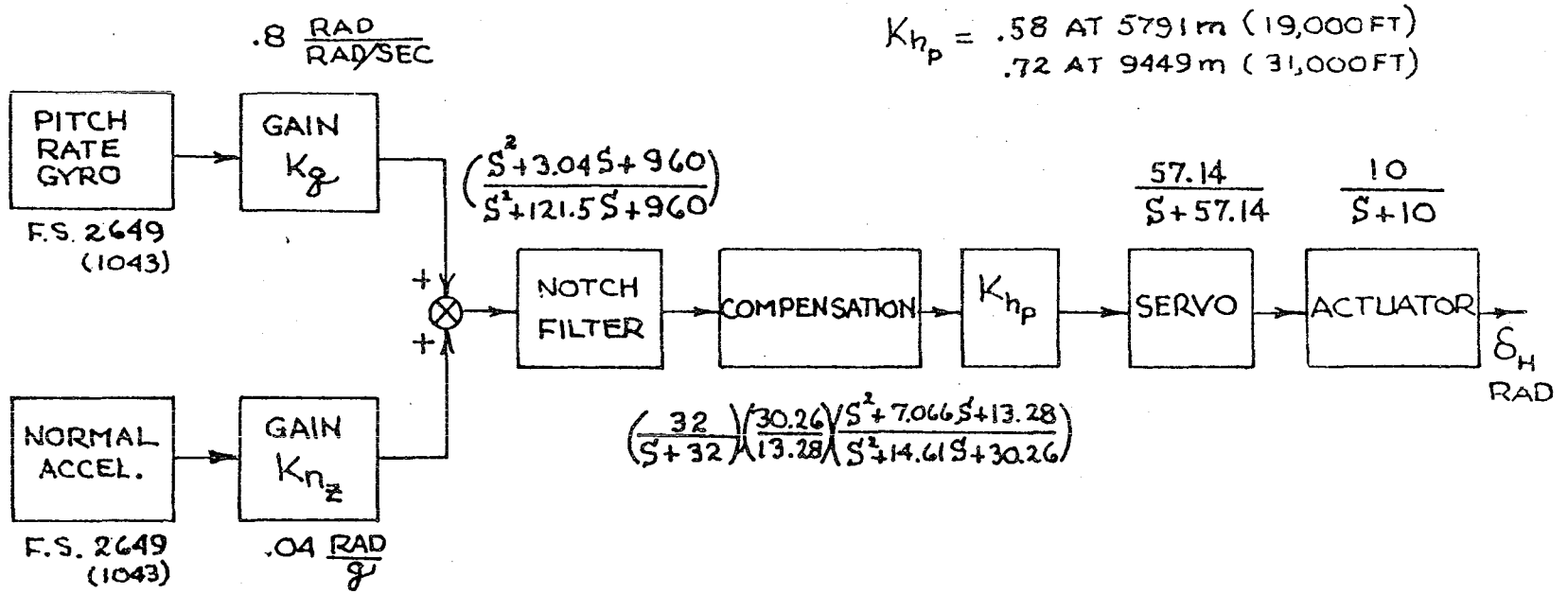

$$(\delta_H)_{GYRO} = +\underbrace{(32)(.8)\left(\frac{30.26}{13.28}\right)(58)(57.14)(10)}_{19332.1}\left\{\frac{(S+1.5\pm j30.95)}{(S+8.495)(S+113.0047)}\frac{(S+3.533\pm j.893)}{(S+2.498)(S+12.112)}\frac{1}{(S+32)}\frac{1}{(S+57.14)}\frac{1}{(S+10)}\right\}\left[q+\sum_{i=1}^{n}(-\phi_i')S\eta_i\right]$$

RAD

$$(\delta_H)_{ACCEL} = +\underbrace{(32)\left(\frac{.04}{32.2}\right)(58)\left(\frac{30.26}{13.28}\right)(57.14)(10)}_{30.02}\left\{\frac{(S+1.5\pm j30.95)}{(S+8.495)(S+113.0047)}\frac{(S+3.533\pm j.893)}{(S+2.498)(S+12.112)}\frac{1}{(S+32)}\frac{1}{(S+57.14)}\frac{1}{(S+10)}\right\}\left[-V_o S\alpha+I_x\left(S+\frac{V_o}{I_x}\right)\beta+\sum_{i=1}^{n}(-\phi_i)S^2\eta_i\right]$$

RAD

For flight condition of M = 1.2 at 5791 m (19,000ft)

Figure 19. - Pitch axis SCAS analytical model.

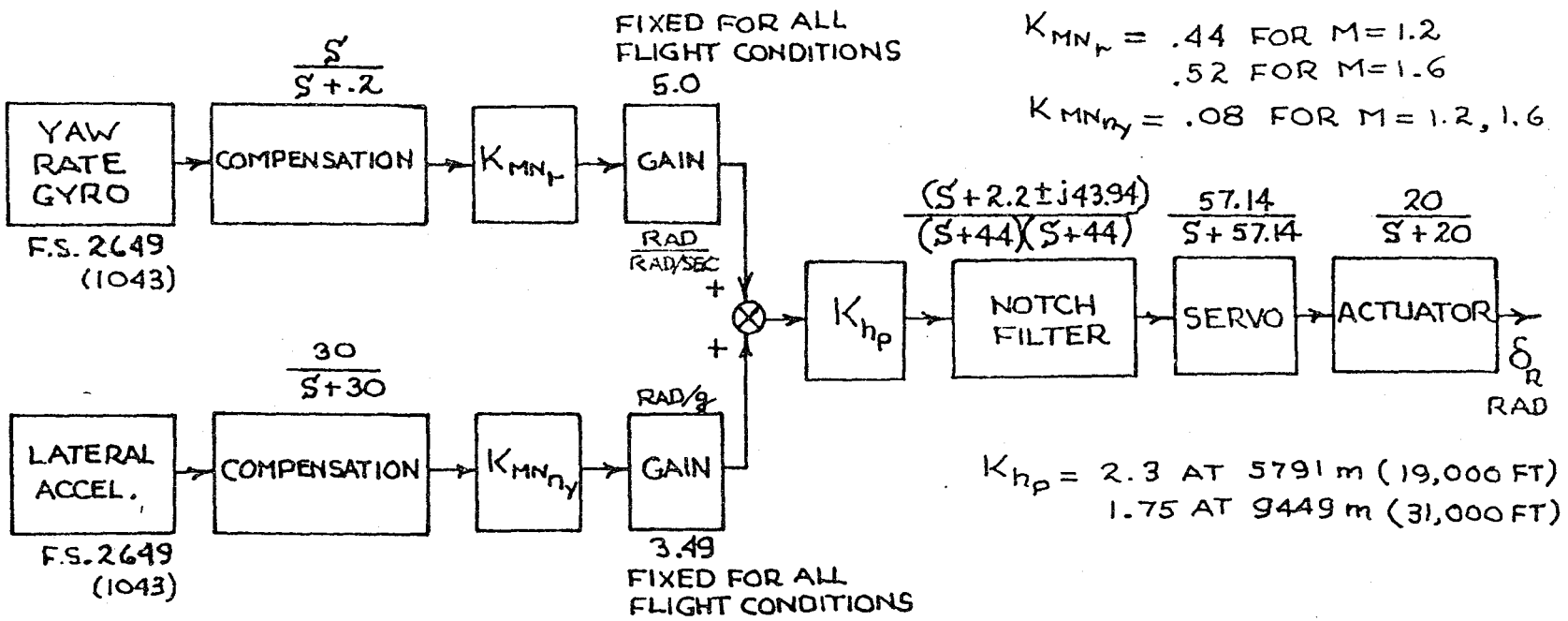

$$(\delta_R)_{GYRO} = \overbrace{(.44)(5.0)(2.3)(57.14)(20)}^{5782.6}\left\{\left(\frac{S}{S+.2}\right)\left(\frac{S+2.2\pm j43.94}{(S+44)(S+44)}\right)\left(\frac{1}{S+57.14}\right)\left(\frac{1}{S+20}\right)\right\}\left[(0)\beta+(1.0)r+(0)p+\sum_{i=1}^{m}\phi_i' S\eta_i\right] \text{ RAD}$$

$$(\delta_R)_{ACCEL.} = +\overbrace{\left(\frac{30}{32.2}\right)(.1)(3.49)(2.3)(57.14)(20)}^{85.47}\left\{\left(\frac{1}{S+30}\right)\left(\frac{S+2.2\pm j43.94}{(S+44)(S+44)}\right)\left(\frac{1}{S+57.14}\right)\left(\frac{1}{S+20}\right)\left(\frac{1}{S}\right)\right\}\left[V_o S^2\beta+l_x S\left(S+\frac{V_o}{l_x}\right)r-V_o\alpha_T\left(S+\frac{32.2}{V_o\alpha_T}\right)p+\sum_{i=1}^{m}\phi_i S^3\eta_i\right] \text{ RAD}$$

See note on figure 22

For flight condition of M = 1.2 at 5791 m (19,000ft)

Figure 20. - Yaw axis SCAS analytical model.

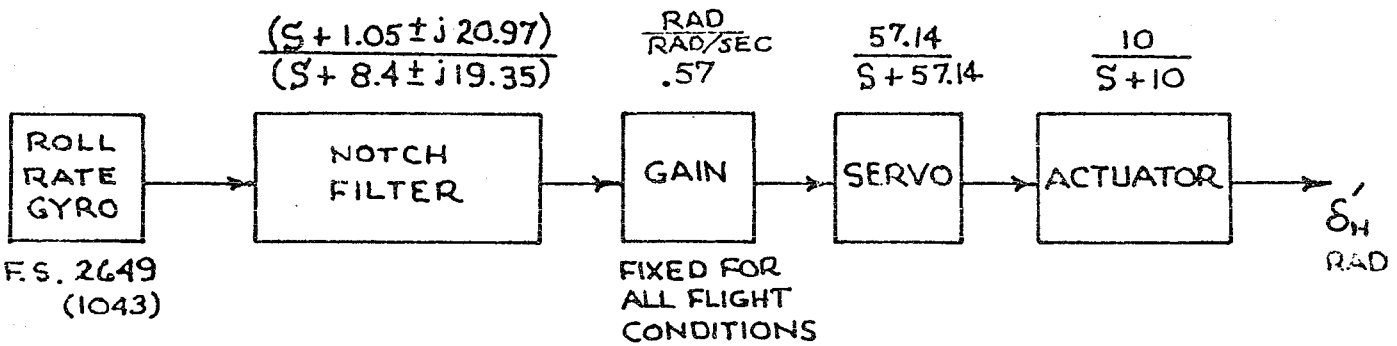

$$\delta'_{H_{RAD}} = -\overbrace{(.57)(57.14)(10)}^{325.7}\left\{\frac{(S+1.05\pm j20.97)}{(S+8.4\pm j19.35)}\left(\frac{1}{S+57.14}\right)\left(\frac{1}{S+10}\right)\right\}\left[(0)\beta+(0)r+(1.0)p+\sum_{i=1}^{m}\phi_i^r S\eta_i\right]$$

For flight condition of M = 1.2 at 5791 m (19,000ft)
= 1.6 at 9449 m (31,000ft)

Figure 21. - Roll axis SCAS analytical model.

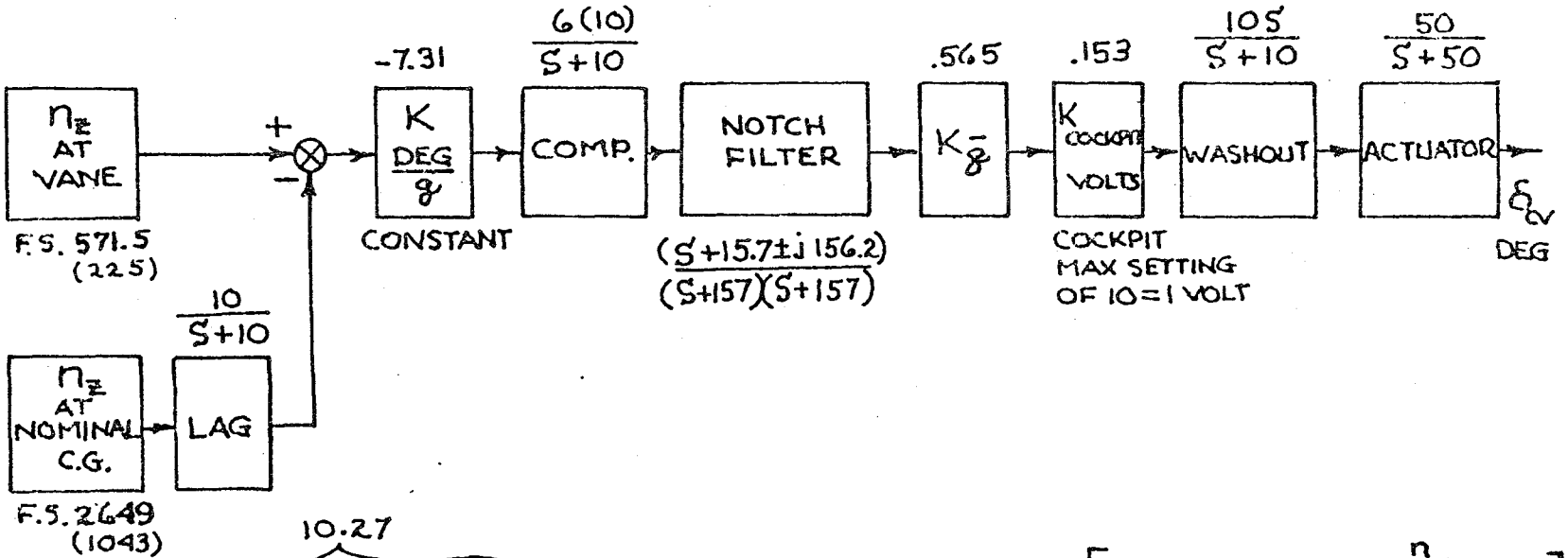

$$(\delta_{cv})_{225\ RAD} = -\overbrace{\frac{(.153)(6)(7.31)(.565)(10)(10)(50)}{(57.3)(32.2)}}^{10.27}\left\{\left(\frac{1}{S+10}\right)\frac{(S+15.7\pm j156.2)}{(S+157)(S+157)}\left(\frac{S}{S+10}\right)\left(\frac{1}{S+50}\right)\right\}\left[-V_o S\alpha + l_x\left(S+\frac{V_o}{l_x}\right)\bar{g} + \sum_{i=1}^{n}(-\phi_i)S^2\eta_i\right]$$

$$(\delta_{cv})_{1043\ RAD} = +\overbrace{\frac{(.153)(6)(7.31)(.565)(10)(10)(10)(50)}{(57.3)(32.2)}}^{102.7}\left\{\left(\frac{1}{S+10}\right)\left(\frac{1}{S+10}\right)\frac{(S+15.7\pm j156.2)}{(S+157)(S+157)}\left(\frac{S}{S+10}\right)\left(\frac{1}{S+50}\right)\right\}\left[-V_o S\alpha + l_x\left(S+\frac{V_o}{l_x}\right)\bar{g} + \sum_{i=1}^{n}(-\phi_i)S^2\eta_i\right]$$

For flight condition of M = 1.2 at 5791 m (19,000ft)
= 1.6 at 9449 m (31,000ft)

Figure 22. - Vertical SMCS analytical model.

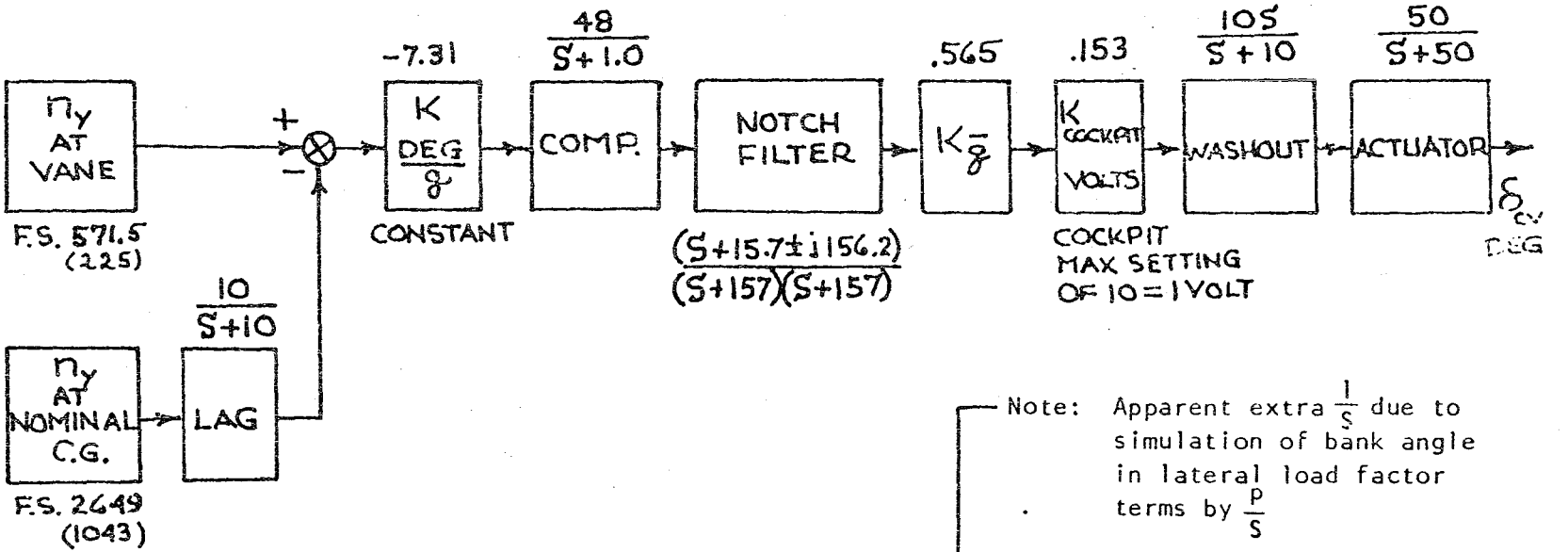

Note: Apparent extra $\frac{1}{S}$ due to simulation of bank angle in lateral load factor terms by $\frac{P}{S}$

$$(\delta_{cv})_{225} = -\overbrace{\frac{(.153)(7.31)(48)(.565)(10)(50)}{(57.3)(32.2)}}^{8.06} \left\{\frac{1}{S+1.0}\right\}\left\{\frac{(S+15.7\pm j156.2)}{(S+157)(S+157)}\right\}\left\{\frac{S}{S+10}\right\}\left\{\frac{1}{S+50}\right\}\left\{\frac{1}{S}\right\}\left\{V_o S^2\beta + l_x S\left(S+\frac{V_o}{l_x}\right)r - V_o\alpha_1\left(S+\frac{32.2}{V_o\alpha_1}\right)p + \sum_{i=1}^{m}\phi_i S^3\eta_i\right\} \text{ RAD}$$

$$(\delta_{cv})_{1043} = +\overbrace{\frac{(.153)(7.31)(48)(.565)(10)(10)(50)}{(57.3)(32.2)}}^{80.6} \left\{\frac{1}{S+10}\right\}\left\{\frac{1}{S+1.0}\right\}\left\{\frac{(S+15.7\pm j156.2)}{(S+157)(S+157)}\right\}\left\{\frac{S}{S+10}\right\}\left\{\frac{1}{S+50}\right\}\left\{\frac{1}{S}\right\}\left\{V_o S^2\beta + l_x S\left(S+\frac{V_o}{l_x}\right)r - V_o\alpha_1\left(S+\frac{32.2}{V_o\alpha_1}\right)p + \sum_{i=1}^{m}\phi_i S^3\eta_i\right\} \text{ RAD}$$

For flight condition of M = 1.2 at 5791 m (19,000ft)
= 1.6 at 9449 m (31,000ft)

Figure 23. - Lateral SMCS analytical model.

Since the focus of this report is the SMCS, a more elaborate block diagram is presented in figure 24 highlighting a number of mechanization features not seen in figures 22 and 23.

The system consists of two basic functional parts; one is associated with operating the vane panels in unison to control symmetric structural motion (vertical system), and the other is associated with operating them differentially to control antisymmetric side bending structural motion (lateral system).

The implementation of the basic ILAF (identical location of accelerometer and force) concept can be seen in the placement of the vertical and lateral accelerometers at the same general location as the control vanes. To augment this principle by eliminating most of the rigid-body motion, a second set of accelerometers is placed near the center of gravity. Because the rigid-body motion content and lower structural modes are desired only from the signal of the center-of-gravity accelerometer, the signal is passed through a simple lag which eliminates higher frequency structural mode content.

After the difference signal from the accelerometers at the vane and at the center of gravity is obtained, it is passed through shaping and a notch filter designed to eliminate the primary natural frequencies of the vane-actuator installation. The signal then passes through a gain which is scheduled by dynamic pressure from the central air data system. The primary utilization of the SMCS will be during low-altitude high-speed flight. The speed and altitude, however, will vary over a limited range; thus dynamic pressure gain scheduling was selected to maintain control force effectiveness.

The functional intent of the system is to produce structural damping; therefore, the signal to the force actuation devices must be proportional to structural velocity. This velocity signal is obtained by appropriate gains and shaping networks. Selections of the gains and shaping networks are a function of the structural, aerodynamic, and actuator dynamic characteristics. Basically, simple lags are used to approximate integration of the structural acceleration signals to obtain the required velocity signals.

Washout networks are used to effectively disengage the vertical or lateral functional parts of the system in event of hardover failures. In addition to isolating hardover failures, the washout networks attenuate rigid-body (whole-vehicle) response acceleration signals that cannot be canceled by the accelerometer signal differencing.

After the washout circuits, the signals are divided and proceed to the independent left and right vane-actuator assemblies. Before reaching the actuators, however, the signals pass through electronic limiters in the circuits. These limiters prevent the vane actuators from making hard contact with the physical actuator throw stops.

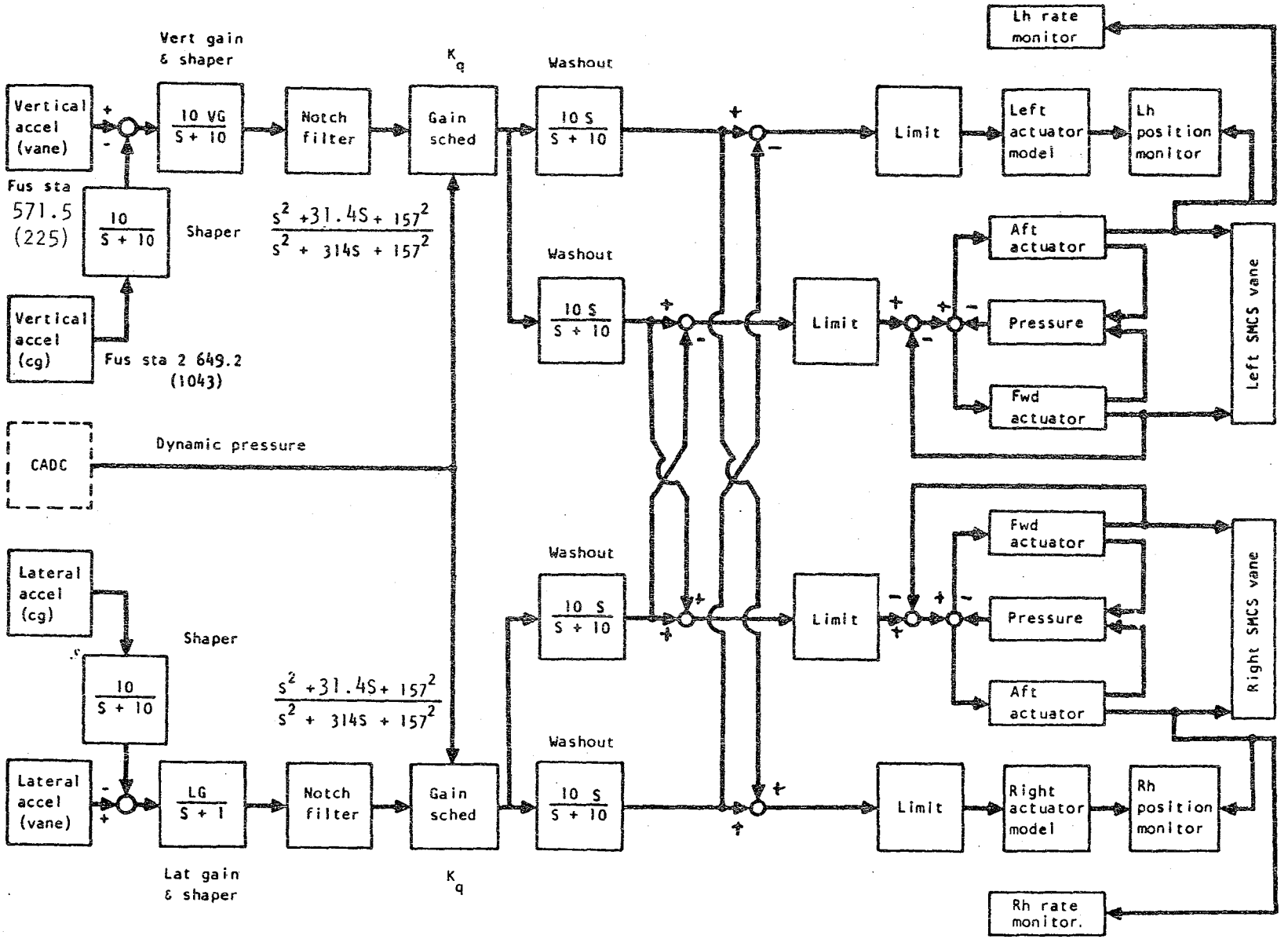

Figure 24. - Structural mode control system block diagram.

Depending upon whether the signals come from the vertical or lateral motion sensing part of the system, the actuators move the left and right vanes in unison or differentially to produce the required aerodynamic control forces. The system will also respond to mixed signals from the vertical and lateral sensor systems. Pressure sensors coordinate the force output between the forward and aft actuators.

Two actuators are associated with each vane so that a free-floating vane can be avoided in event of a malfunction. Use of the dual hydromechanical components insures that the vanes can be returned to neutral position, and held when disengaged manually by the pilot or automatically by the SMCS monitors. The monitors use vane deflection and maximum vane rate information to detect malfunctions. The part of the monitor that uses vane deflection information consists of a duplicate of the electronics from the shaping network output to the actuator input and an electronic model of the actuator. Thus, differences between the command vane position and the actual vane position exceeding certain values for a specified time interval are used to automatically disengage the SMCS. The part of the monitor that uses vane maximum rate information disengages the SMCS when maximum rate is sustained for more than an accumulated number of seconds during a specified time interval. This latter monitor is designed to handle dynamic instability possibilities such as limit cycling.

In the early design phases, it was thought prudent to design the SMCS so that it would operate only in conjunction with the SCAS. Thus, any unforseen hardover vane failure effects on rigid-body motion would be attenuated. In retrospect, it appears that this design approach is overly conservative because of the small size of the SMCS vane.

The SMCS is not designed to operate continuously. A cockpit switch enables the crew to turn the system on prior to low-level flight and turn it off afterward. Also, while not specifically noted on the block diagram, there is a switch mechanized so that the system is disabled automatically as the landing gear is lowered and enabled as the gear is raised. This feature is necessary to preclude the vane from inducing inertia reaction forces in the absence of aerodynamic forces which will cause instabilities (the so-called "tail wags dog" phenomenon) if the switch is accidently left on or during ground testing.

FLIGHT TEST DATA

The test data for this study were obtained on two separate flights; M = 1.6 data were obtained on flight 3-137, and M = 1.2 data were obtained on flight 3-138. It is the intent of this section to display and discuss the results of these data as they pertain to the effects of mach number and SMCS performance.

The vertical data are discussed first and are displayed in figures 25 through 36, followed by the lateral data in figures 37 through 48. At each mach number, the data are presented in the following sequence: Basic aircraft (no active system operating), SCAS operating, and SCAS + SMCS operating; first for the pilot station F.S. 746.8 (294) and then the vane station F.S. 571.5 (225).

In order to facilitate visual comparisons among plots, scales for the vertical and lateral load factor responses have been kept fixed.

In the interest of not repeating data, the flight test and analyses results are displayed together on data plots of figures 25 through 36 and 43 through 48. These analyses results, however, are not discussed at this point but are reserved for a following section.

Vertical Axis Data

Looking first at M = 1.2 vertical response data at the pilot station in figures 25 through 27, the response data show three response peaks within the 10 Hz frequency range of interest, the first being the first fuselage bending mode and of primary interest to the vehicle ride quality and SMCS operation. Operating the SCAS at this mach number causes the first fuselage structural response to increase slightly as shown by figure 26; this effect is characteristic of the pitch SCAS, as reference 2 indicates. The SMCS does the job it is intended to do as indicated in figure 27 by the marked reduction in the first fuselage mode response near 3 Hz. There is a slight increase in response of the highest frequency mode shown.

Figures 28 through 30 show the similar M = 1.2 vertical response data at the vane station. The three modal peaks seen in the previous data are seen in these data with the high frequency modes being relatively more responsive. Figure 29 shows that the pitch SCAS increases the response of the first fuselage bending mode. Figure 30 shows the impact of SMCS in reducing the first fuselage bending response. The impact at highest frequency mode is now more obvious than in figure 27.

The vertical response data for M = 1.6 are shown in figures 31 through 36. The features seen in the M = 1.2 data are seen in the M = 1.6 data with some exceptions. Contrary to what was seen in the M = 1.2 data, operating the pitch SCAS does not excite the first mode response. The first bending mode is less responsive at M = 1.6 than at M = 1.2. On the other hand, the adverse impact of the SMCS at the highest frequency is greater as seen at the vane station at M = 1.6 than at M = 1.2.

Note: δ_{cv} is control surface deflection. The flight-test data measurements of the forcing command were analytically processed to remove effects of actuator dynamics, which were measured, in order to permit comparisons with analytical results on this and similar subsequent figures.

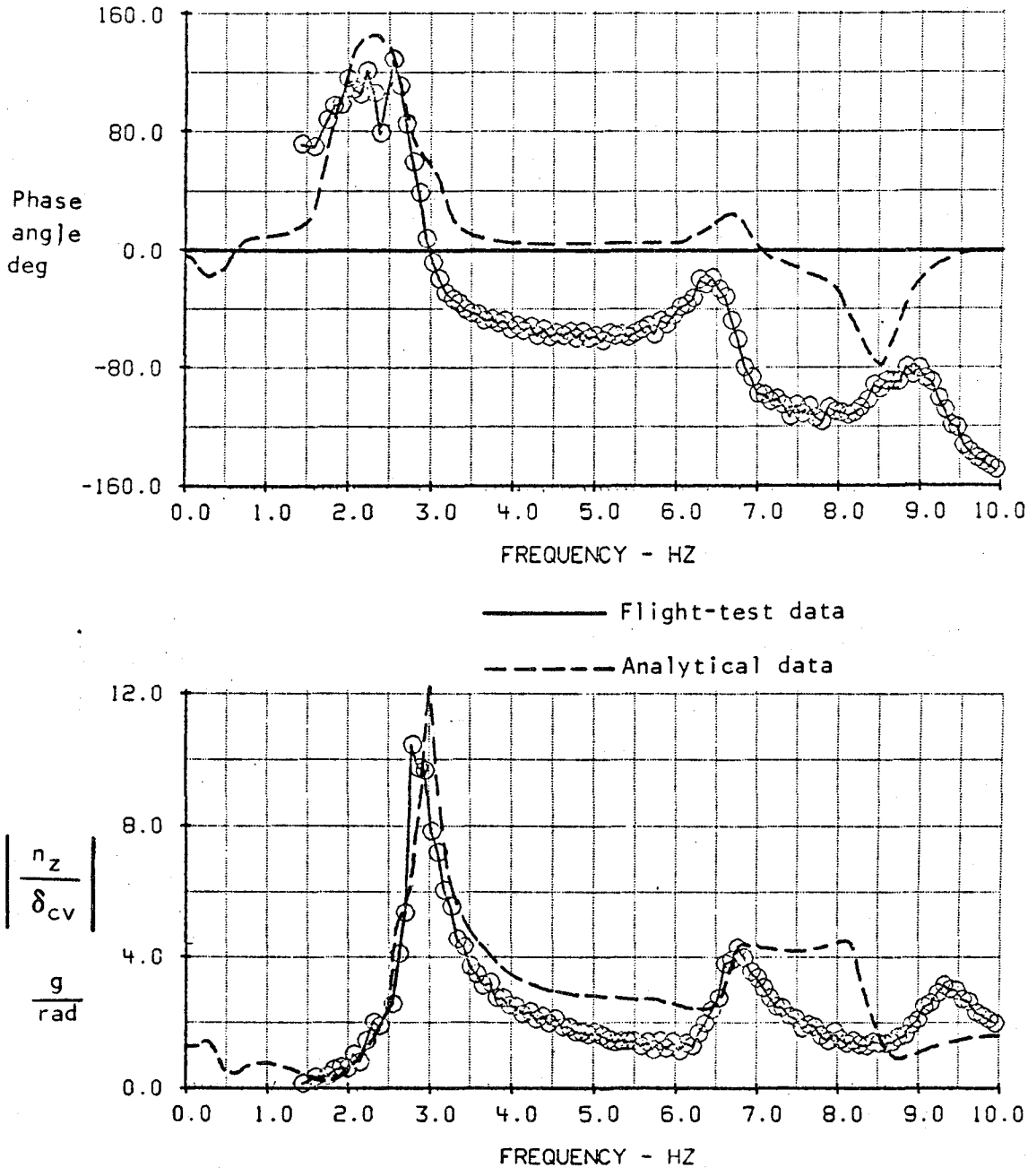

Figure 25. - Comparison of analytical and flight-test results, frequency response of normal load factor at pilot station (FS 746.8 (294)) due to SMCS vane deflection, M = 1.2, h_p = 5,791 m (19,000 ft), Λ = 67.5°, SCAS off, SMCS off.

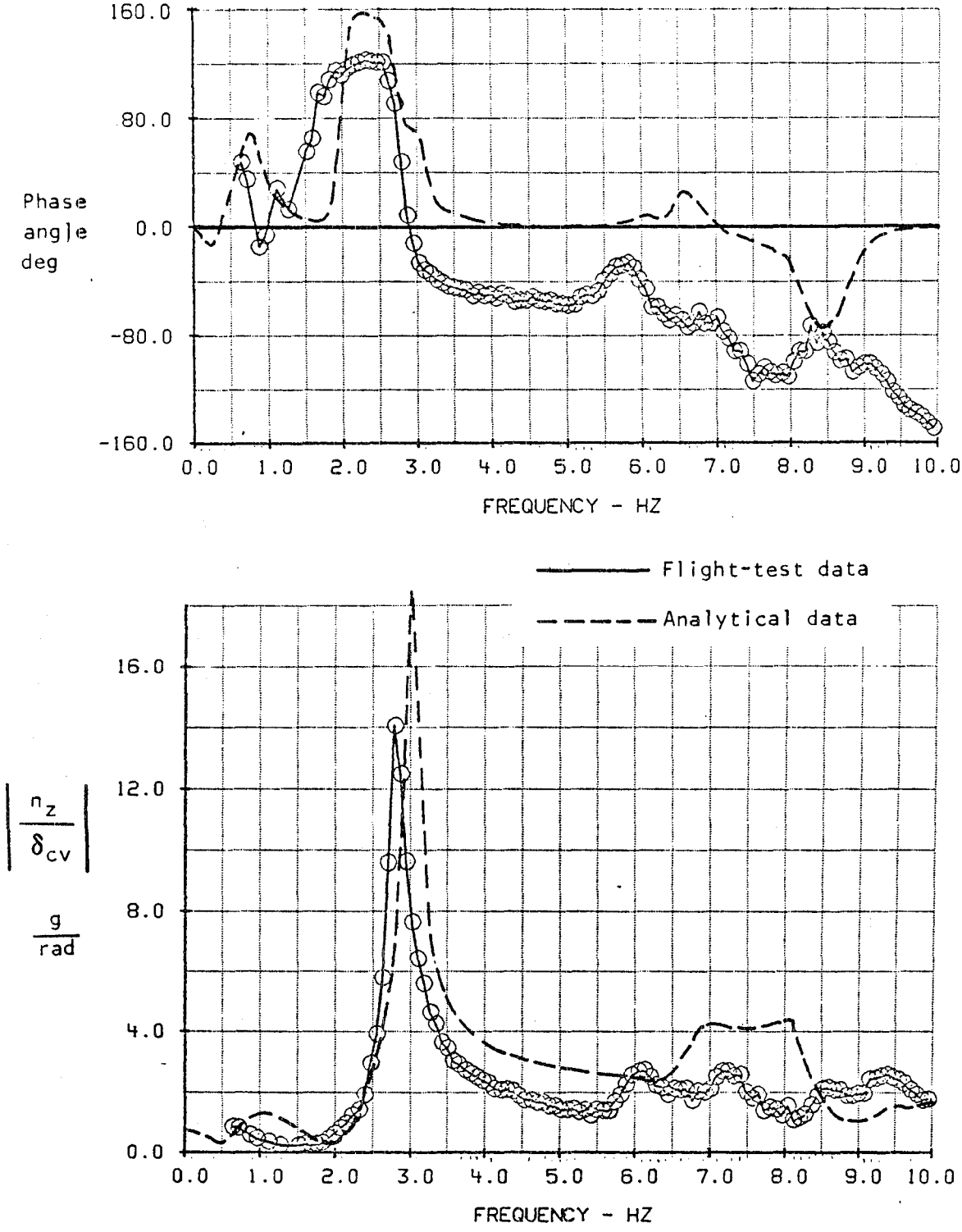

Figure 26. - Comparison of analytical and flight-test results, frequency response of normal load factor at pilot station (FS 746.8 (294)) due to SMCS vane deflection, M = 1.2, h_p = 5,791 m (19,000 ft), Λ = 67.5°, SCAS on, SMCS off.

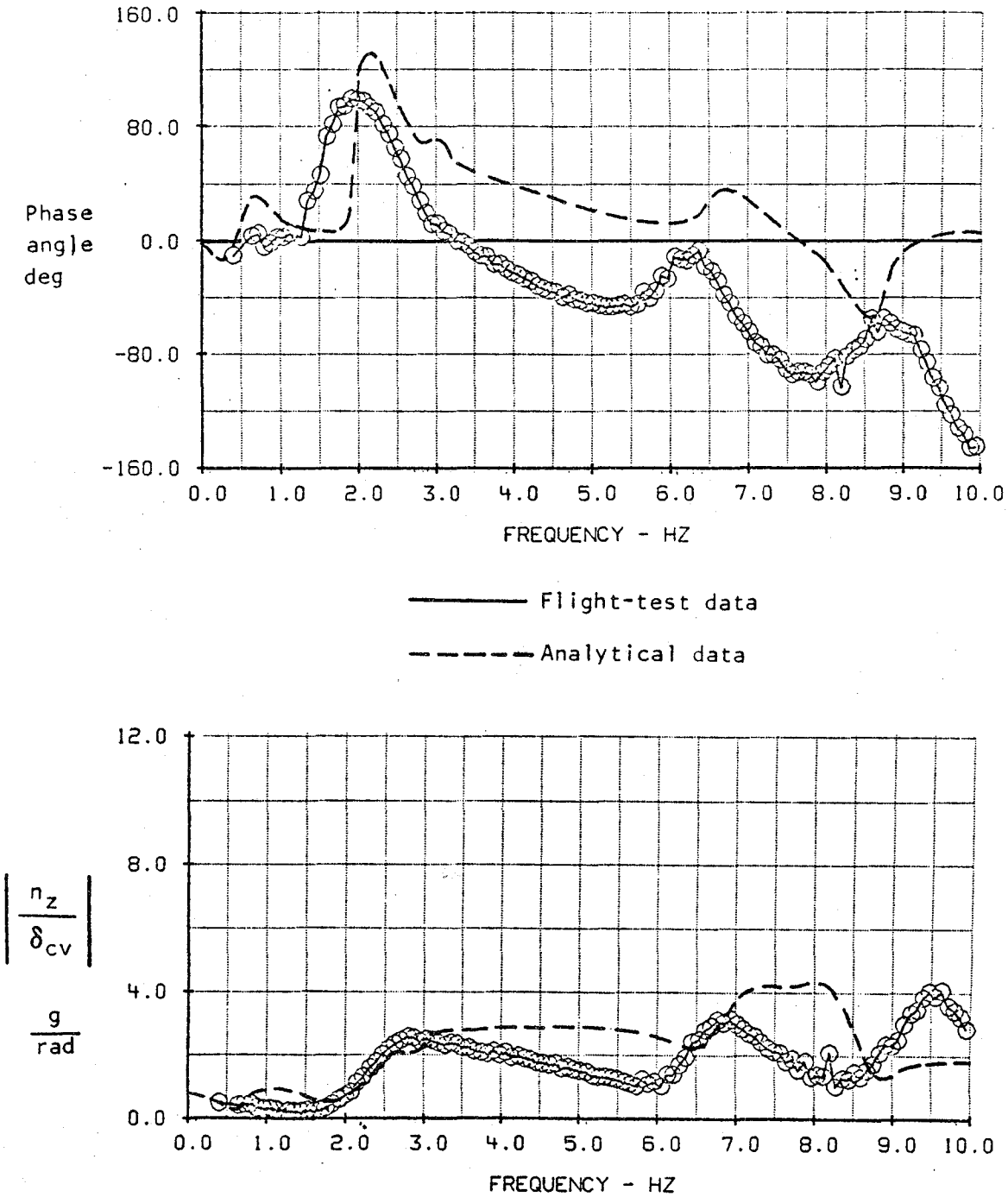

Figure 27. - Comparison of analytical and flight-test results, frequency response of normal load factor at pilot station (FS 746.8 (294)) due to SMCS vane deflection, M = 1.2, h_p = 5,791 m (19,000 ft), Λ = 67.5°, SCAS on, SMCS on.

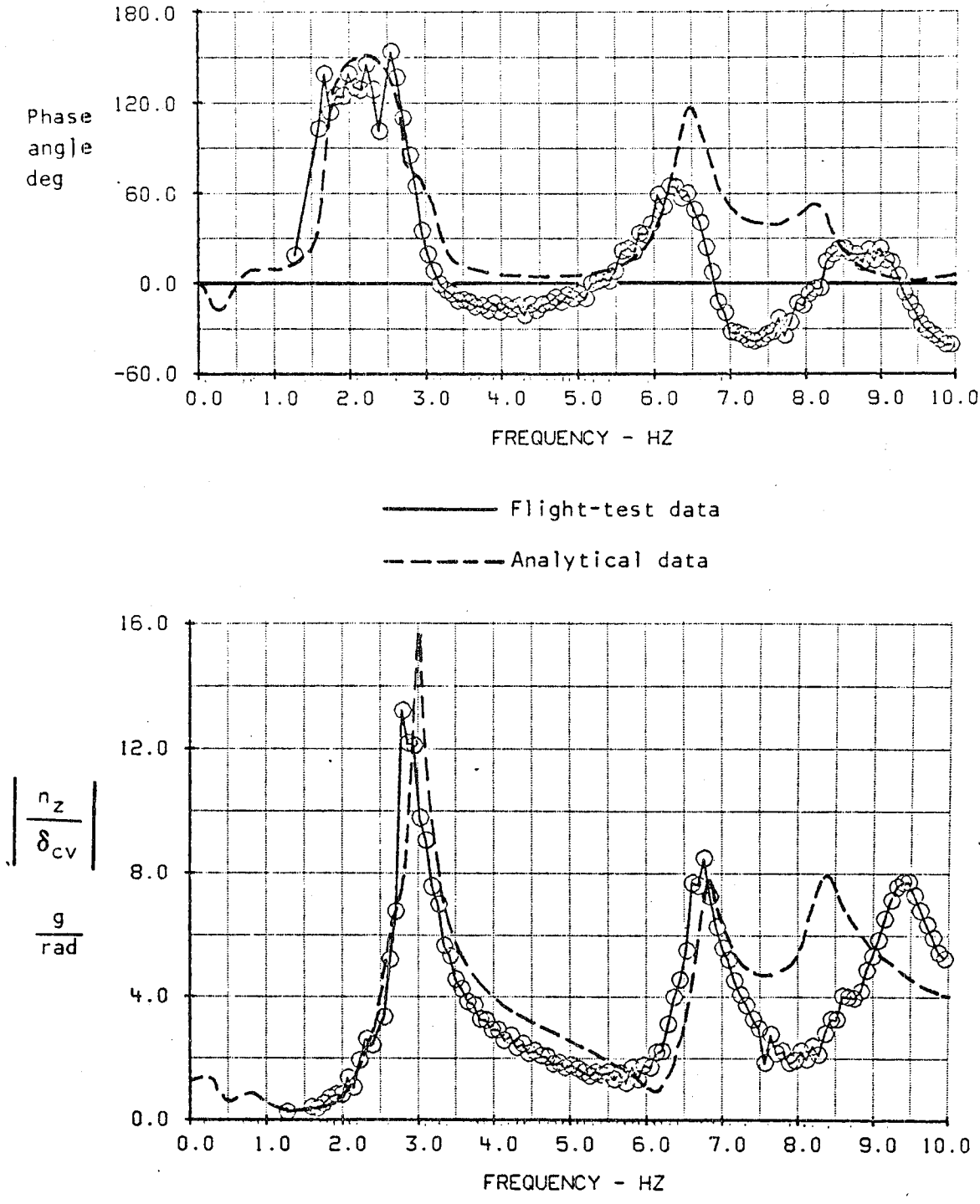

Figure 28. - Comparison of analytical and flight-test results, frequency response of normal load factor at vane station (FS 571.5 (225)) due to SMCS vane deflection, M = 1.2, h_p = 5,791 m (19,000 ft), Λ = 67.5°, SCAS off, SMCS off.

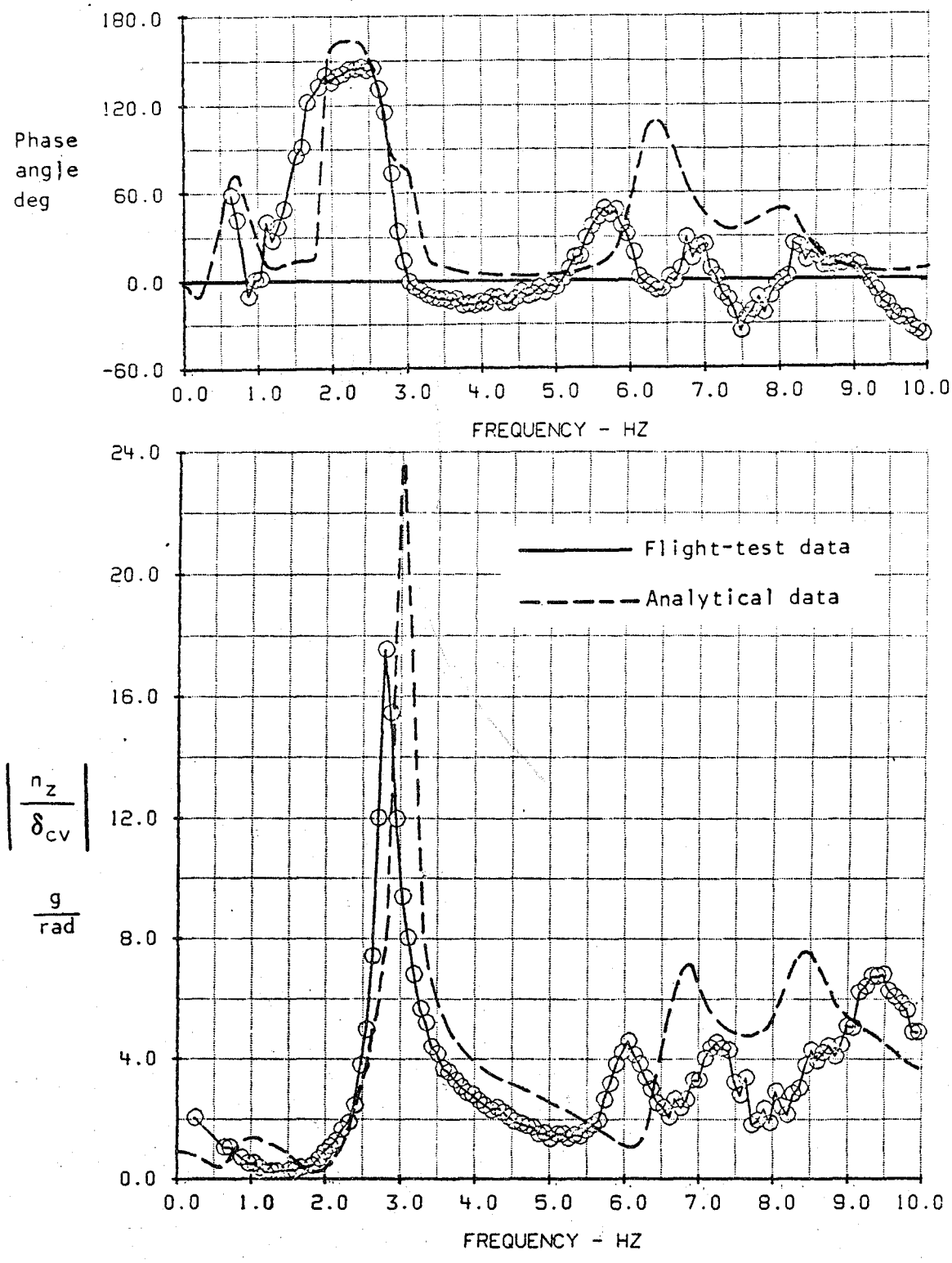

Figure 29. - Comparison of analytical and flight-test results, frequency response of normal load factor at vane station (FS 571.5 (225)) due to SMCS vane deflection, M = 1.2, h_p = 5,791 m (19,000 ft), Λ = 67.5°, SCAS on, SMCS off.

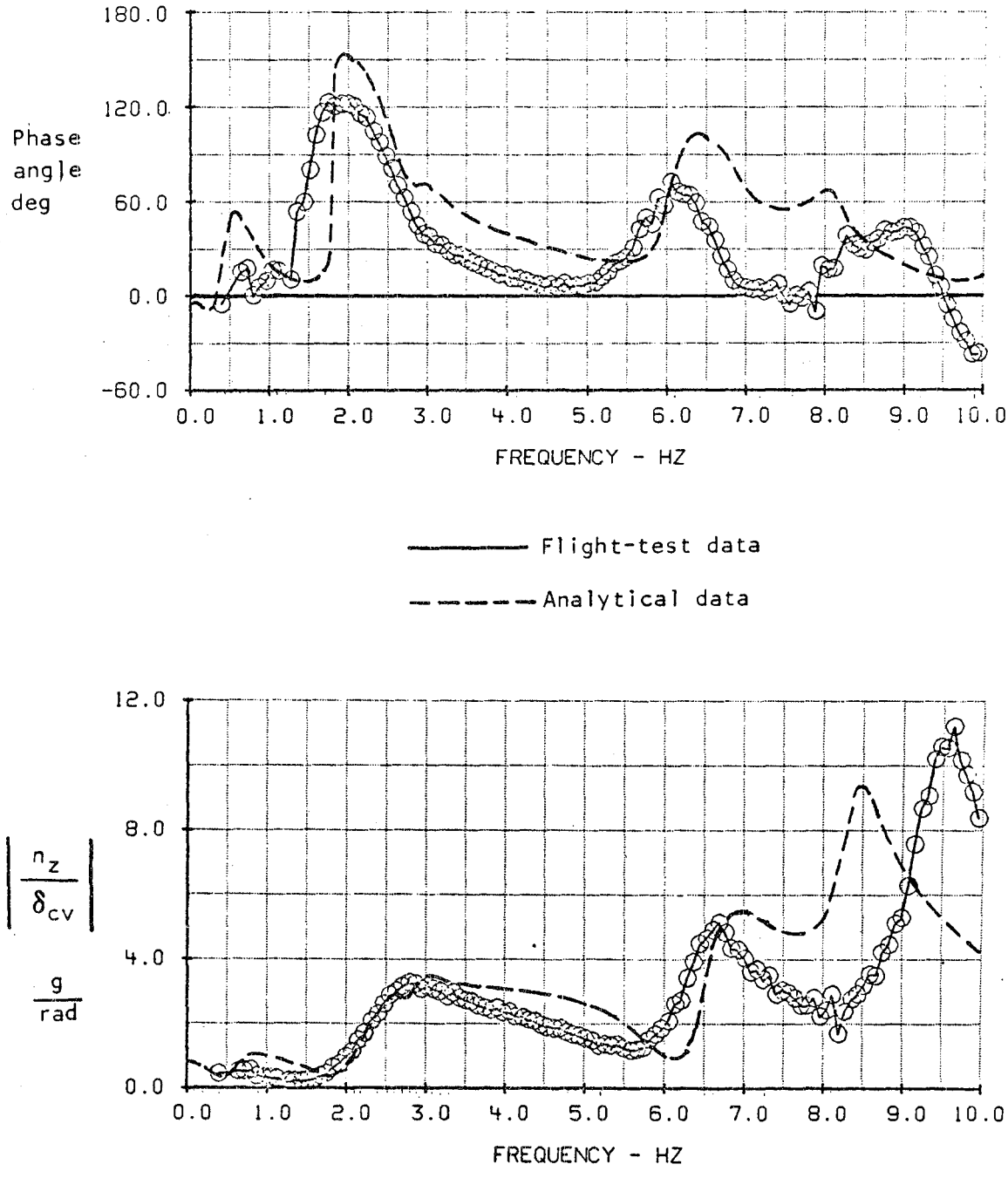

Figure 30. - Comparison of analytical and flight-test results, frequency response of normal load factor at vane station (FS 571.5 (225)) due to SMCS vane deflection, M = 1.2, h_p = 5,791 m (19,000 ft), Λ = 67.5°, SCAS on, SMCS on.

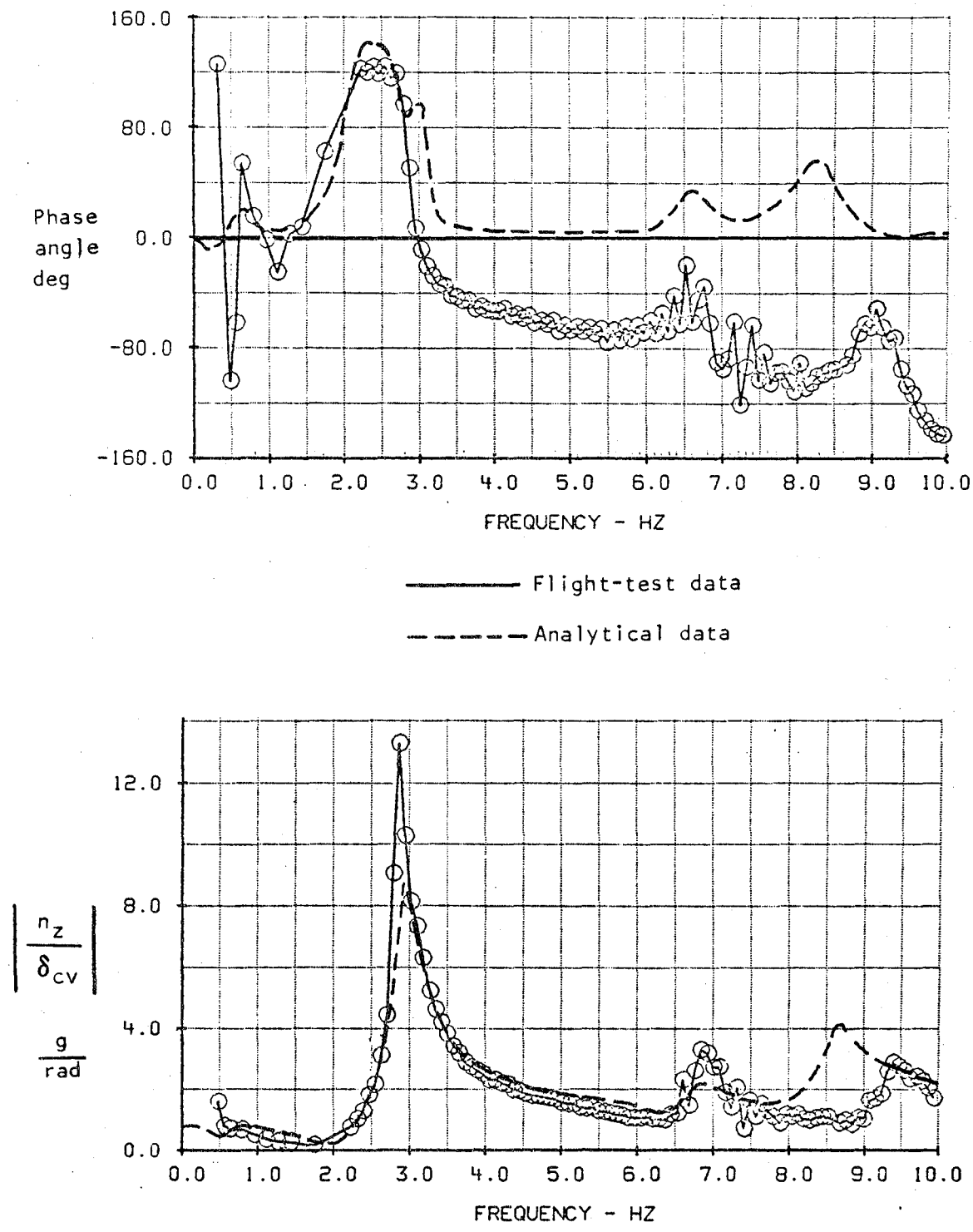

Figure 31. - Comparison of analytical and flight-test results, frequency response of normal load factor at pilot station (FS 746.8 (294)) due to SMCS vane deflection, M = 1.6, h_p = 9,449 m (31,000 ft), Λ = 67.5°, SCAS off, SMCS off.

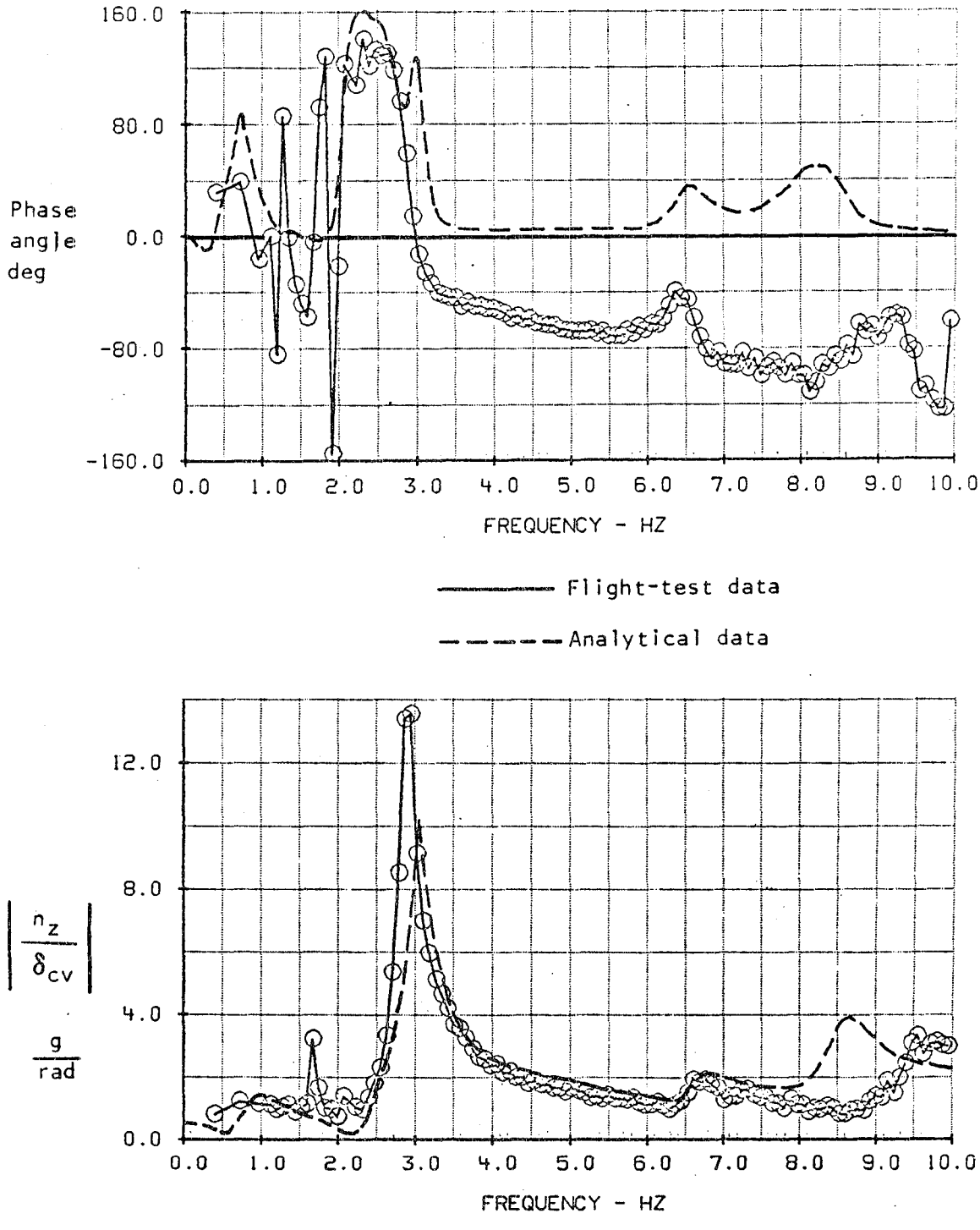

Figure 32. - Comparison of analytical and flight-test results, frequency response of normal load factor at pilot station (FS 746.8 (294)) due to SMCS vane deflection, M = 1.6, h_p = 9,449 m (31,000 ft), Λ = 67.5°, SCAS on, SMCS off.

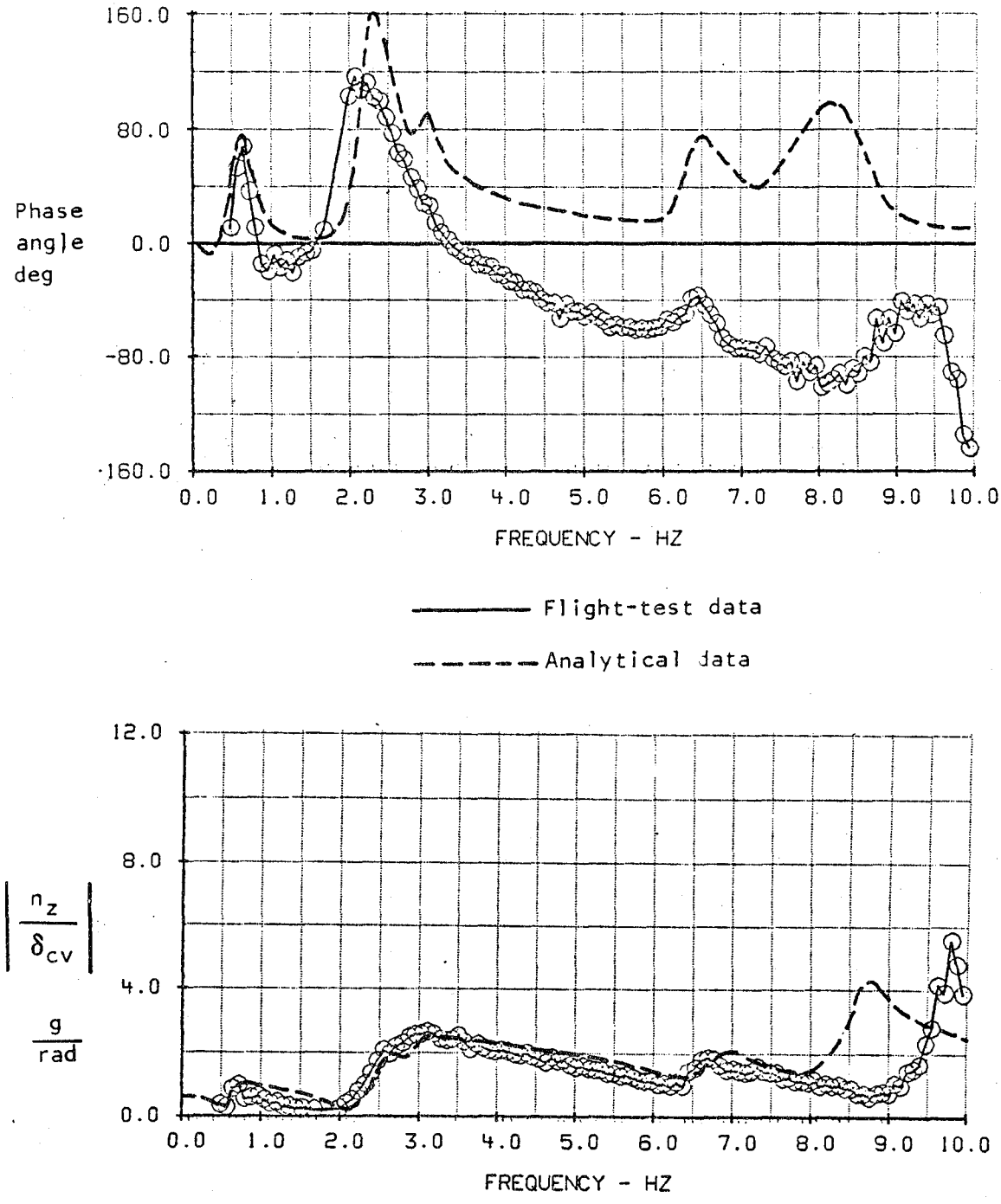

Figure 33. - Comparison of analytical and flight-test results, frequency response of normal load factor at pilot station (FS 746.8 (294)) due to SMCS vane deflection, M = 1.6, h_p = 9,449 m (31,000 ft), Λ = 67.5°, SCAS on, SMCS on.

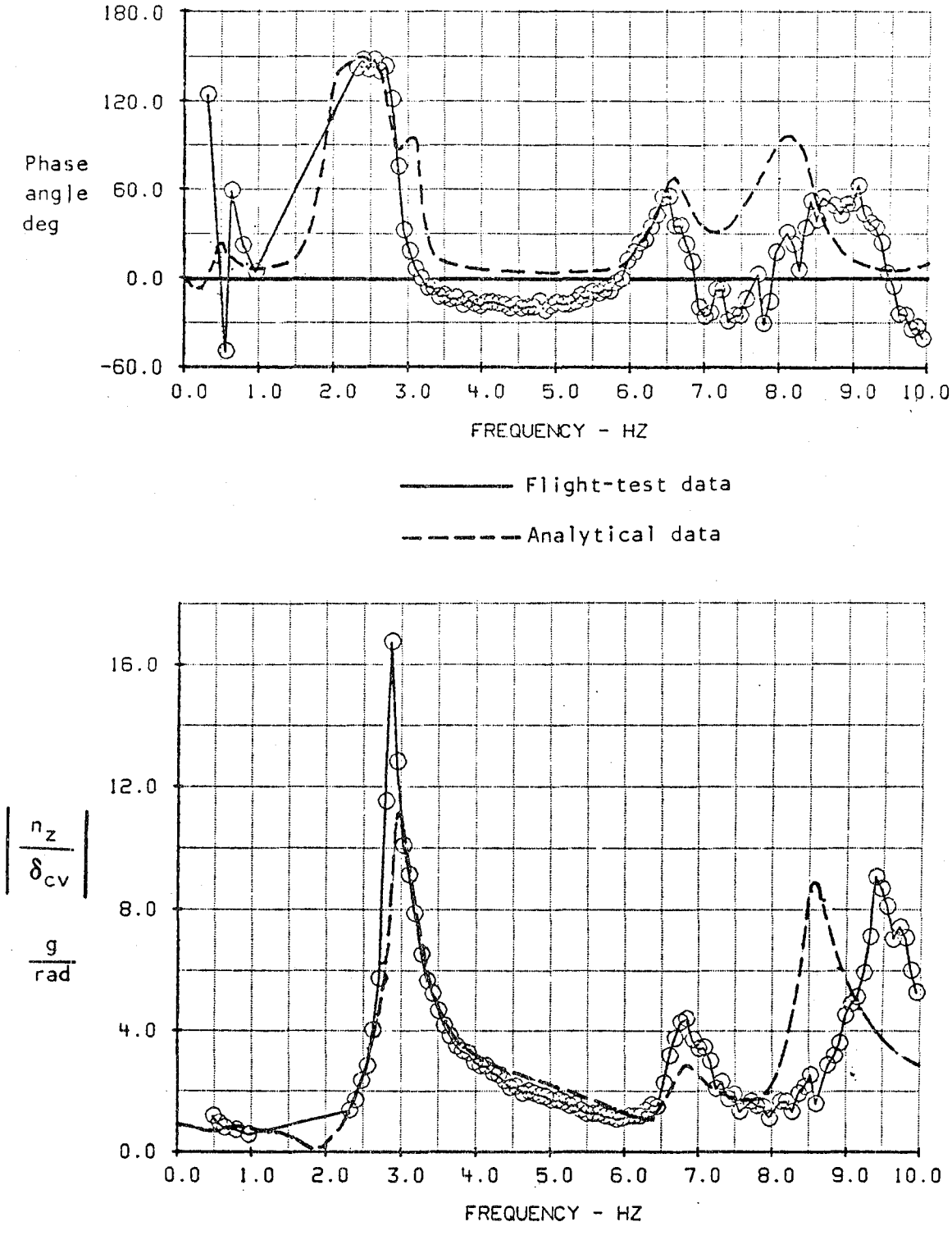

Figure 34. - Comparison of analytical and flight-test results, frequency response of normal load factor at vane station (FS 571.5 (225)) due to SMCS vane deflection, M = 1.6, h_p = 9,449 m (31,000 ft), Λ = 67.5°, SCAS off, SMCS off.

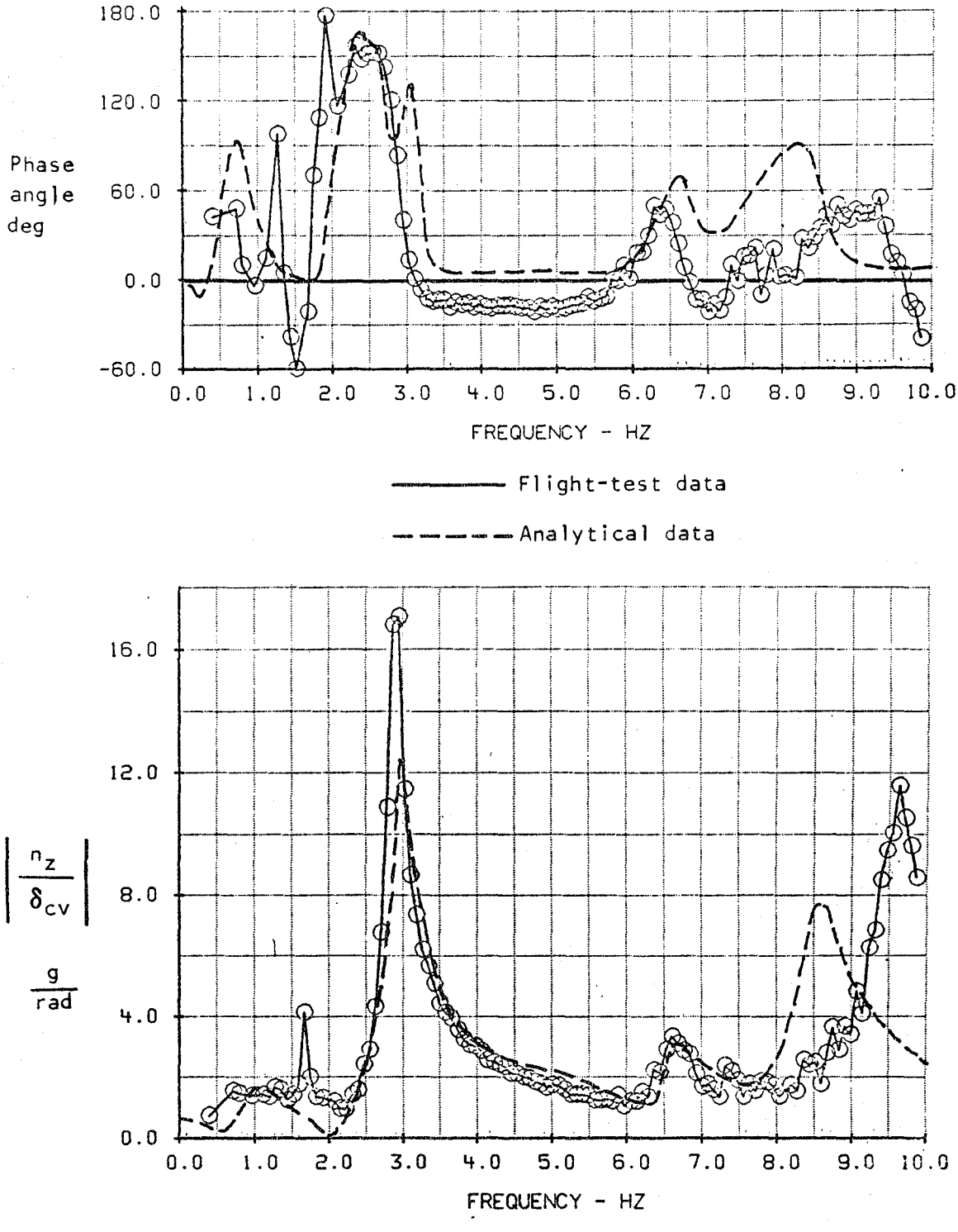

Figure 35. - Comparison of analytical and flight-test results, frequency response of normal load factor at vane station (FS 571.5 (225)) due to SMCS vane deflection, M = 1.6, h_p 9,449 m (31,000 ft), Λ = 67.5°, SCAS on, SMCS off.

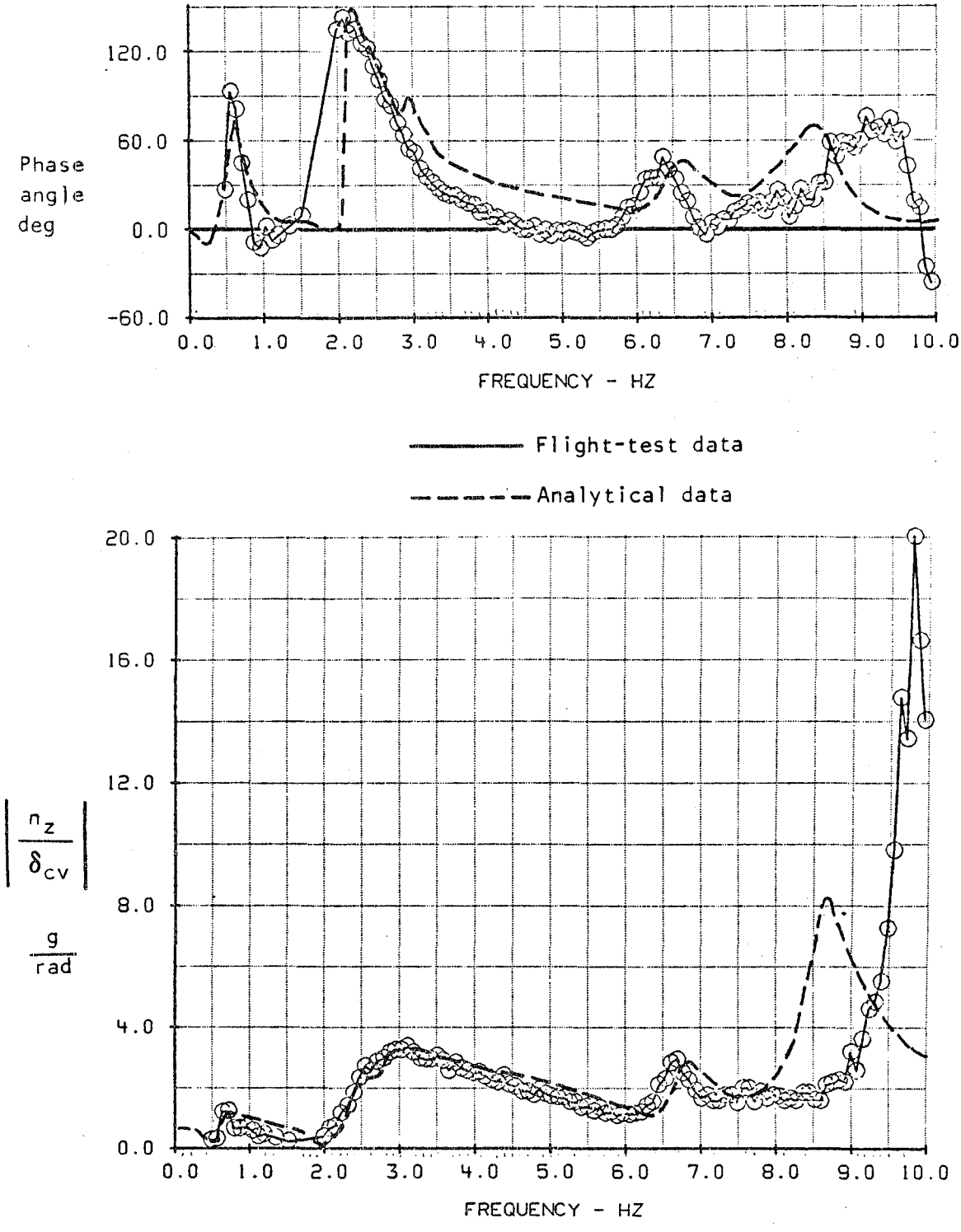

Figure 36. - Comparison of analytical and flight-test results, frequency response of normal load factor at vane station (FS 571.5 (225)) due to SMCS vane deflection, M = 1.6, h_p = 9,449 m (31,000 ft), Λ = 67.5°, SCAS on, SMCS on.

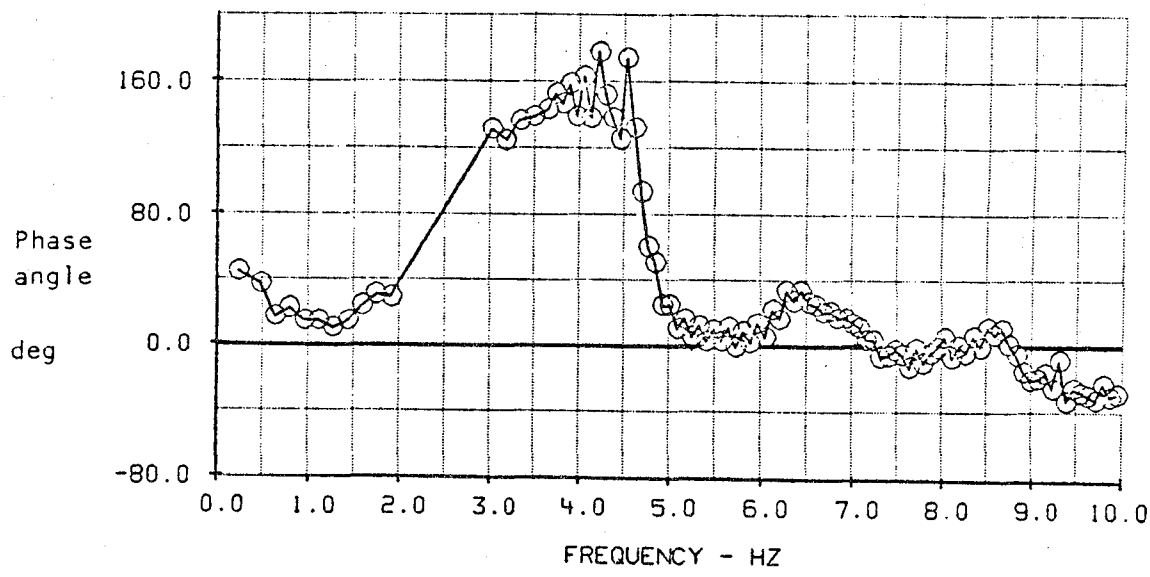

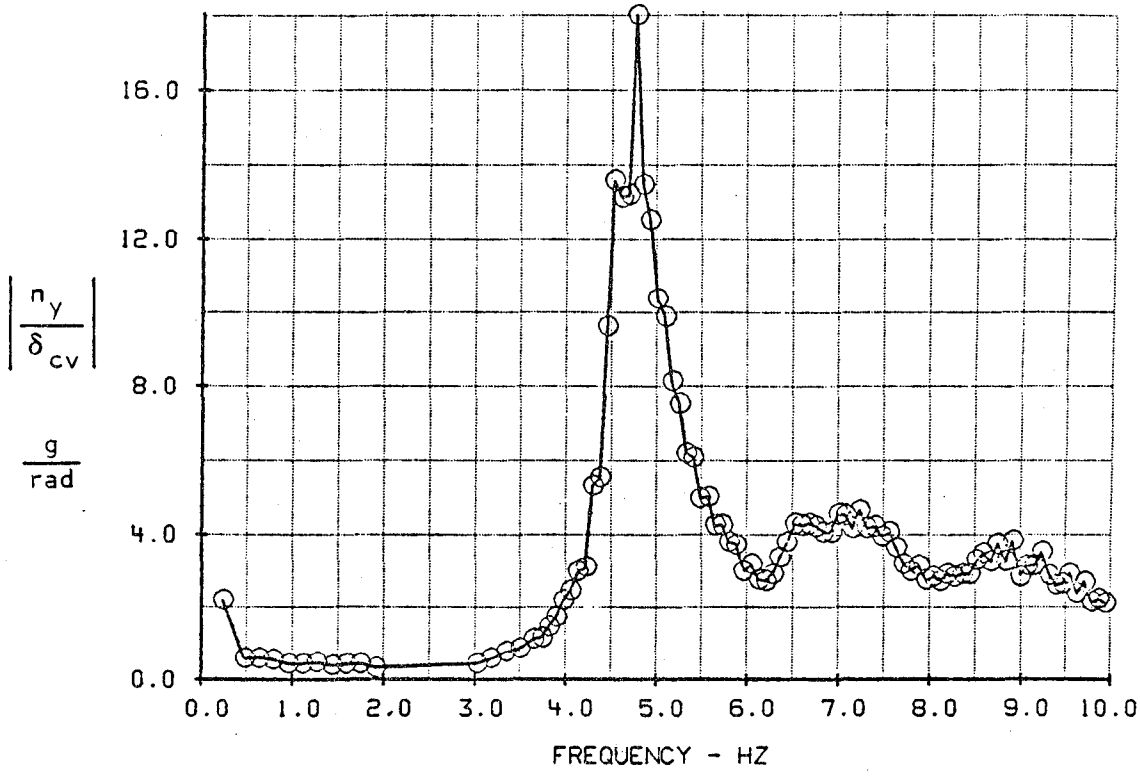

Figure 37. - Flight-test results, frequency response of lateral load factor at pilot station (FS 746.8 (294)) due to SMCS vane deflection, M = 1.2, h_p = 579 m (19,000 ft), Λ = 67.5°, SCAS off, SMCS off.

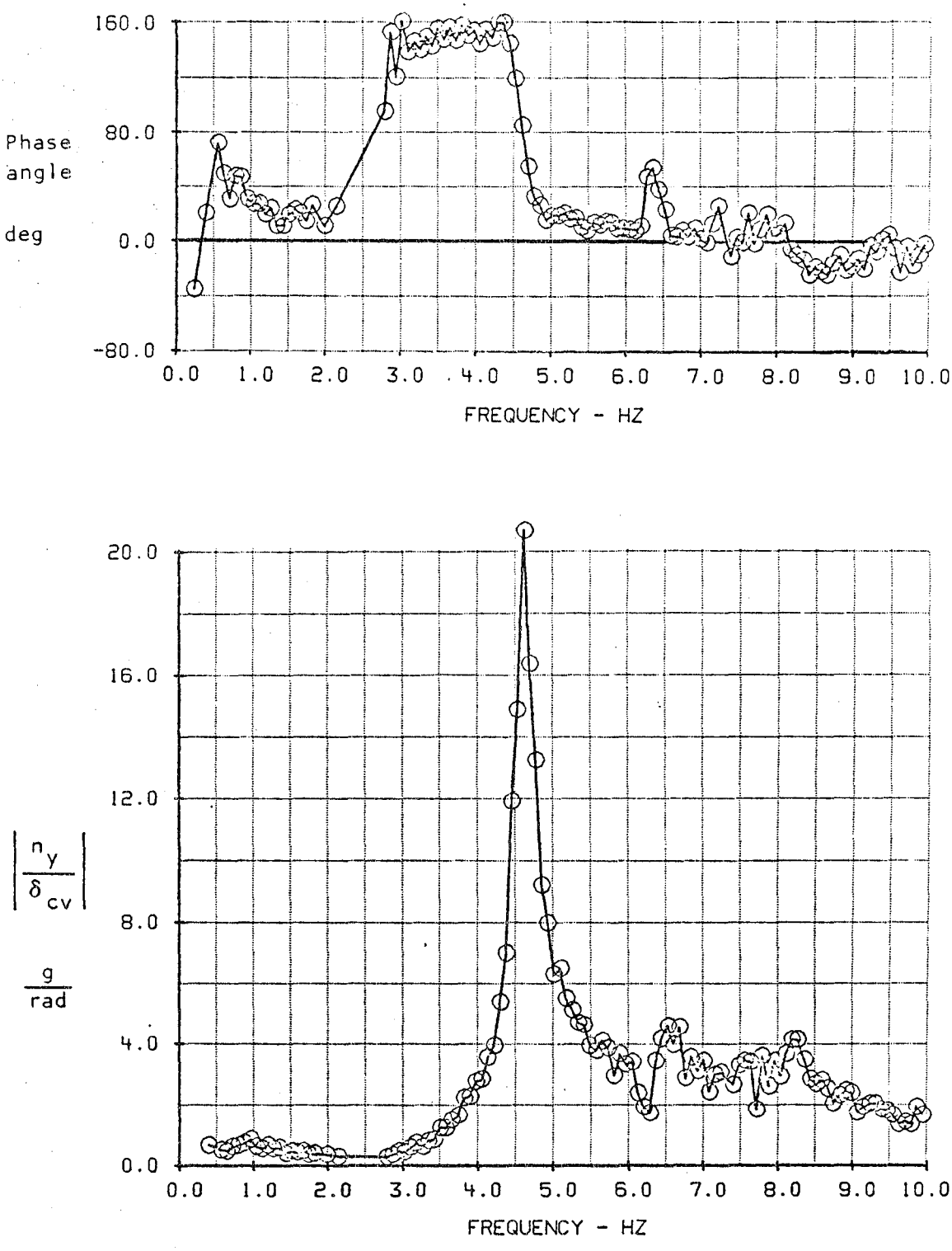

Figure 38. - Flight-test results, frequency response of lateral load factor at pilot station (FS 746.8 (294)) due to SMCS vane deflection, M = 1.2, h_p = 579 m (19,000 ft), Λ = 67.5°, SCAS on, SMCS off.

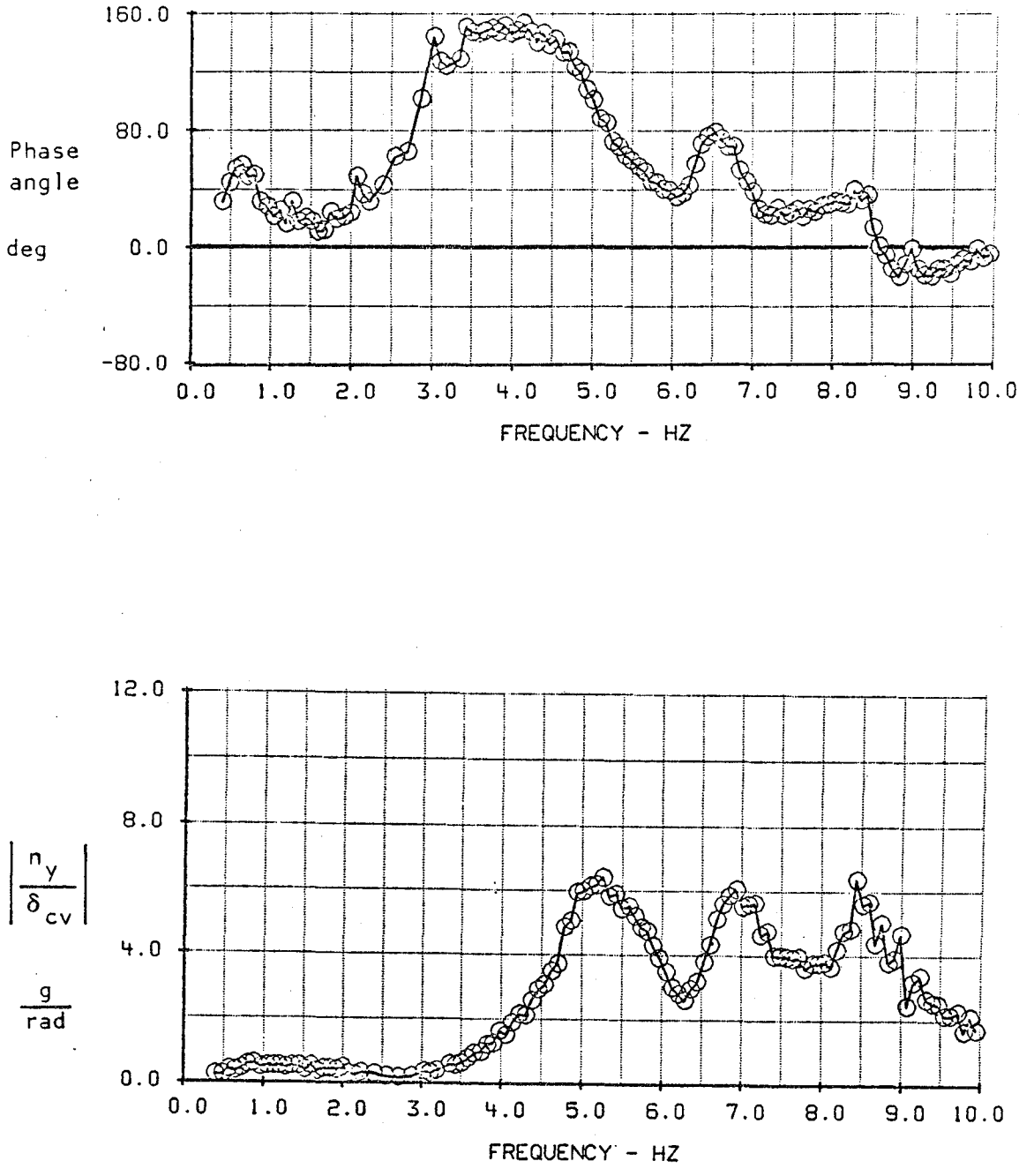

Figure 39. - Flight-test results, frequency response of lateral load factor at pilot station (FS 746.8 (294)) due to SMCS vane deflection, M = 1.2, h_p = 579 m (19,000 ft), Λ = 67.5°, SCAS on, SMCS on.

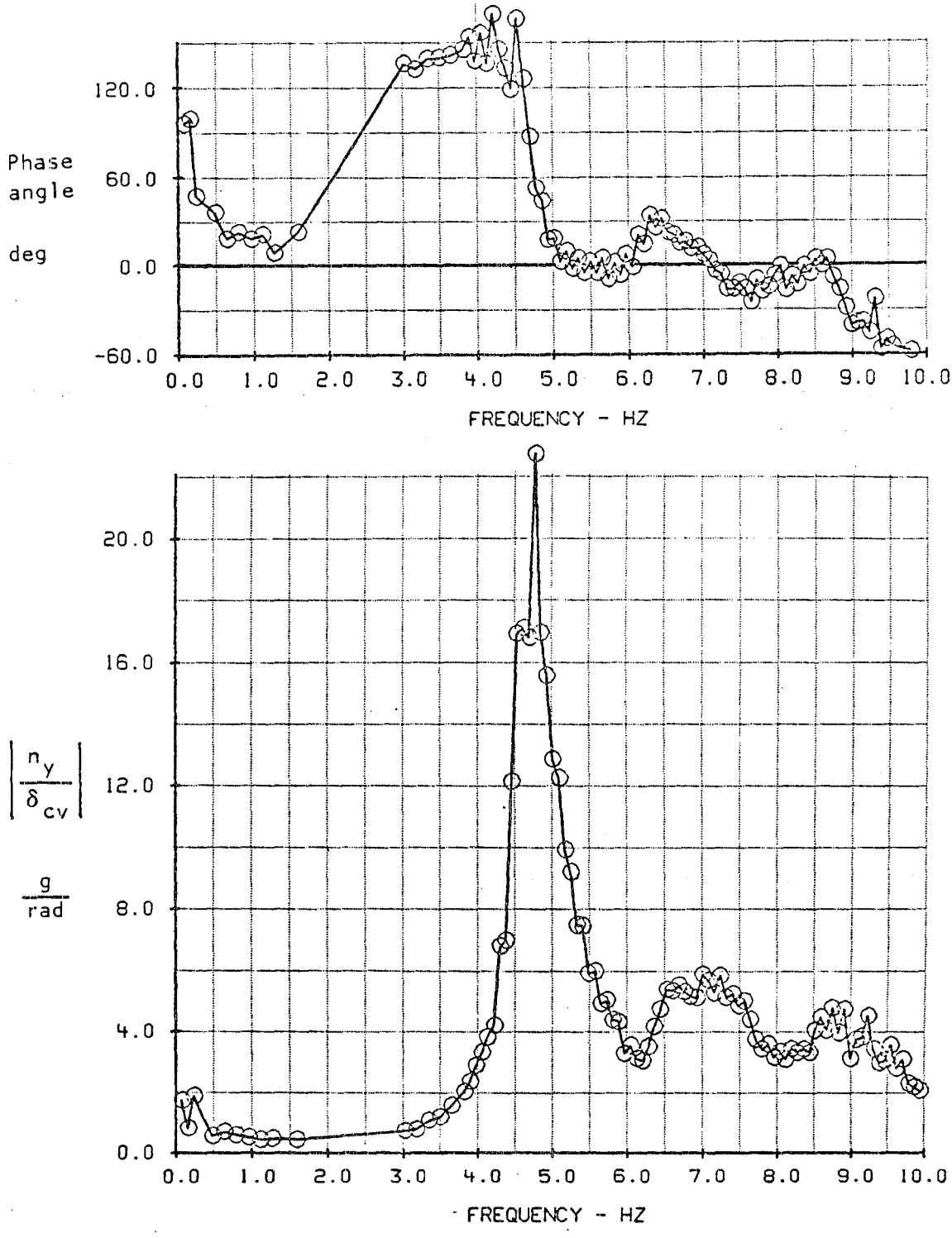

Figure 40. - Flight-test results, frequency response of lateral load factor at vane station (FS 571.5 (225)) due to SMCS vane deflection, M = 1.2, h_p = 5,791 m (19,000 ft), Λ = 67.5°, SCAS off, SMCS off.

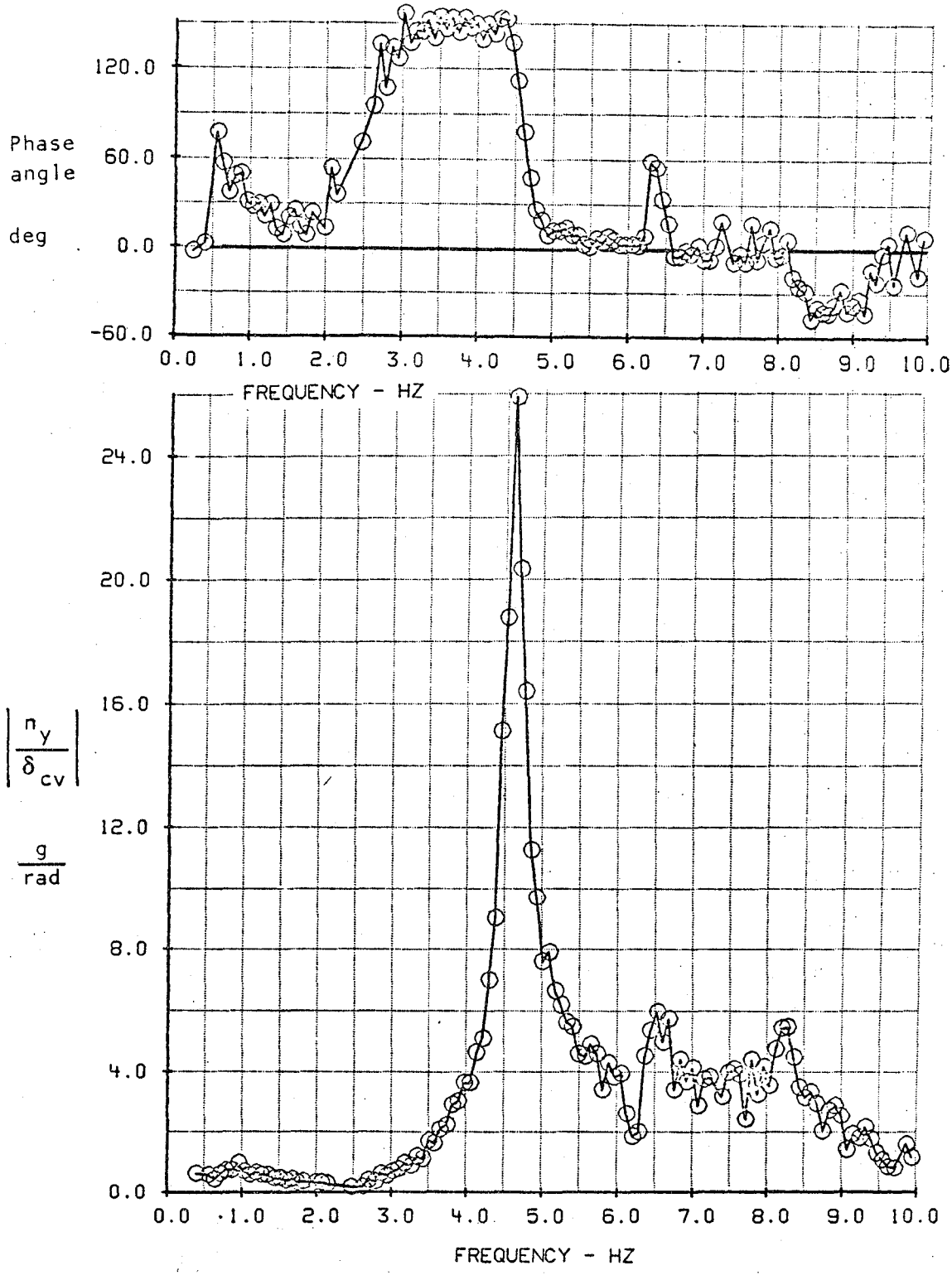

Figure 41. - Flight-test results, frequency response of lateral load factor at vane station (FS 571.5 (225)) due to SMCS vane deflection, M = 1.2, h_p = 5,791 m (19,000 ft), Λ = 67.5°, SCAS on, SMCS off.

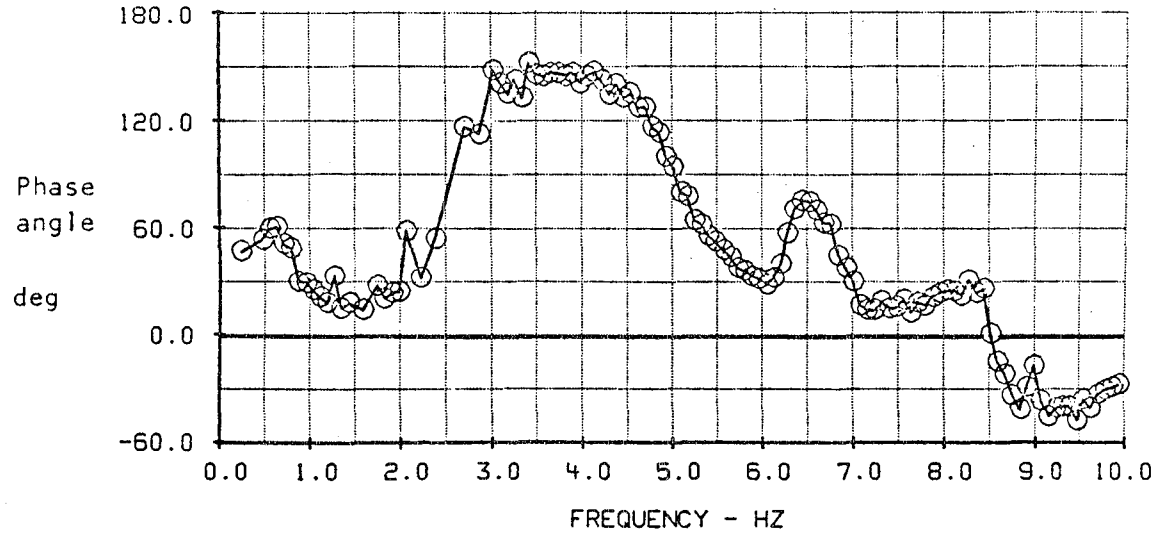

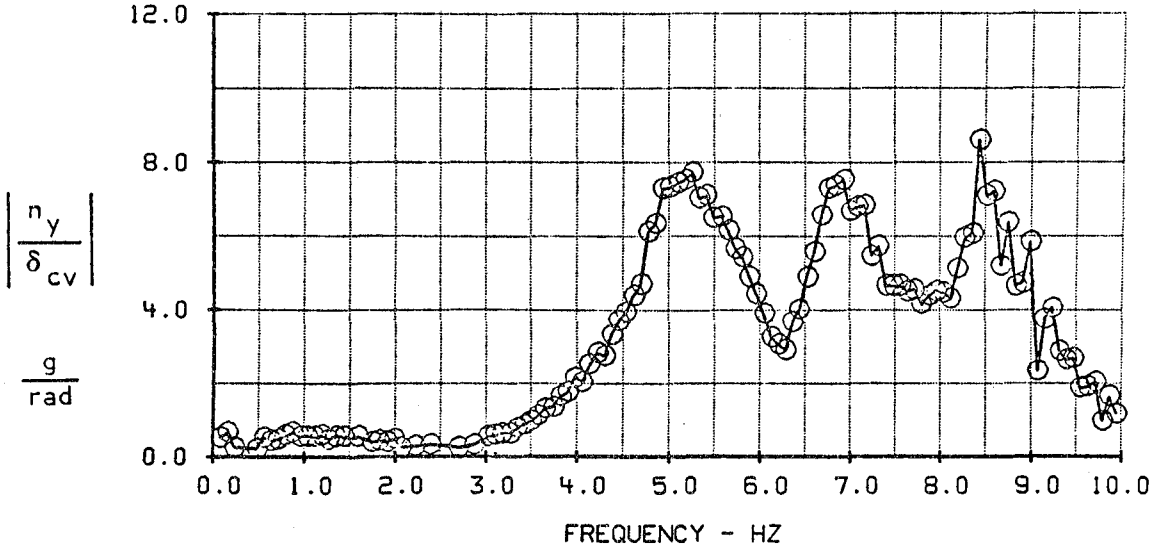

Figure 42. - Flight-test results, frequency response of lateral load factor at vane station (FS 571.5 (225)) due to SMCS vane deflection, M = 1.2, h_p = 5,791 m (19,000 ft), Λ = 67.5°, SCAS on, SMCS on.

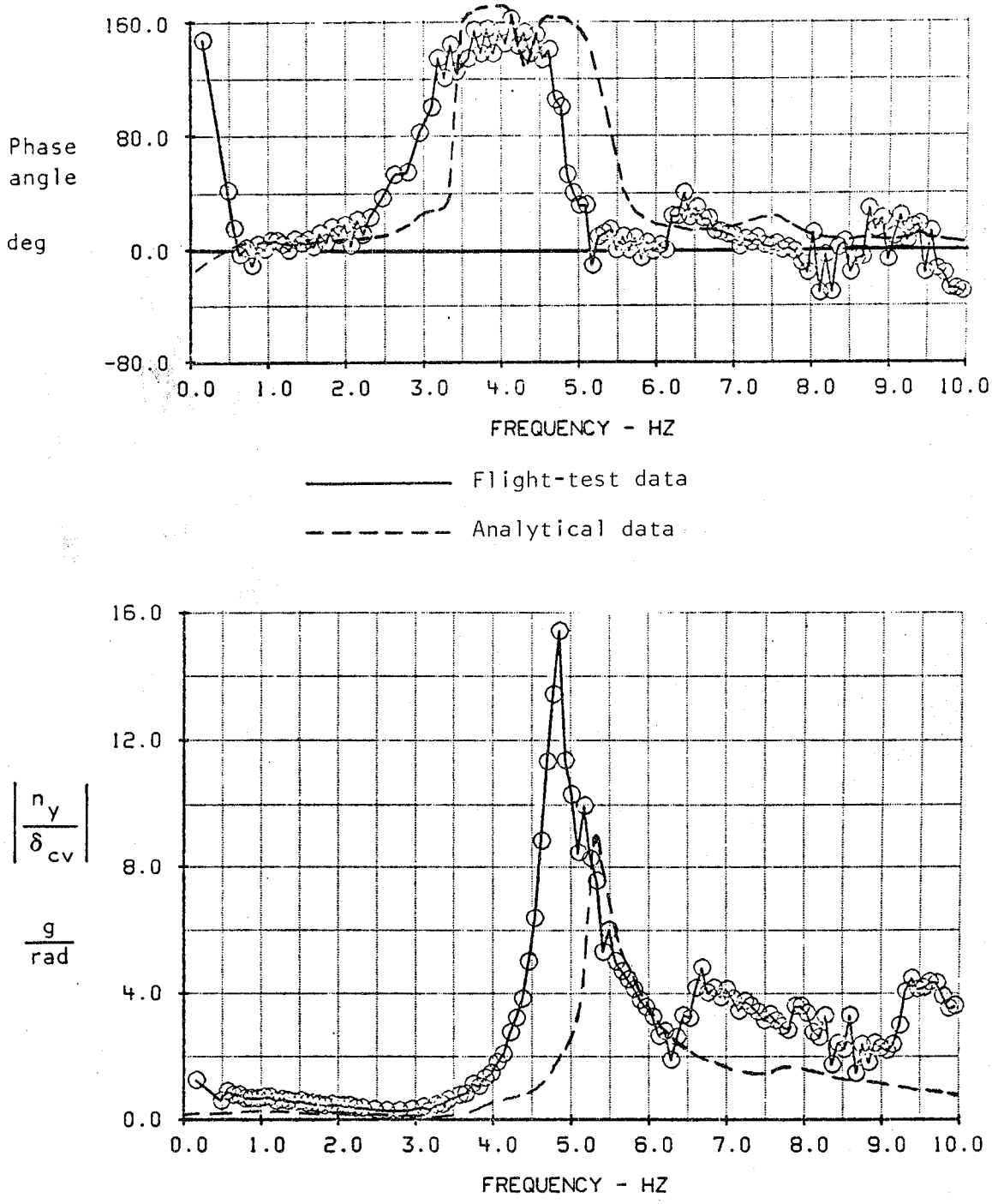

Figure 43. - Comparison of analytical and flight-test results, frequency response of lateral load factor at pilot station (FS 746.8 (294)) due to SMCS vane deflection, M = 1.6, h_p = 9,449 m (31,000 ft), Λ = 67.5°, SCAS off, SMCS off.

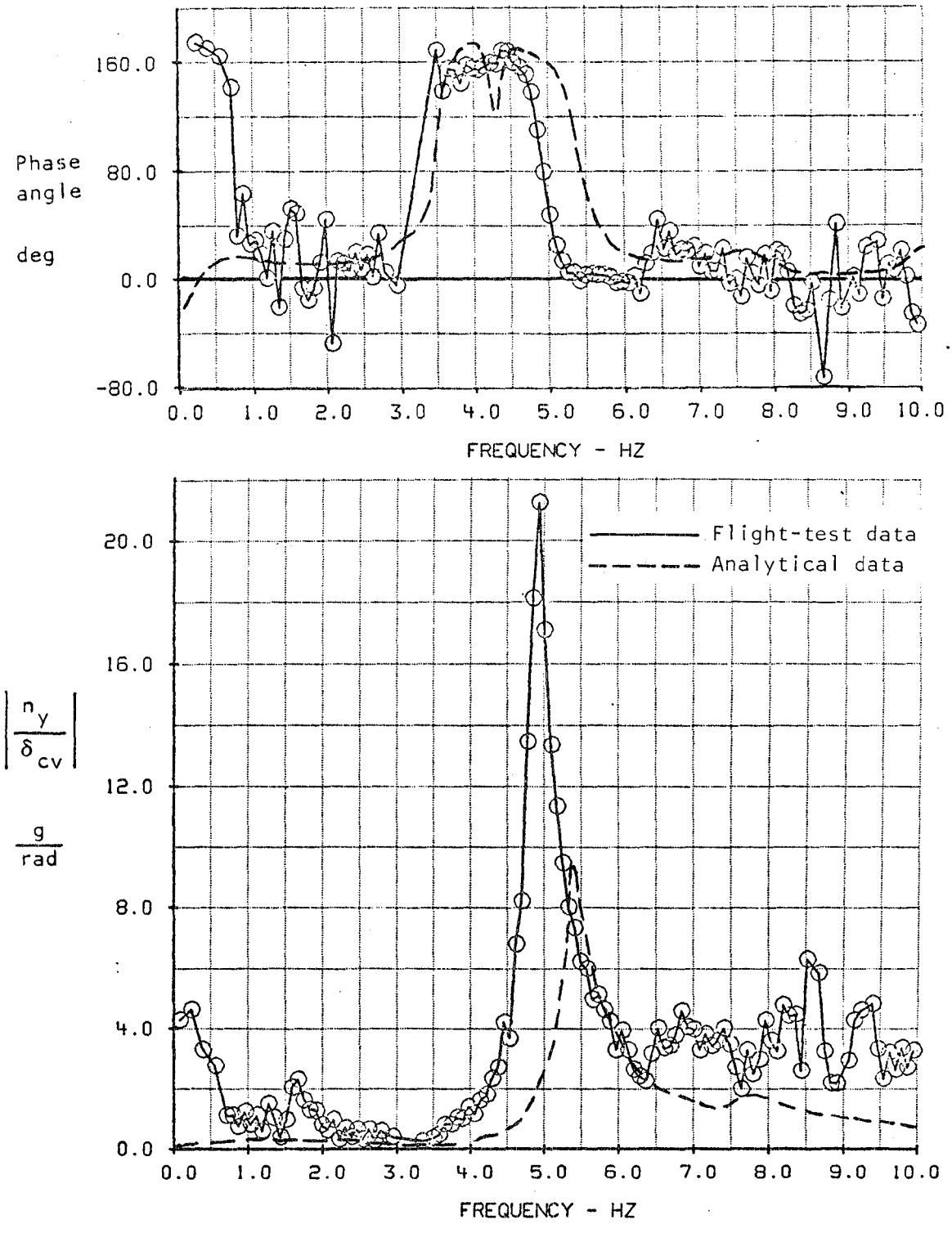

Figure 44. - Comparison of analytical and flight-test results, frequency response of lateral load factor at pilot station (FS 746.8 (294)) due to SMCS vane deflection, M = 1.6, h_p = 9,449 m (31,000 ft), Λ = 67.5°, SCAS on, SMCS off.

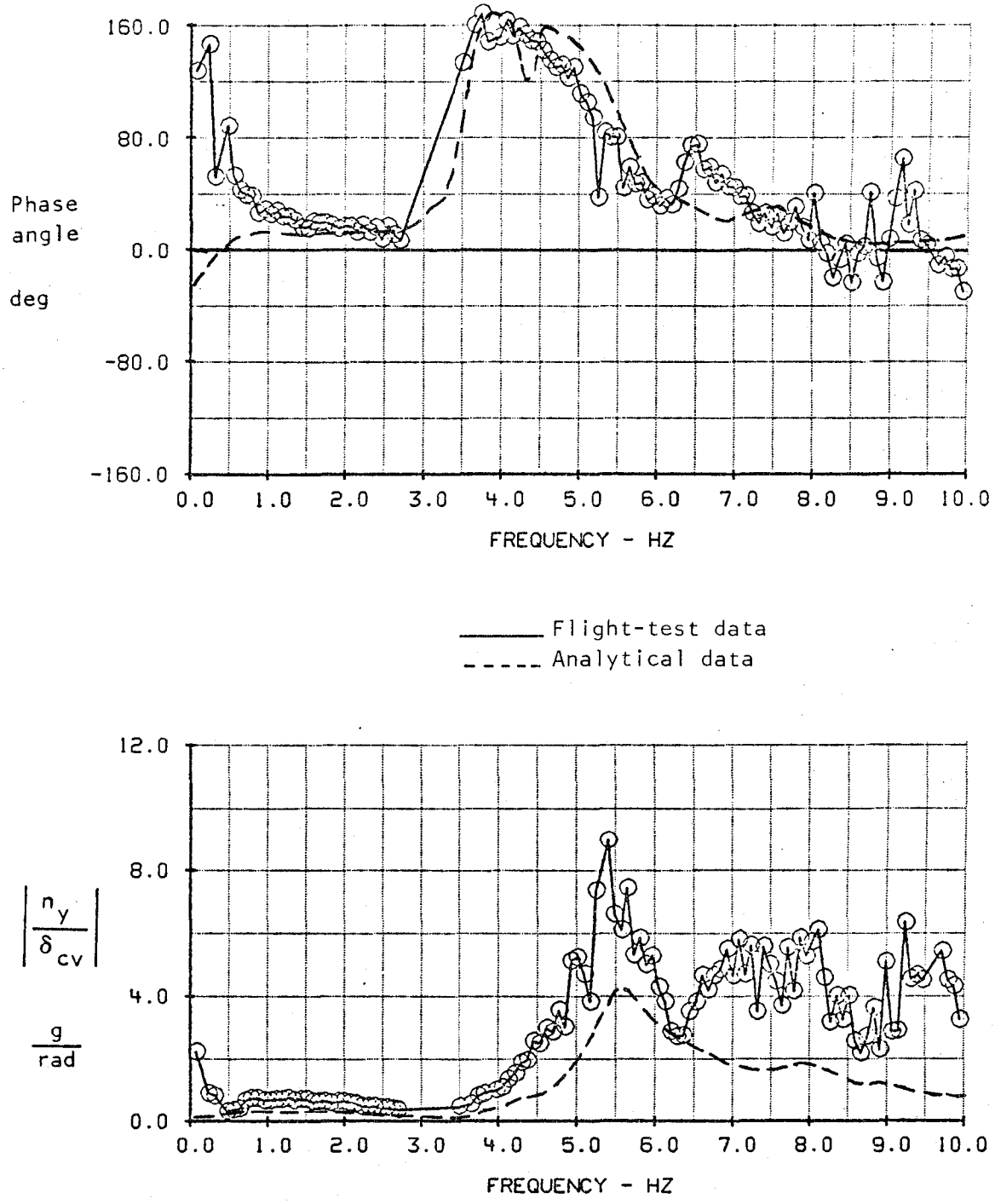

Figure 45. - Comparison of Analytical and flight-test results, frequency response of lateral load factor at pilot station (FS 746.8 (294)) due to SMCS vane deflection, M = 1.6, h_p = 9,449 m (31,000 ft), Λ = 67.5°, SCAS on, SMCS on.

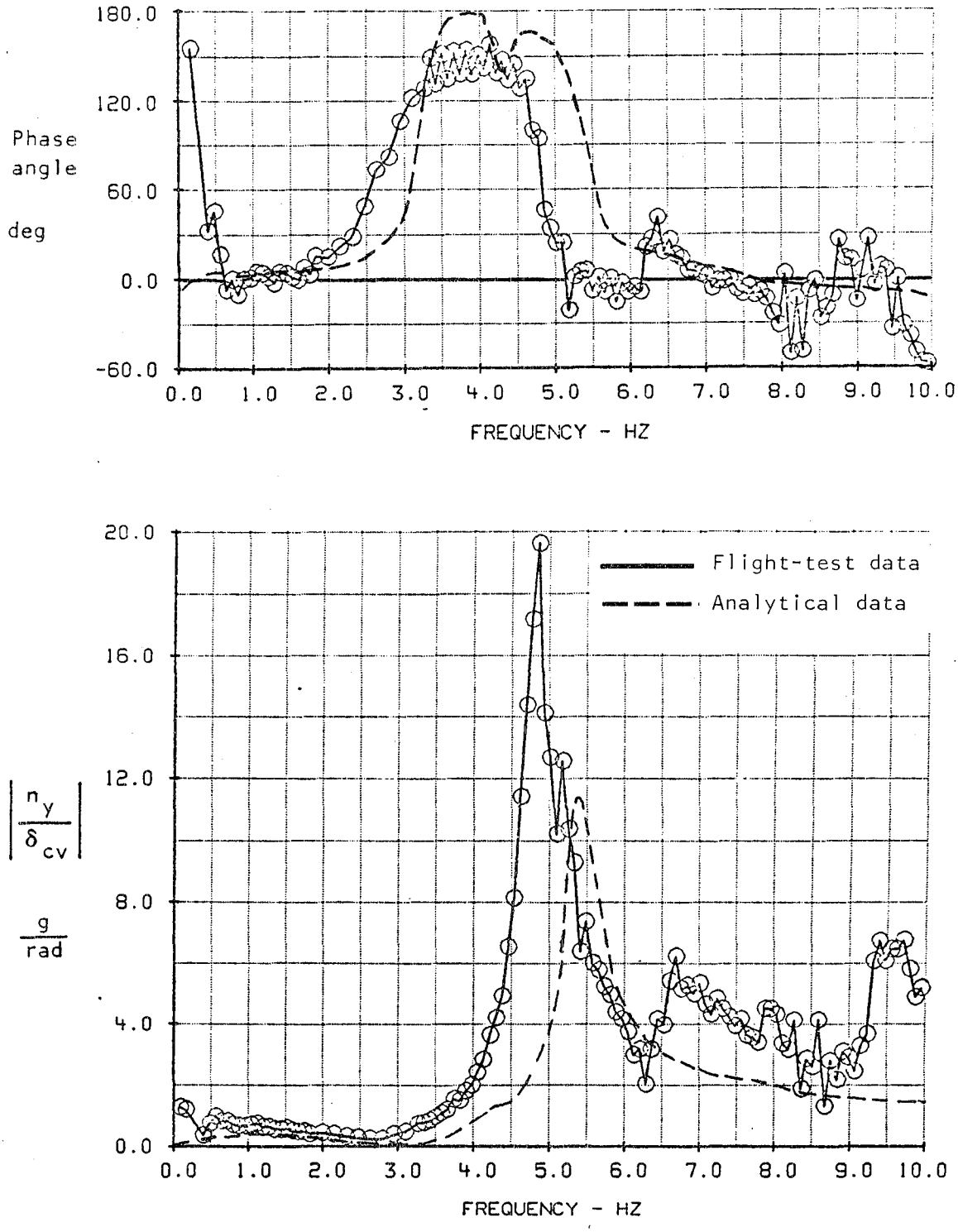

Figure 46. - Comparison of analytical and flight-test results, frequency response of lateral load factor at vane station (FS 571.5 (225)) due to SMCS vane deflection, M = 1.6, h_p = 9,449 m (31,000 ft), A = 67.5°, SCAS off, SMCS off.

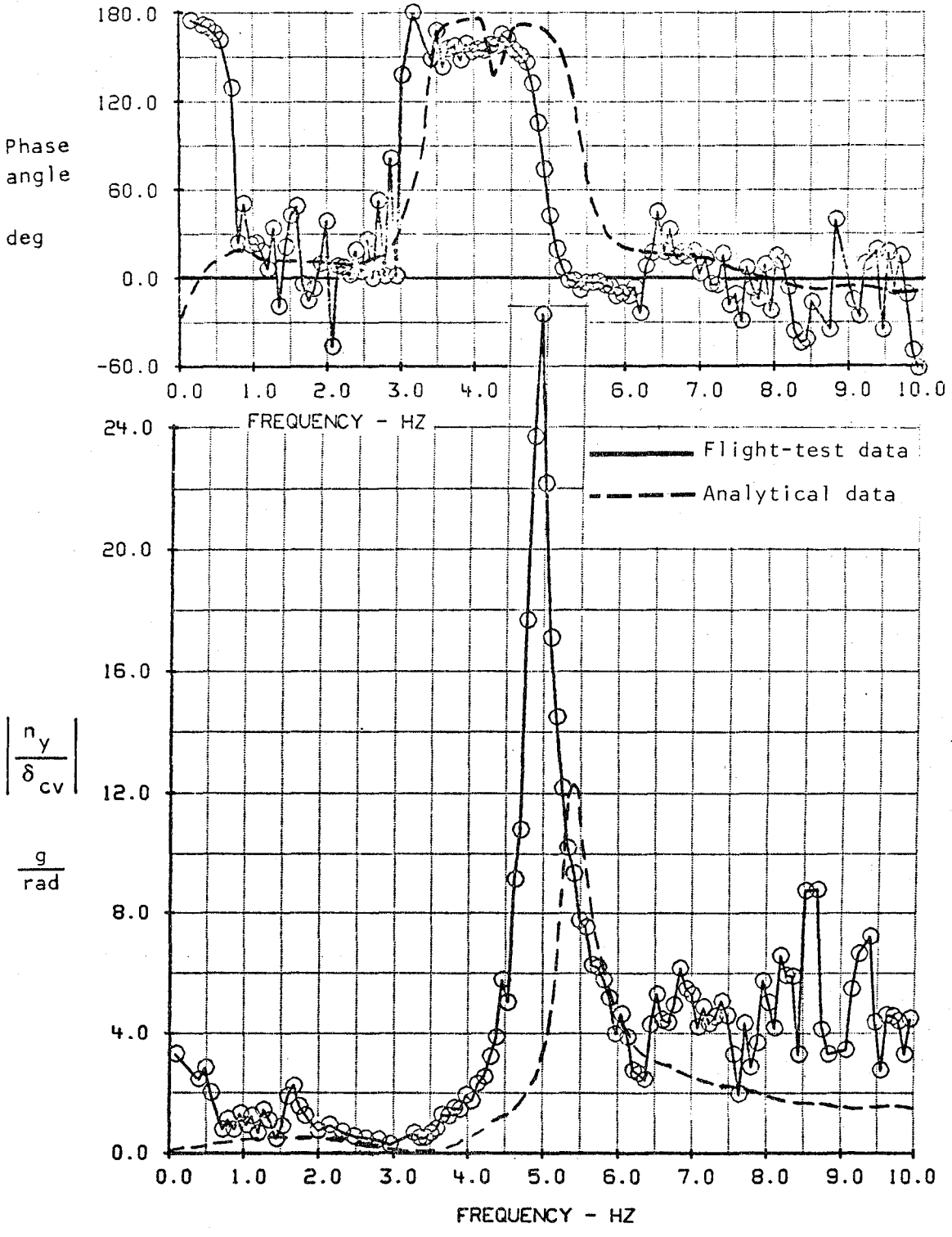

Figure 47. - Comparison of analytical and flight-test results, frequency response of lateral load factor at vane station (FS 571.5 (225)) due to SMCS vane deflection, M = 1.6, h_p = 9,449 m (31,000 ft), A = 67.5°, SCAS on, SMCS off.

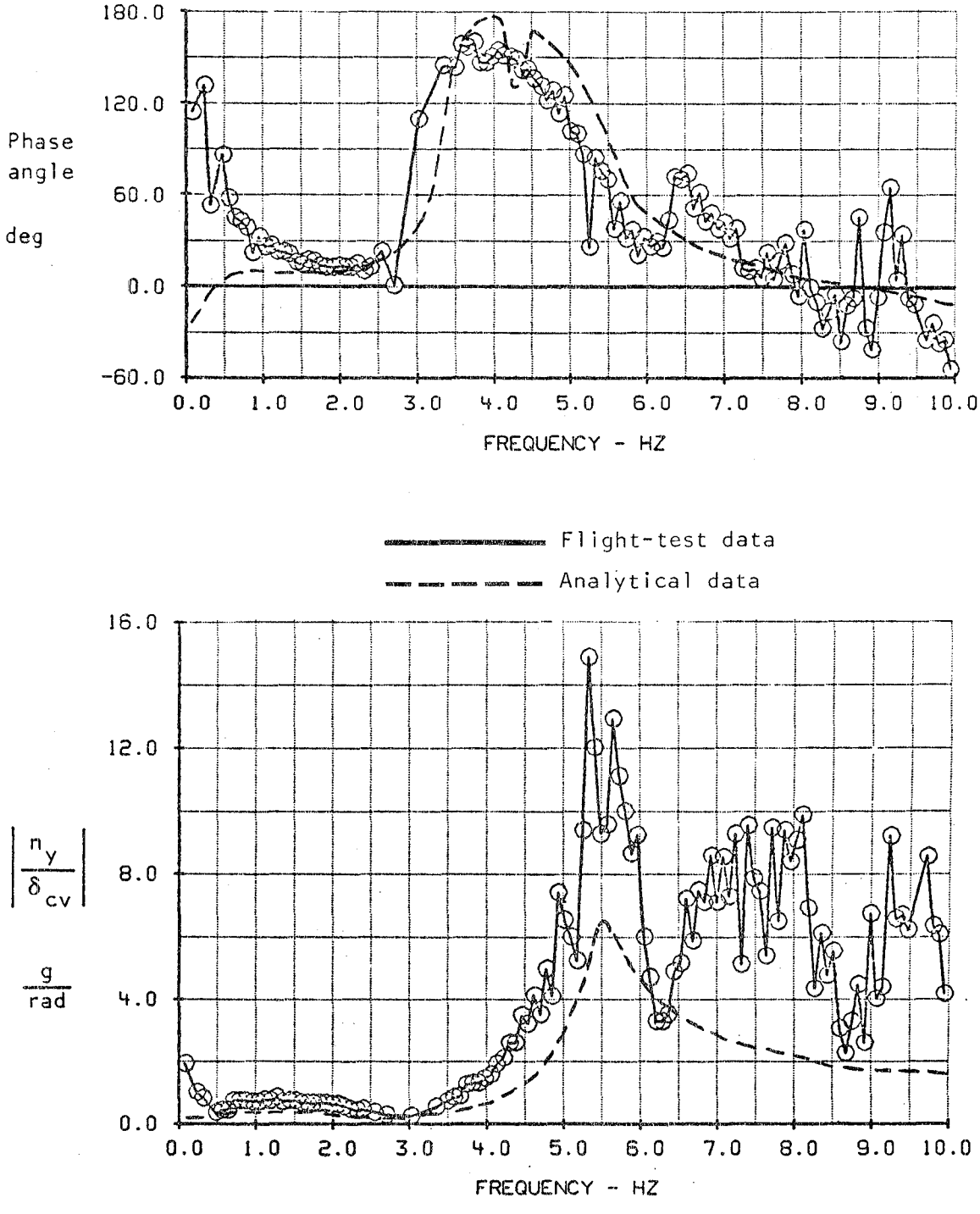

Figure 48. - Comparison of Analytical and flight-test results, frequency response of lateral load factor at vane station (FS 571.5 (225)) due to SMCS vane deflection, M = 1.6, h_p = 9,449 m (31,000 ft), A = 67.5°, SCAS on, SMCS on.

Lateral Axis Data

The lateral response data at M = 1.2 at the pilot station shown in figures 37 through 39 exhibit similar characteristics as the companion vertical axis data; namely, there is a large peak due to first fuselage bending and several less distinct modal peaks at the higher test frequencies. Operating the SCAS caused increased response at the first fuselage side bending frequency (figure 38). This peak is significantly reduced by the SMCS, as figure 39 shows.

The lateral responses at the vane station shown in figures 40 through 42 are significantly higher than the similar data in figures 37 through 39. The characteristic response features and trends are similar.

The M = 1.6 data for the pilot station, figures 43 through 45, exhibit similar characteristics to the M = 1.2 data in figures 37 through 39. The same may be said for the M = 1.6 vane station data of figures 46 through 48 when compared to the M = 1.2 data in figures 34 through 36.

COMPARISONS OF FLIGHT TEST AND ANALYSES RESULTS

Vertical Axis Results

The vertical axis analyses results have been overlayed on the flight test data results of figures 25 through 36. As was the case when reviewing the flight test results previously, the format is M = 1.2 data are presented first allowed by M = 1.6 data. Under a given mach number, frequency response data at the pilot station (F.S. 746.8 (294)) are presented first followed by data at the vane station (F.S. 571.5 (225)) forward of the pilot station. At each location, data with all active controls system off are shown first, followed by data for SCAS only on, and finally for SCAS + SMCS on.

Looking at the M = 1.2 data as a whole, it is observed that the analyses match the first low-frequency response peak magnitude and phase angle (first fuselage bending) quite well. The vane station data are better matched than the pilot station data; the phase angle trends at the pilot station are predicted but are not close in magnitudes. The analyses third response peaks on the data are seen to be lower in frequency than flight test data. This can be best seen on the vane station data of figures 28 through 30.

It is particularly heartening to see the good first peak matches which may be directly related to the Mach Box levels for $C_{N_{\delta_{CV}}}$ calculated as part of these analyses and presented in figure 18.

The analyses data predict quite well the impact of the SCAS and SMCS systems. As noted before, the SCAS at M = 1.2 tended to raise the first response peak for the pilot station (figure 26) and the vane station (figure 29). The SMCS effectiveness in reducing the first response peak was accurately calculated (figures 27 and 30). The analyses show the tendency of the SMCS to amplify the third response peak but underpredict the magnitude as shown in figure 30.

Generally, what has been said about the M = 1.2 results may be said about the M = 1.6 data of figures 31 through 36.

Considering the comparison results as a whole, the following may be said. For this airplane and for the mach numbers analyzed, the Mach Box theory did a creditable job of predicting the required aerodynamics. Of particular significance was the ability to predict the SMCS vane normal force effectiveness even though flight test data suggests it is low at M = 1.6. Before this project began, some knowledgeable people were predicting nearly useless results from the Mach Box theory at M = 1.2.

The consistent discrepancy in the vertical phase comparison at the pilot station location in light of the equally consistent general agreement at the vane station is thought to be due to some instrument anomaly in the pilot station sensor. This allegation is uncheckable.

The higher frequency modal response differences observed between the analyses and the test data are thought to be due to stiffness and mass distribution arguments. As reported in reference 2, the highest frequency modes were off some in those analyses also; and the same stiffness description was employed for this study. The mass distributions, however, are thought to be the larger element of this difference. As previously explained, the analyses reflect a midtest run time point; and as shown on table I, there was a considerable weight increment difference between the beginning and end of a particular test series. It is also to be recalled the fuel distribution in the wings could only be guessed at for lack of detailed instrumentation in this area.

Lateral Axis Results

The lateral axis analyses results have been overlaid on the flight test data results of figures 43 through 48. Analyses were conducted for only the M = 1.6 case. The data follow the same display format as discussed in connection with the vertical axis analyses.

The response data in figures 43 through 48 are uniformly low. This trend is also observed in the first peak of controls off and SCAS on vertical axis response data at M= 1.6, but is much more pronounced across the frequency spectrum of the lateral data. The first frequency peak was missed in figures 43, 44, 46, and 47; at the exact condition for which the weight characteristics were determined (table III) (reflected in figure 45 and 48), the peak frequency is well matched.

Except for the frequency shift noted, the phase characteristics calculated match the flight test data quite well.

The accuracy of the flight test data was checked using the knowledge that the SMCS forcing was kicked off line by the safety monitor several times when n_y at the vane station exceeded $\pm.3$ g. The amplitude setting of 080 for the shaker system for the active systems-off case kicked the shaker system off line, whereas the setting of 050 permitted the shaker system to operate. Using the flight test frequency response data, the amplitude data of figure 4, and the known amplitude settings, calculations showed the n_y = .30 g to be bracketed by the amplituded settings.

The data of figures 45 and 48, for which the mass characteristics were most accurately determined, suggest that the vane lateral effectiveness is low. This fact, plus the observed low effectiveness in the vertical axis, suggests that the analytical techniques utilized in calculating vane effectiveness are in need of refinement or augmentation by wind tunnel test data.

RIDE QUALITY

Ride quality analyses were accomplished using the analytical models developed in matching the frequency response test data at the flight conditions of M = 1.2 at 5,791 meters (19,000 feet) and M = 1.6 at 9,449 meters (31,000 feet). The criterion used to evaluate the ride quality is the $\overline{H}$, or crew sensitivity index, used to evaluate the B-1 long-term exposure ride quality. Reference 1 has a short discourse on the contributing elements of the criterion. The von Karman gust spectrum was employed with a characteristic length, L, of 762 meters (2,500 feet).

Vertical Axis

The long-term (over 3 hours) requirement level of $\overline{H}_z$ for the B-1 is 0.092 in international units and 0.028 in English units.

Figure 49 shows the power spectral density curve for $\overline{H}_z$ at M = 1.2 at 5,791 meters (19,000 feet). This curve shows the relative contributions of short period motion and structural motion. The overall criterion level is determined by the square root of the area under this curve. It is immediately seen that the actual $\overline{H}_z$ levels for all vehicle configurations are below the long-term requirement level. Turbulence is known to exist at altitude for relatively short periods of time in patches. These two facts then suggest that the B-1 (or a similar vehicle) would have no vertical ride quality problem at supersonic speeds at altitude. The data also show that the SMCS system is extremely effective in reducing the primary structural mode response near 3 Hz.

The ride quality data in figure 50 for the flight condition of M = 1.6 at 9,449 meters (31,000 feet) have similar characteristics to those observed at M = 1.2 in figure 49; thus, the observations made on those data apply to the data of figure 50.

Lateral Axis

The long-term (over 3 hours) requirement level of $\overline{H}_y$ for the B-1 is .023 in international units and .007 in English units.

Figure 51 shows the power spectral density curve for $\overline{H}_y$ at M = 1.6 at 9,449 meters (31,000 feet). This curve shows the relative contributions of the Dutch roll and structural motions. As for the vertical axis, the overall criterion level is determined by the square root of the area under this curve. Contrary to the vertical results, the $\overline{H}_y$ levels for all vehicle configurations are above the long-term level. While all aircraft configuration $\overline{H}_y$ levels are above the long-term requirement (the previous comment about short turbulence patches is still applicable), the SMCS operation is still effective in the lateral axis in improving the ride quality.

Time Histories of SMCS Operation in Turbulence

Time history data obtained while flying in turbulence provide one of the best formats for evaluating the impact of the SMCS on ride quality. Some such data were obtained on flight 3-138. Since the basic theme of this report is supersonic flight at altitude, and the data obtained were recorded at transonic speeds at low altitude, these data have been placed in Appendix C, figure 55.

$$\bar{H}_z = \left[6.28 \int_{f=o}^{f=c.o.} \Phi_{\bar{H}_Z}(\omega)\, df \right]^{1/2} \frac{1}{ft/sec}$$

$$\bar{H}_z = \left[\left(\frac{6.28}{.0929} \right) \int_{f=o}^{f=c.o.} \Phi_{\bar{H}_Z}(\omega)\, df \right]^{1/2} \frac{1}{m/sec}$$

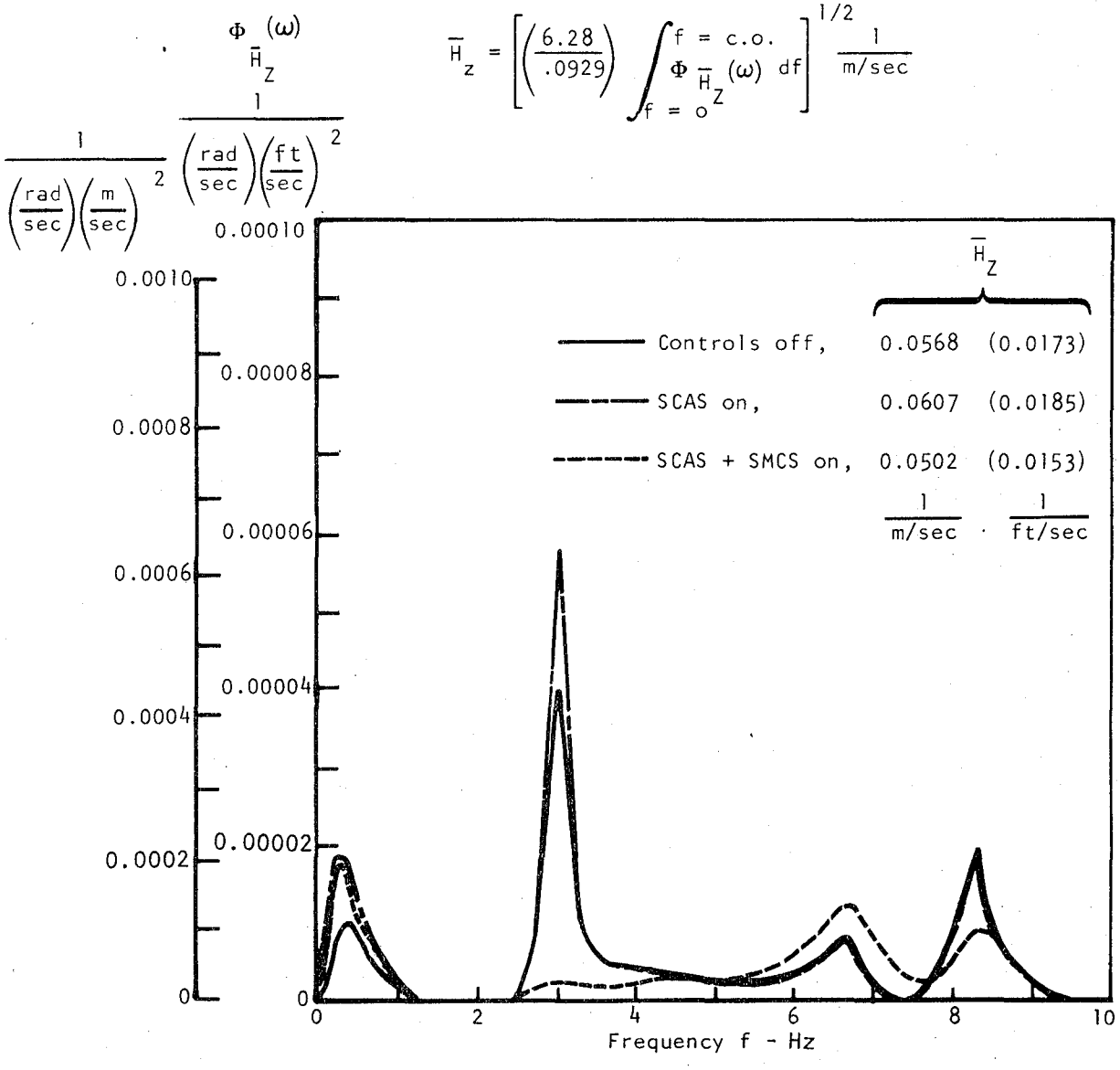

Figure 49. - Vertical ride quality index, $\bar{H}_Z$, power Spectral density at M = 1.2, 5,791 m (19,000 ft), with and without active controls.

$$\bar{H}_z = \left[6.28 \int_{f=o.}^{f = c.o.} \Phi_{\bar{H}_Z}(\omega)\, df \right]^{1/2} \frac{1}{ft/sec}$$

$$\bar{H}_z = \left[\left(\frac{6.28}{0.0929} \right) \int_{f = o}^{f = c.o.} \Phi_{\bar{H}_Z}(\omega)\, df \right] \frac{1}{m/sec}$$

$$\frac{1}{\left(\frac{rad}{sec}\right)\left(\frac{m}{sec}\right)^2} \qquad \frac{\Phi_{\bar{H}_Z}(\omega)}{\left(\frac{rad}{sec}\right)\left(\frac{ft}{sec}\right)^2}$$

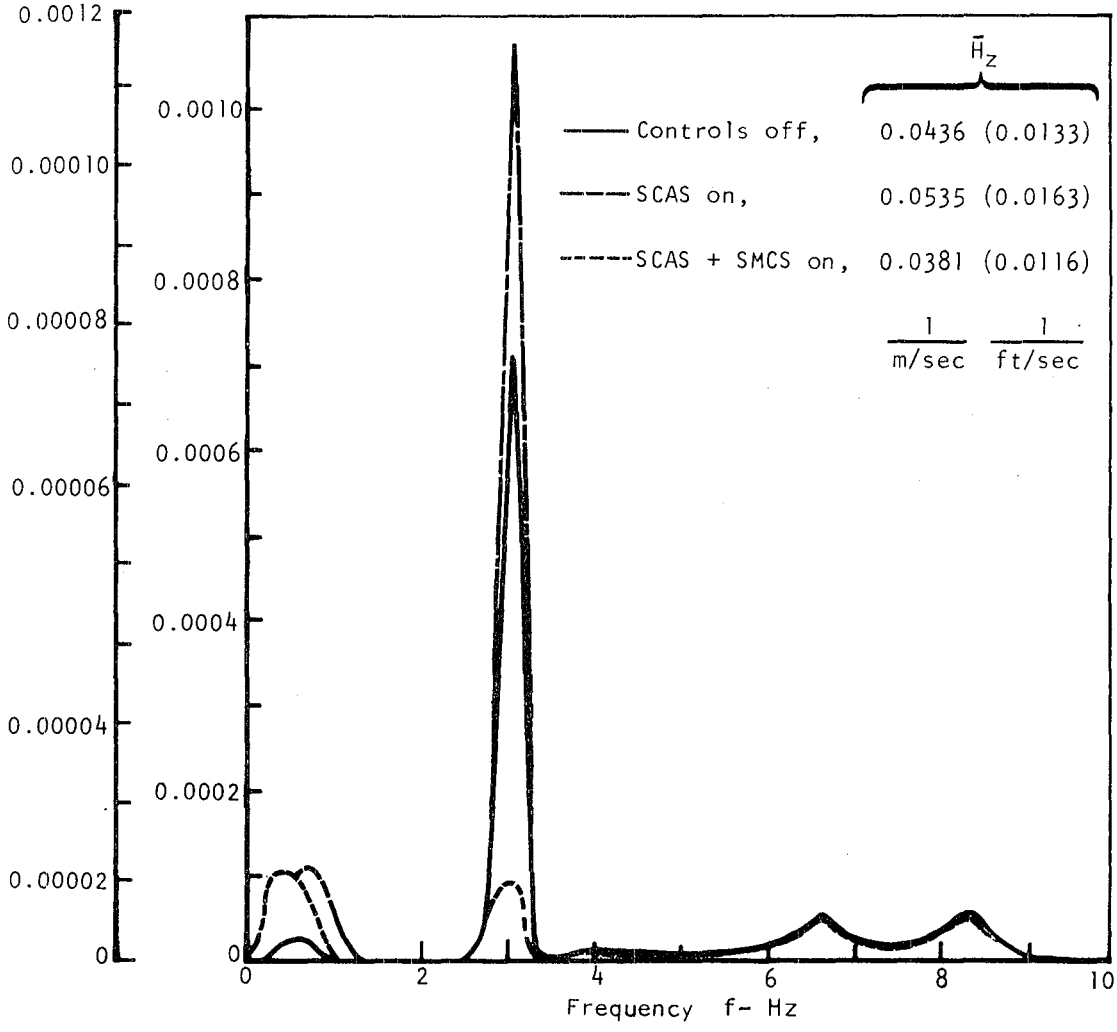

Figure 50. - Vertical ride quality index, $\bar{H}_z$, power spectral density at M = 1.6, 9,449 m (31,000 ft) with and without active controls.

$$\bar{H}_y = \left[6.28 \int_{f=0}^{f=c.o.} \Phi_{\bar{H}_y}(\omega)\, df \right]^{1/2} \frac{1}{ft/sec}$$

$$\bar{H}_y = \left[\left(\frac{6.28}{0.0929}\right) \int_{f=0}^{f=c.o.} \Phi_{\bar{H}_y}(\omega).df \right]^{1/2} \frac{1}{m/sec}$$

$\Phi_{\bar{H}_y}(\omega)$

$\frac{1}{\left(\frac{rad}{sec}\right)\left(\frac{ft}{sec}\right)^2}$ $\quad$ $\frac{1}{\left(\frac{rad}{sec}\right)\left(\frac{ft}{sec}\right)^2}$

	$\bar{H}_y$	
——— Controls off	.0390	(.0119)
– – – – SCAS on	.0394	(.0120)
– – – – – SCAS + SMCS on	.0285	(.0087)
	$\frac{1}{m/sec}$	$\frac{1}{ft/sec}$

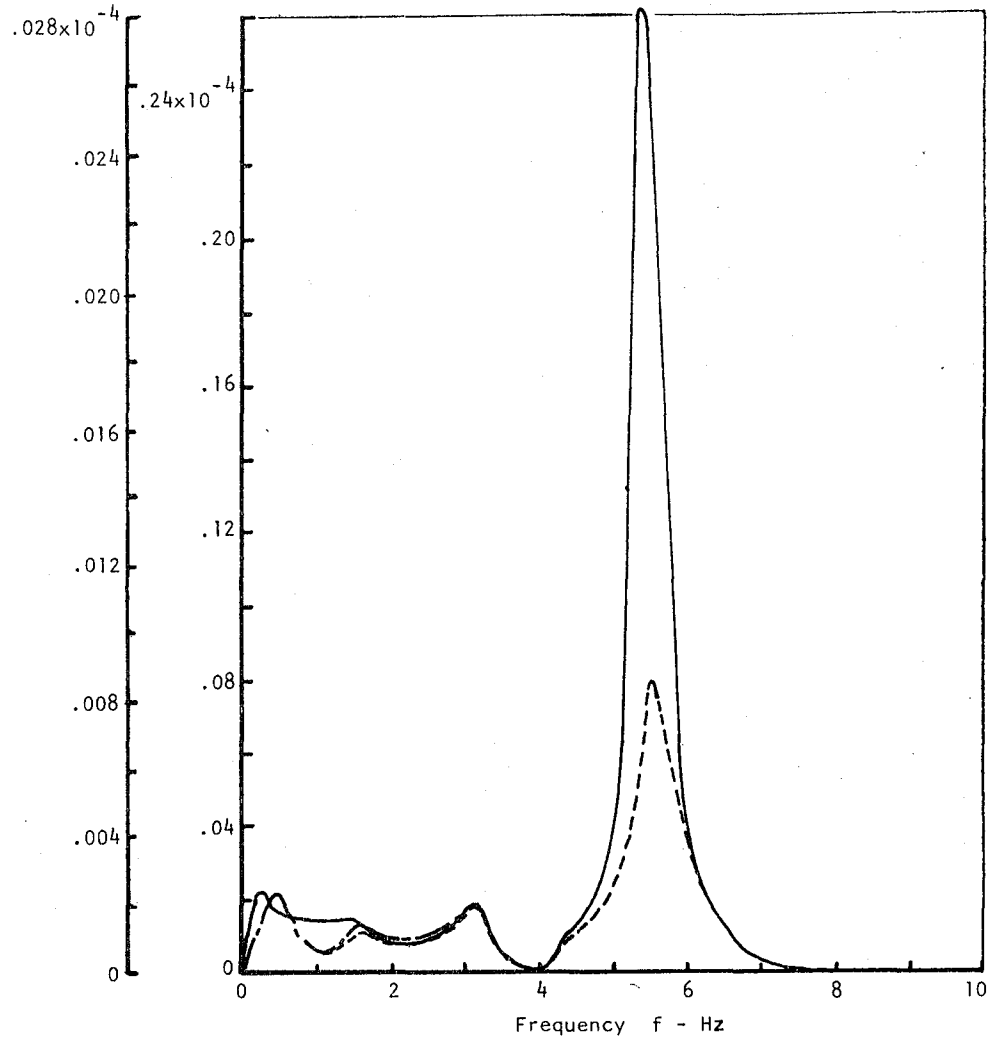

Figure 51. - Lateral ride quality index, $\bar{H}_y$, power spectral density at M = 1.6, 9449 m (31,000 ft), with and without active controls.

CONCLUSIONS

The primary objective of demonstrating the possibility of designing an SMCS that could be turned on at takeoff and be left on for the whole flight without further attention (as is the case for all regular augmentation systems) has been met. The SMCS system even appears to be more effective in damping the key fuselage bending modes at supersonic speeds than at the design point of M = 0.85 (for fixed system gains). The adverse effect of the SMCS on higher frequency symmetric modes is similar to that at the subsonic design point but is slightly more adverse. However, this adverse effect did not make the system unstable and does not appear to affect ride quality performance.

The vertical ride quality analyses indicate that the basic configuration without active systems is satisfactory even for long-term exposure (which is improbable at altitude). If clear air turbulence were to be encountered, it is indicated that the SMCS would be very effective in reducing the adverse accelerations. On the other hand, lateral ride quality analyses indicate that the aircraft with the SMCS on does not quite meet the long-term exposure criteria, but would be satisfactory for more probable short-term exposure at altitude. Again, the lateral SMCS was shown to be very effective in reducing peak lateral accelerations.

The secondary objective of evaluating existing analyses techniques in the supersonic speed range has been accomplished. The Mach Box theory has been shown to provide creditable data for active control systems evaluations even at M = 1.2, which is approaching the lower speed bounds on the theory. However, the ability of the theory to predict force effectiveness of small SMC vanes on a fuselage appears to be only good to fair, the vertical force effectiveness being more accurately calculated than the lateral force effectiveness, and the force effectiveness data at M = 1.6 being less accurate than the data at M = 1.2, as evidenced by flight test data matching.

APPENDIX A

LIST OF SYMBOLS

A, Ampltd		amplitude setting of B-1 oscillating system for the SMCS vanes
A/C		aircraft
b		lifting surface span
B.P.		butt plane
b_w		wing span
c		lifting surface local chord
$\bar{c}$		mean aerodynamic chord
$\bar{c}_w$		wing mean aerodynamic chord
c_{av}		lifting surface average chord
CG		center of gravity
C_ℓ		local lift coefficient
C_L		total lift coefficient
cm		centimeters
C_m	$= \frac{M}{S_w \bar{c}_w q_o}$	pitching-mcment coefficient
C_{m_α}	$= \frac{\partial C_m}{\partial \alpha}$	pitching-moment curve slope
C_N	$= \frac{N}{S_w q_o}$	normal-force coefficient
C_{N_α}	$= \frac{\partial C_N}{\partial \alpha}$	normal-force curve slope

$C_{N_{\delta_{(\ )}}}$	=	$\frac{\partial C_N}{\partial \delta_{(\ )}}$ normal-force coefficient due to control surface deflection, subscript identifies surface
deg		degrees
EI		bending stiffness
f		frequency, cycles per second
F1B		fuselage first bending mode
F2B		fuselage second bending mode
F3B		fuselage third bending
F1T		fuselage first torsion mode
Flex/Rigid		flexible-to-rigid ratio of an aerodynamic parameter
Flt		flight
F.S.		fuselage station
ft		feet
Fwd		forward
g		acceleration of gravity
GJ		torsional stiffness
g_{s_i}		structural damping constant, mode i
GVT		ground vibration test
$\bar{H}_{(\ )}$		crew sensitivity index; subscript Z denotes vertical axis, Y denotes lateral axis
H1B		horizontal tail first bending mode
h_p		altitude (+ up from sea level)
H1T		horizontal tail first torsional mode
HF&A		horizontal tail fore and aft mode

Hz	hertz (cycles per second)
in.	inches
K	SMCS gain
kg	kilogram
K_{h_p}	SCAS gain scheduled with altitude
$K_{MN_{n_y}}$	yaw SCAS lateral accelerometer gain
K_{MN_r}	yaw SCAS gyro gain
K_{n_z}	pitch SCAS normal acceleration gain
k_q	pitch SCAS gyro gain
$k_{\bar{q}}$	SMCS gain scheduled with dynamic pressure
L	characteristic length of gust power spectral density
lb	pounds
ℓ_x	distance along the X-axis + forward
M	aerodynamic pitching moment about Y-axis
m	meter
M	mach number
N	aerodynamic normal force
NAC1	first nacelle mode
$\left\lvert \frac{n_z}{\delta_{cv}} \right\rvert$	amplitude of frequency response of normal load factor due to SMCS vane symmetric deflections
$\left\lvert \frac{n_y}{\delta_{cv}} \right\rvert$	amplitude of frequency response of lateral load factor due to SMCS vane differential deflection, sense and magnitude of δ_{cv} indexed to right surface, + δ_{cv} gives + (C_y)

p	rolling rate about X-body axis
q_o	$1/2\ \rho V_o^2$, dynamic pressure
q	pitching rate about Y-body axis
r	yawing rate about Z-body axis
rad	radians
S	Laplace variable
SCAS	stability and control augmentation system
SDM	System Definition Manual
sec	second
SIC	structural influence coefficients
SMCS	structural mode control system
S_w	wing area
T_M	time history duration
V_o	resultant velocity of the CG
V_H	maximum level flight speed
V1B	vertical first bending mode
V1T	vertical first torsion mode
W1B	wing first bending mode
W2B	wing second bending mode
W1T	wing first torsional mode
WF&A	wing fore and aft mode
ℓ_y	distance from centerline out span of surface laterally
α	aircraft angle of attack

α_t	trimmed aircraft angle of attack
β	sideslip angle
δ_{CV}	SMCS vane deflection, + symmetric trailing edge down; + differential right side trailing edge down, magnitude indexed to right surface deflection
δ_H	horizontal tail deflection, + trailing edge down
δ_H'	rolling tail control differential deflection, + deflection produces $+C_\ell$, magnitude is differential angle
δ_r	lower rudder panel deflection, + trailing edge left
η_i	deflection of the ith normalized structural mode at normalization point
$\dot{\eta}_i$	rate of change of the ith mode at point of normalization
$\ddot{\eta}_i$	acceleration of the ith mode at point of normalization
Λ	sweep angle of leading edge of lifting surface
ω	frequency, radians per second
$\phi_i^{(\ )}$	the i normalized mode shape; i.e., ratio of local deflection to deflection at normalizing point (nondimensional); ( ) superscript denotes location
$\phi_i'^{(\ )}$	slope of the ith normalized mode; ( ) superscript denotes location
$\Phi_{\bar{H}_z}(\omega)$	power spectral density of the ride quality index $\bar{H}_z$; function of ω
$\Phi_{\bar{H}_y}(\omega)$	power spectral density of the ride quality index $\bar{H}_y$; function of ω
ρ	density of air
τ_M	time duration of covariance function

Appendix B

MODAL DATA

This appendix contains the vibration modes used in the analytical matches of the vertical test data at M = 1.2 (flt 3-138) and M = 1.6 (flt 3-137) and the lateral test data at M = 1.6 (flt 3-137).

The weight condition for the vertical case at M = 1.2 was 134, 690 kg (296,940 lb) with the CG at 0.465 $\bar{c}_w$ (FS 2619.9 (1031.44). The weight condition for the vertical case at M = 1.6 was 128,893 kg (284,160 lb) with the CG at 0.444 $\bar{c}_w$ (FS 2608.6 (1027.0)). The weight condition for the lateral case at M = 1.6 was 114,156 kg (251,670 lb) with the CG at 0.455 $\bar{c}_w$ (FS 2603.8 (1025.1)). The wing sweep was 67.5° in all cases.

For each case, the modes are shown as used in the analyses. In all cases, these modes are not in the sequential order of the original vibration analyses, but retain here their sequential number from the vibration analyses.

The modal data for the vertical case at M=1.6 (flt 3-137) are shown in figure 52. The modal data for the vertical case at M = 1.2 (flt 3-138) are shown in figure 53. The modal data for the lateral case at M = 1.6 are shown in figure 54.

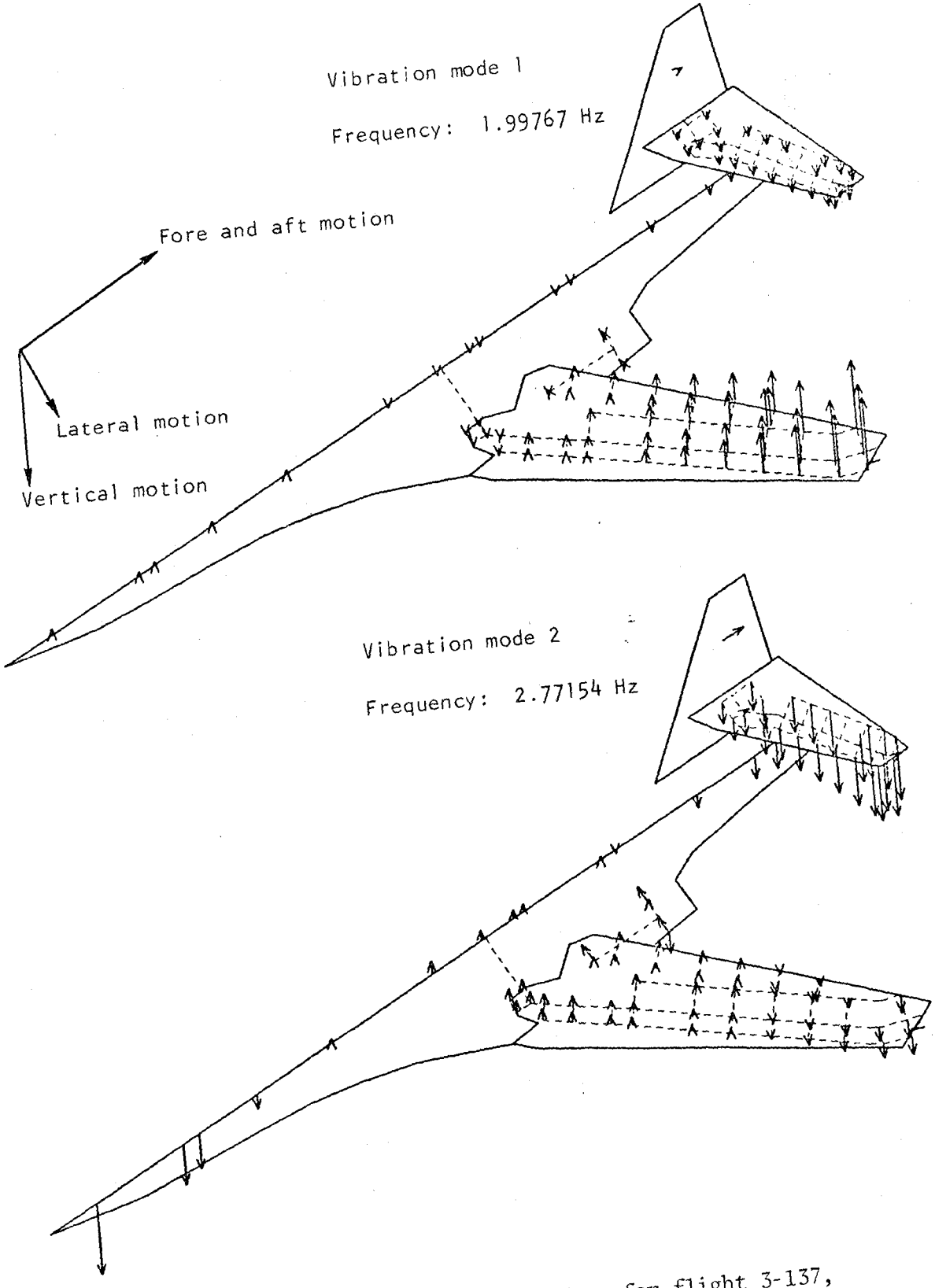

Figure 52. - Symmetric modal data for flight 3-137, weight = 128,893 kg (284,160 lb).

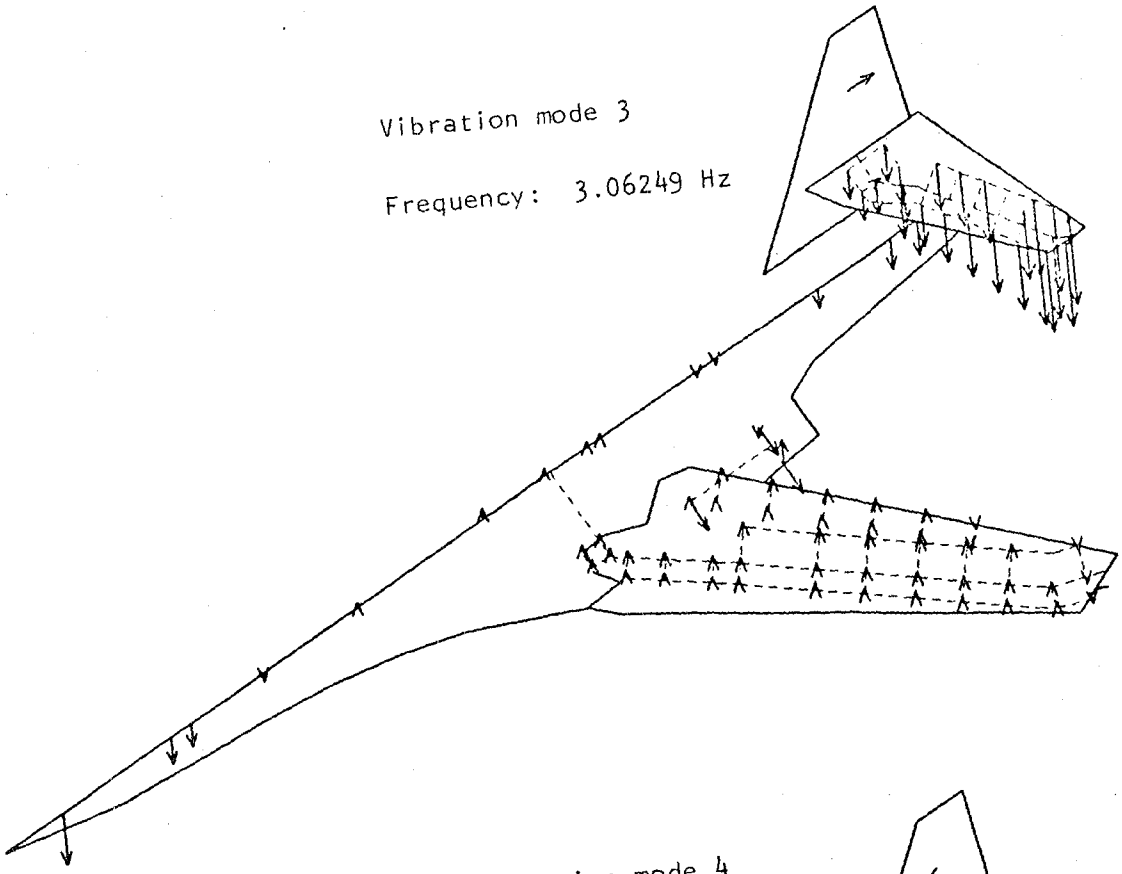

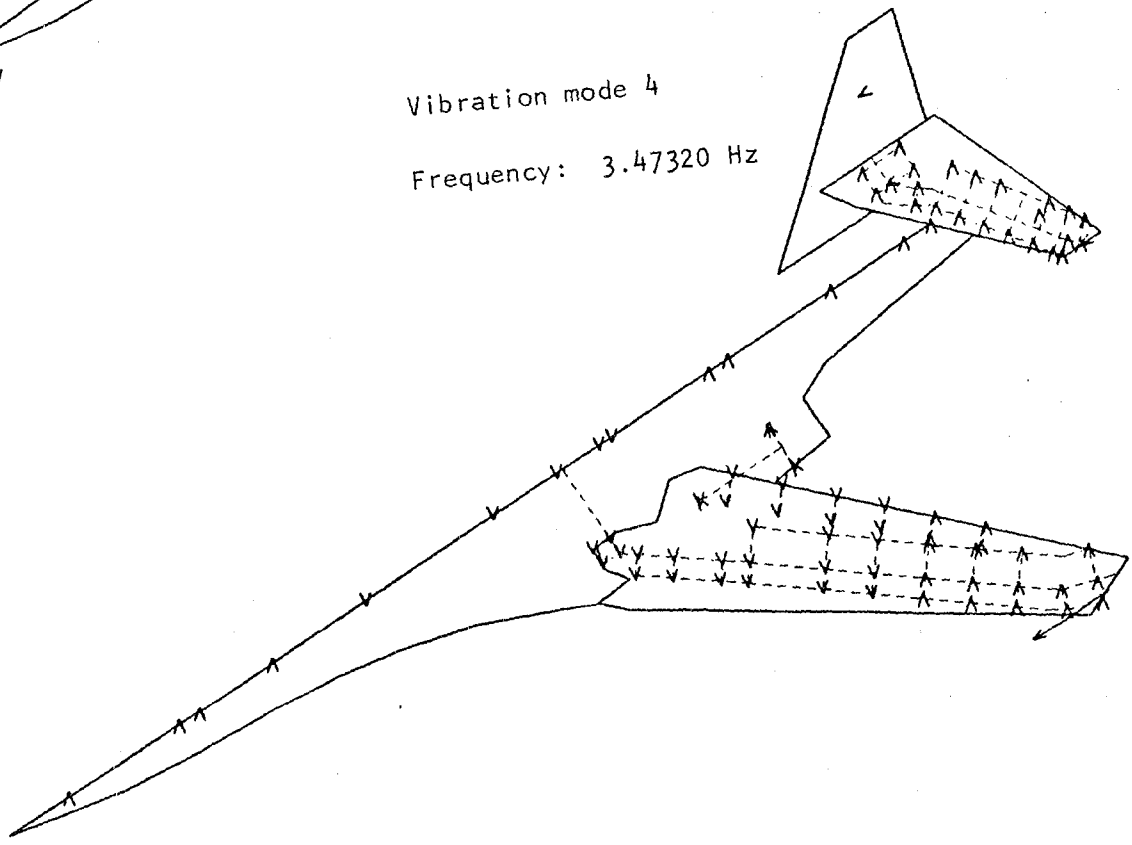

Figure 52. Continued.

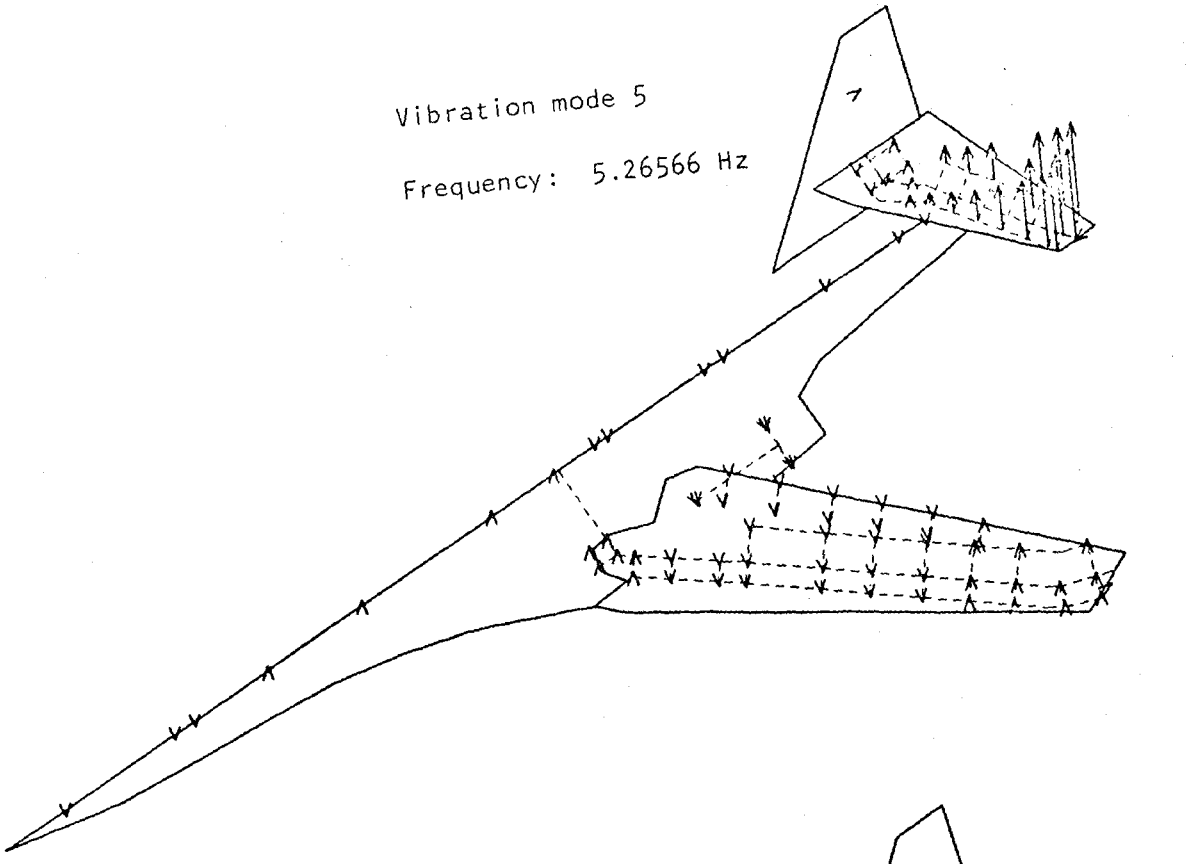

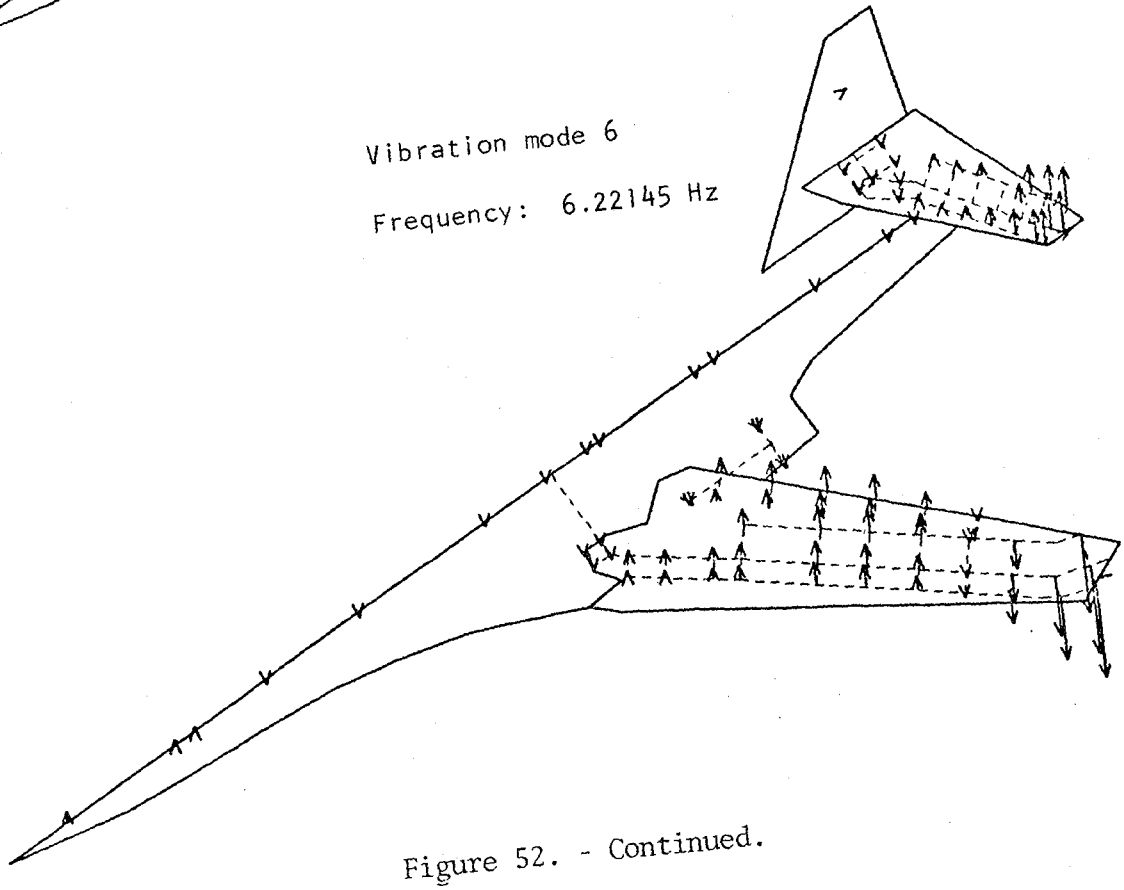

Figure 52. - Continued.

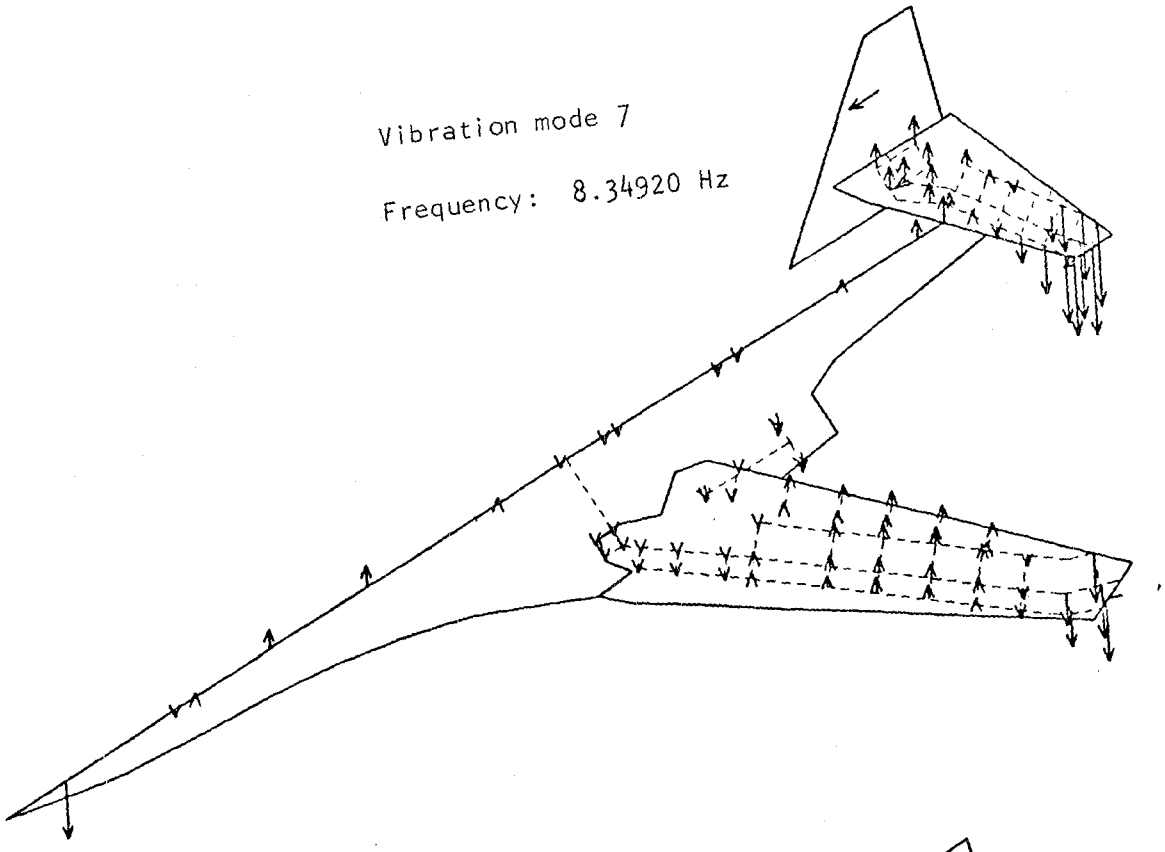

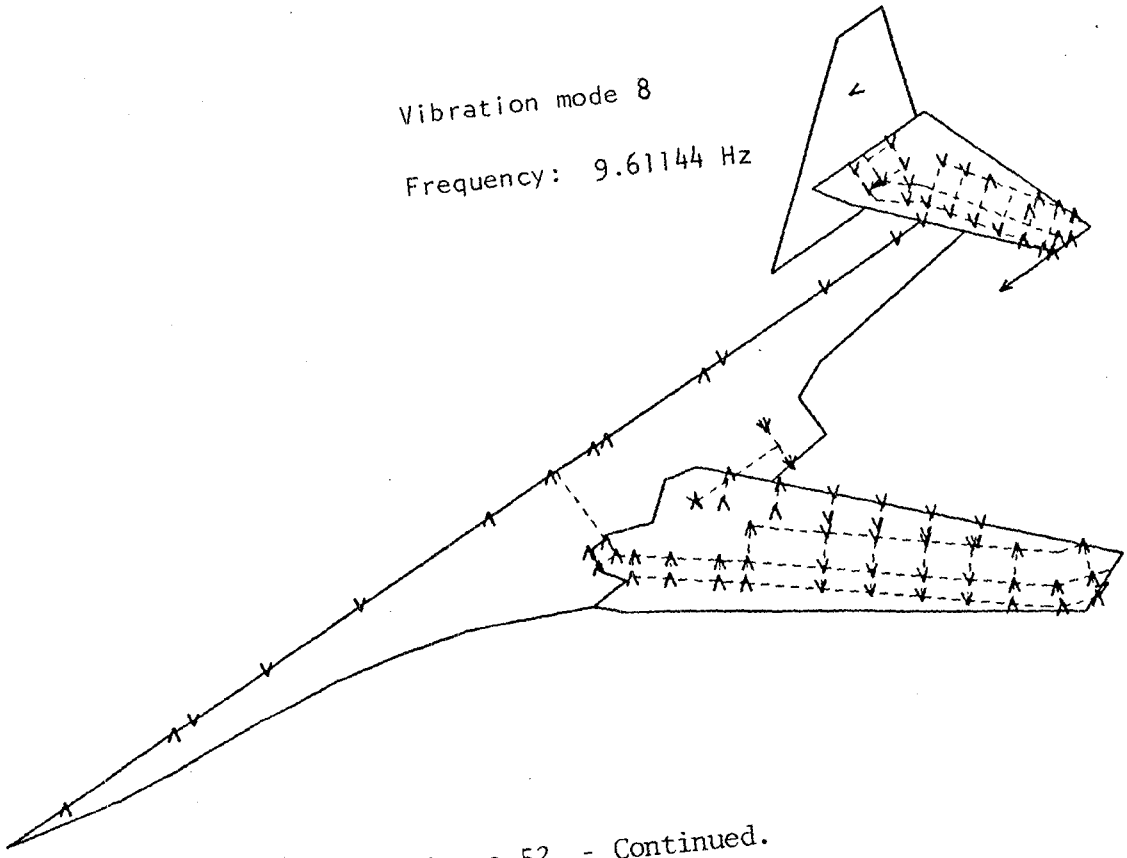

Figure 52. - Continued.

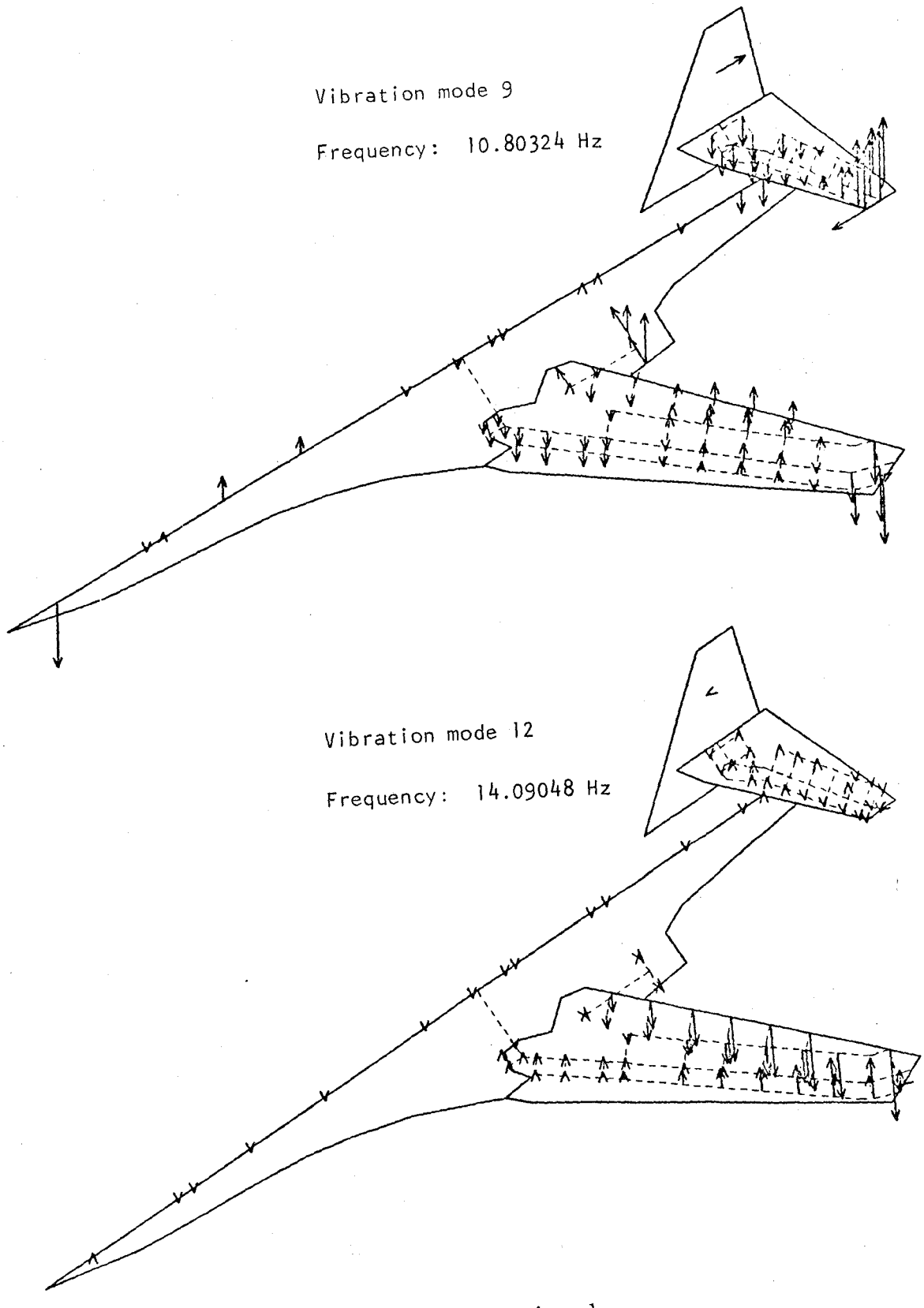

Figure 52. - Continued.

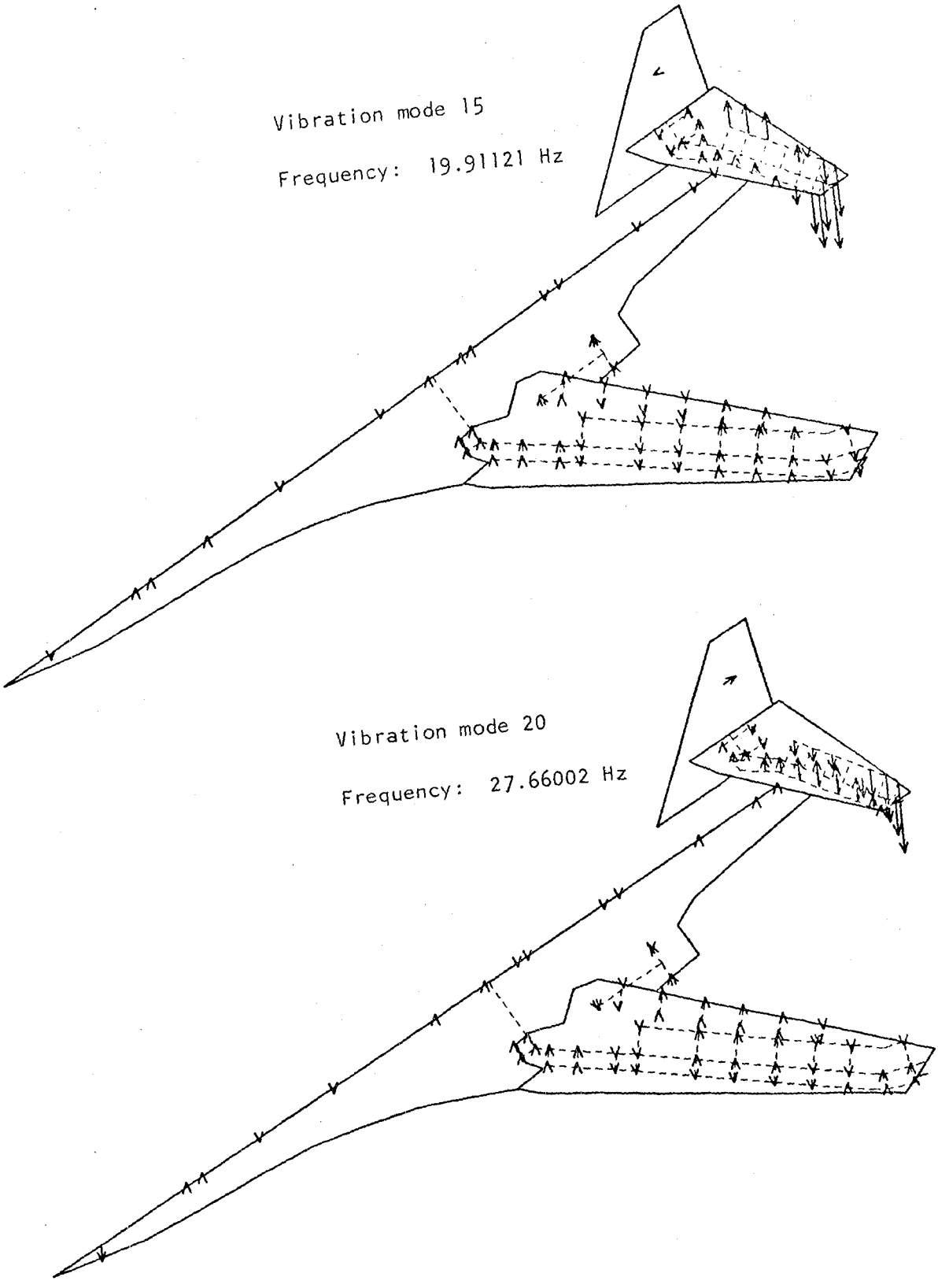

Figure 52. - Concluded.

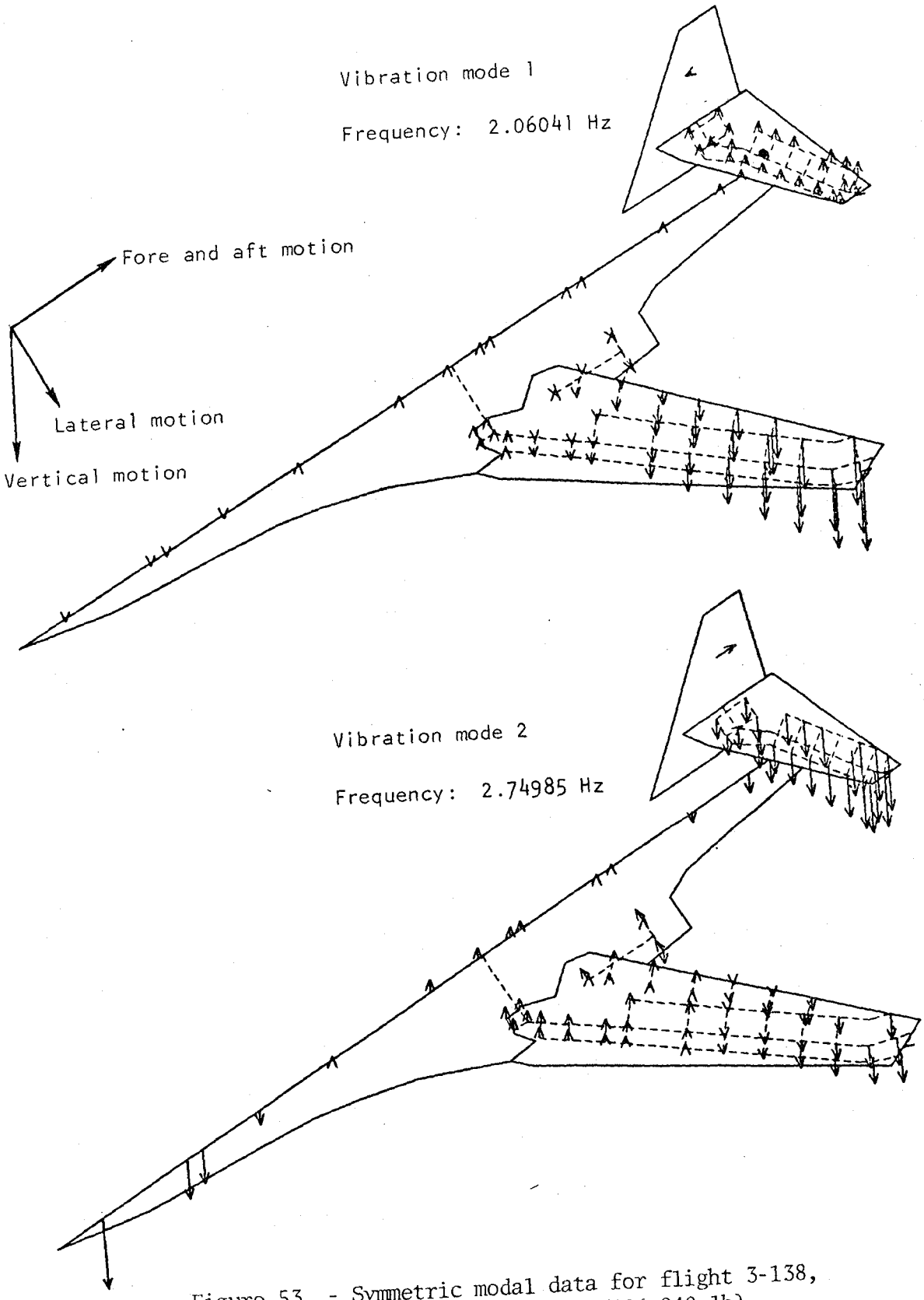

Figure 53. - Symmetric modal data for flight 3-138, weight = 134,690 kg (296,940 lb).

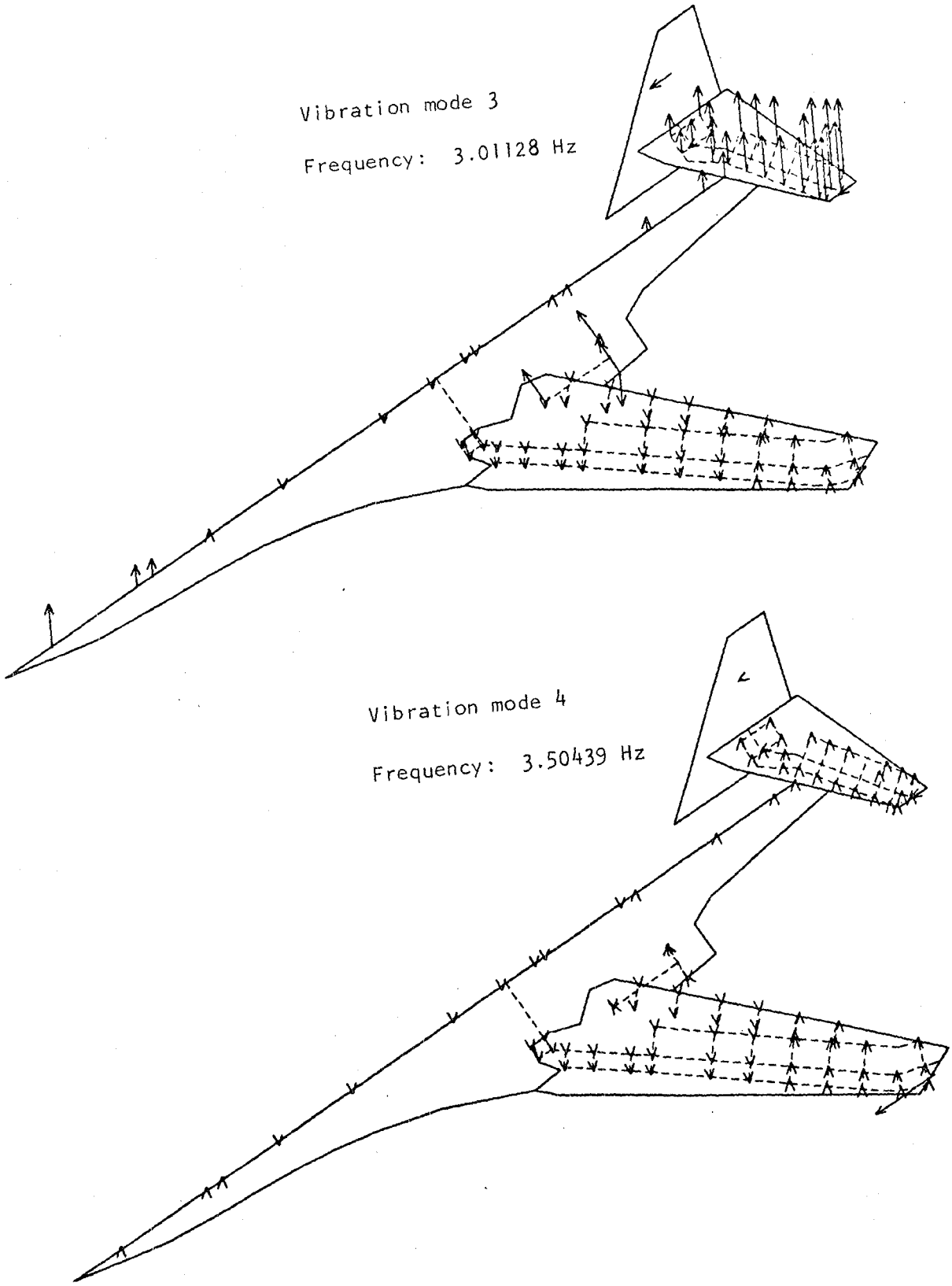

Figure 53. - Continued.

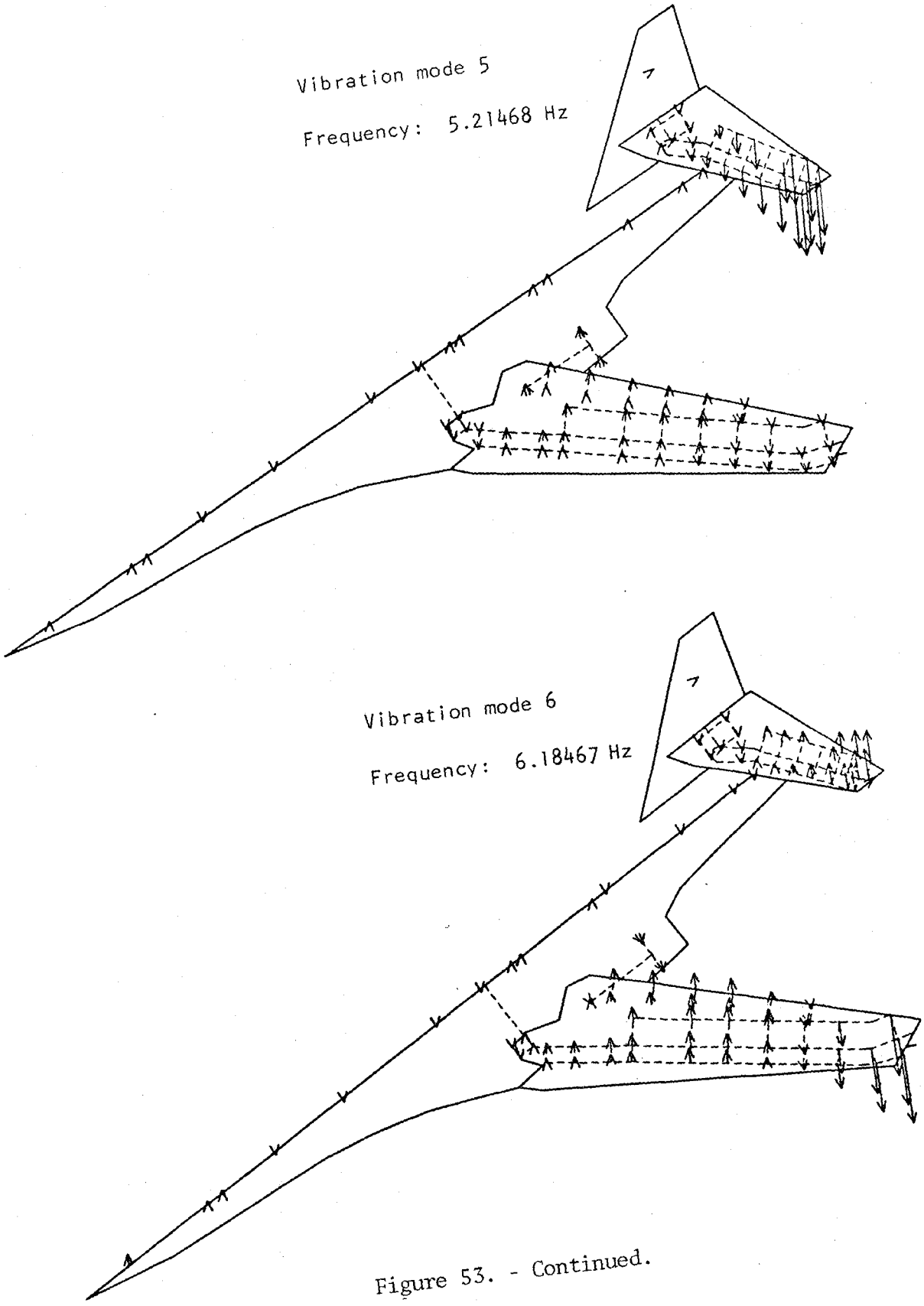

Figure 53. - Continued.

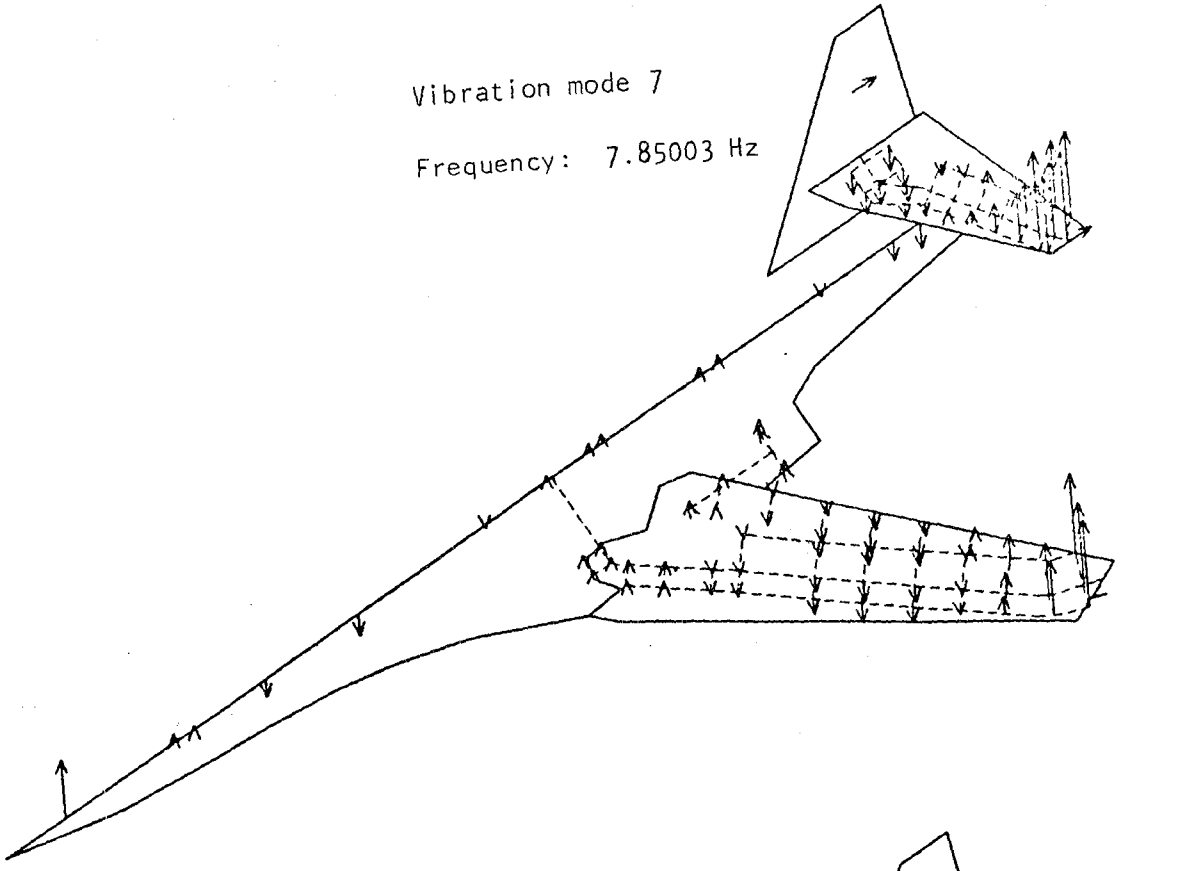

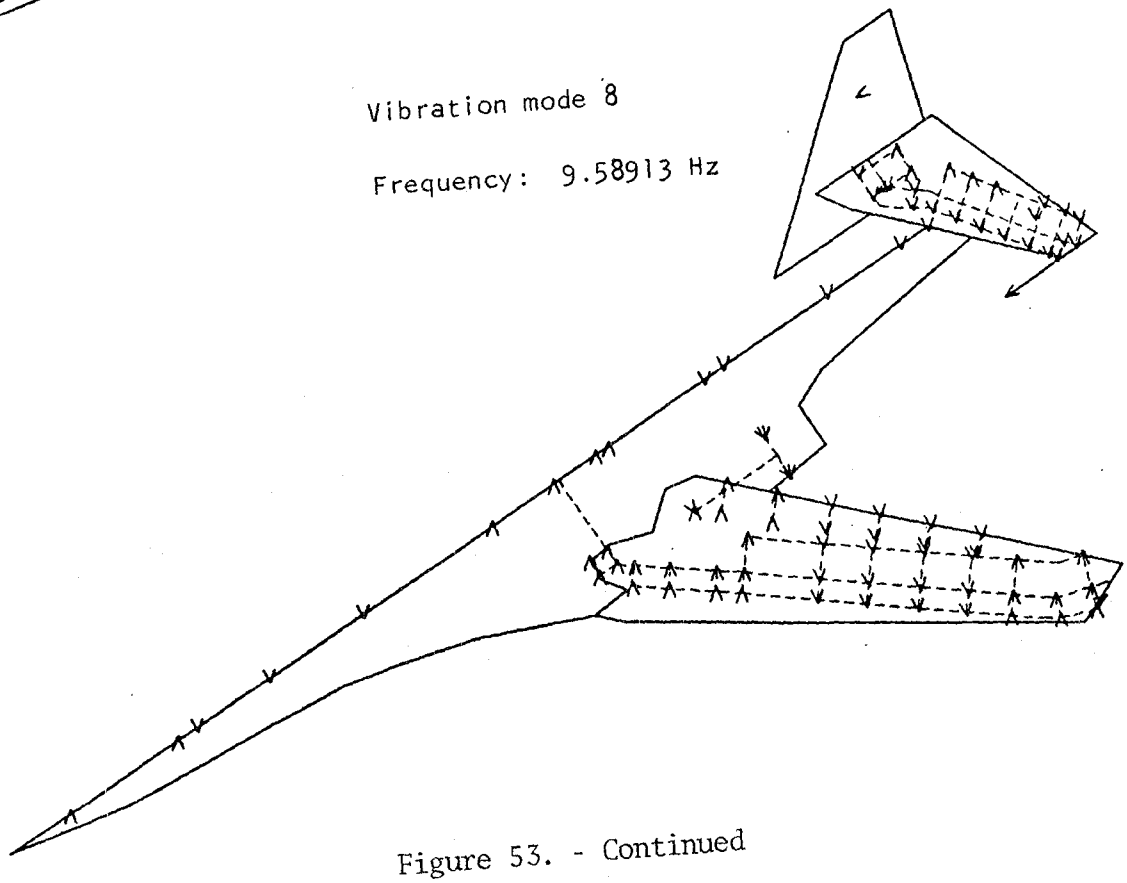

Figure 53. - Continued

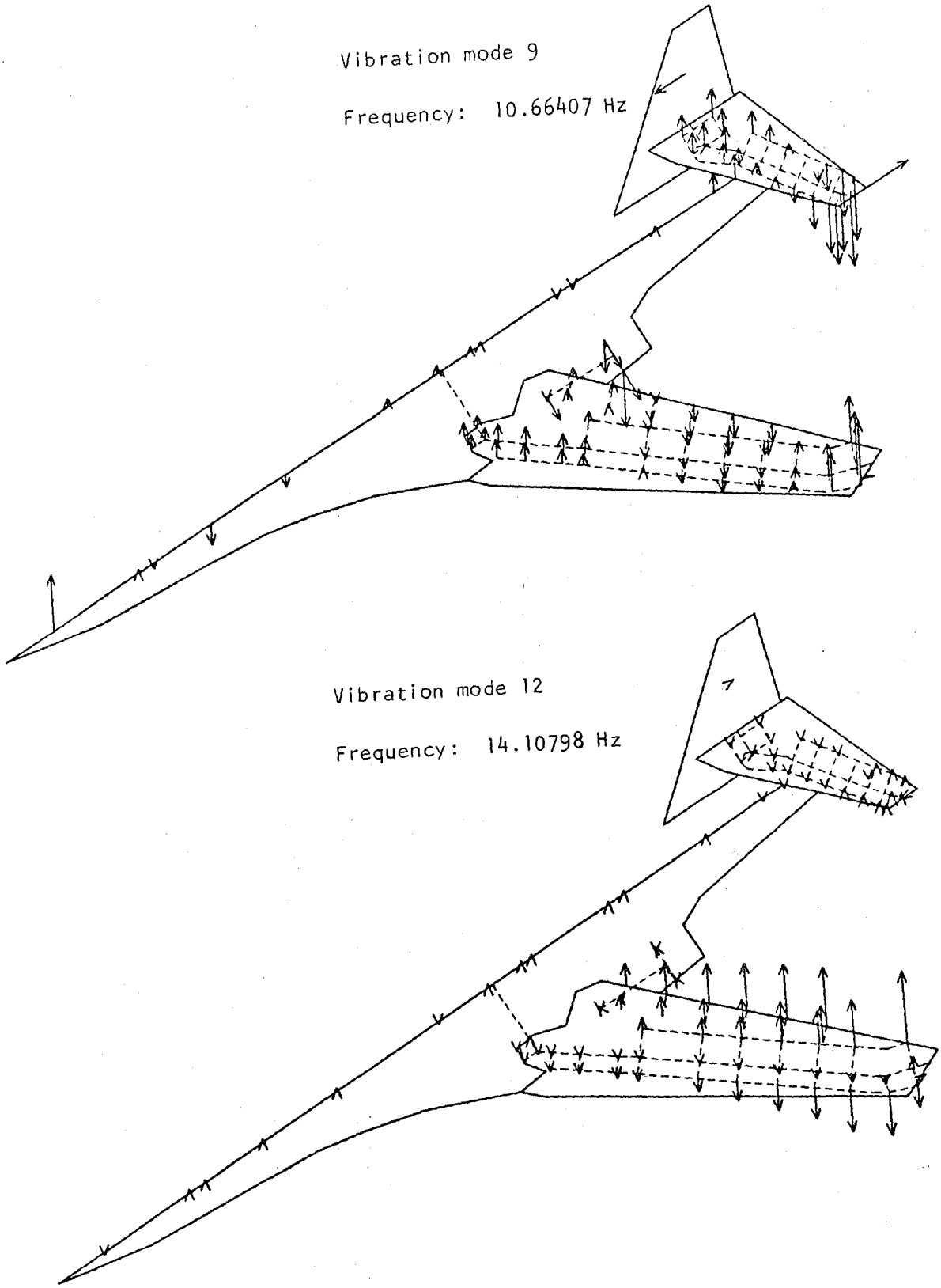

Figure 53. - Continued

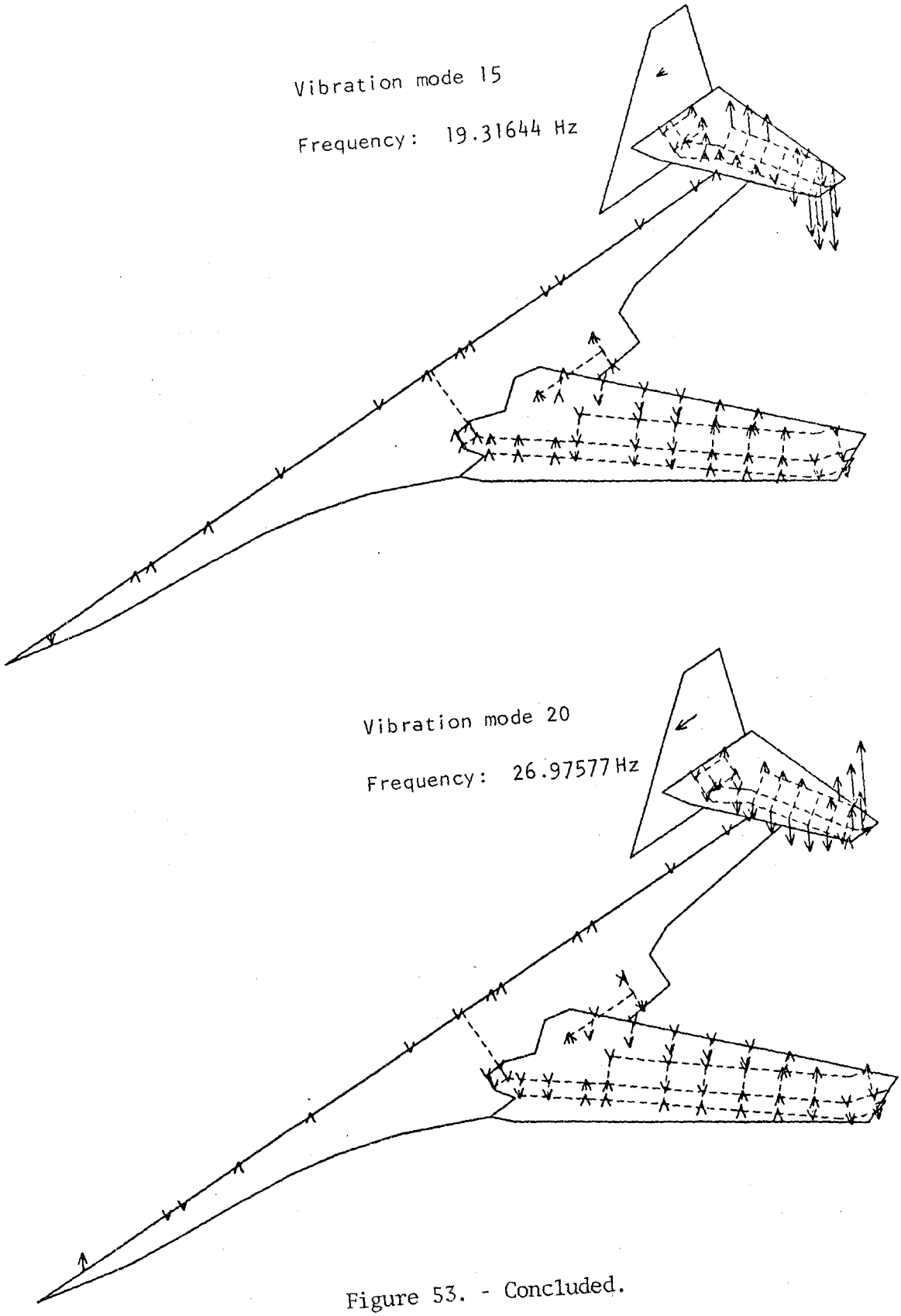

Figure 53. - Concluded.

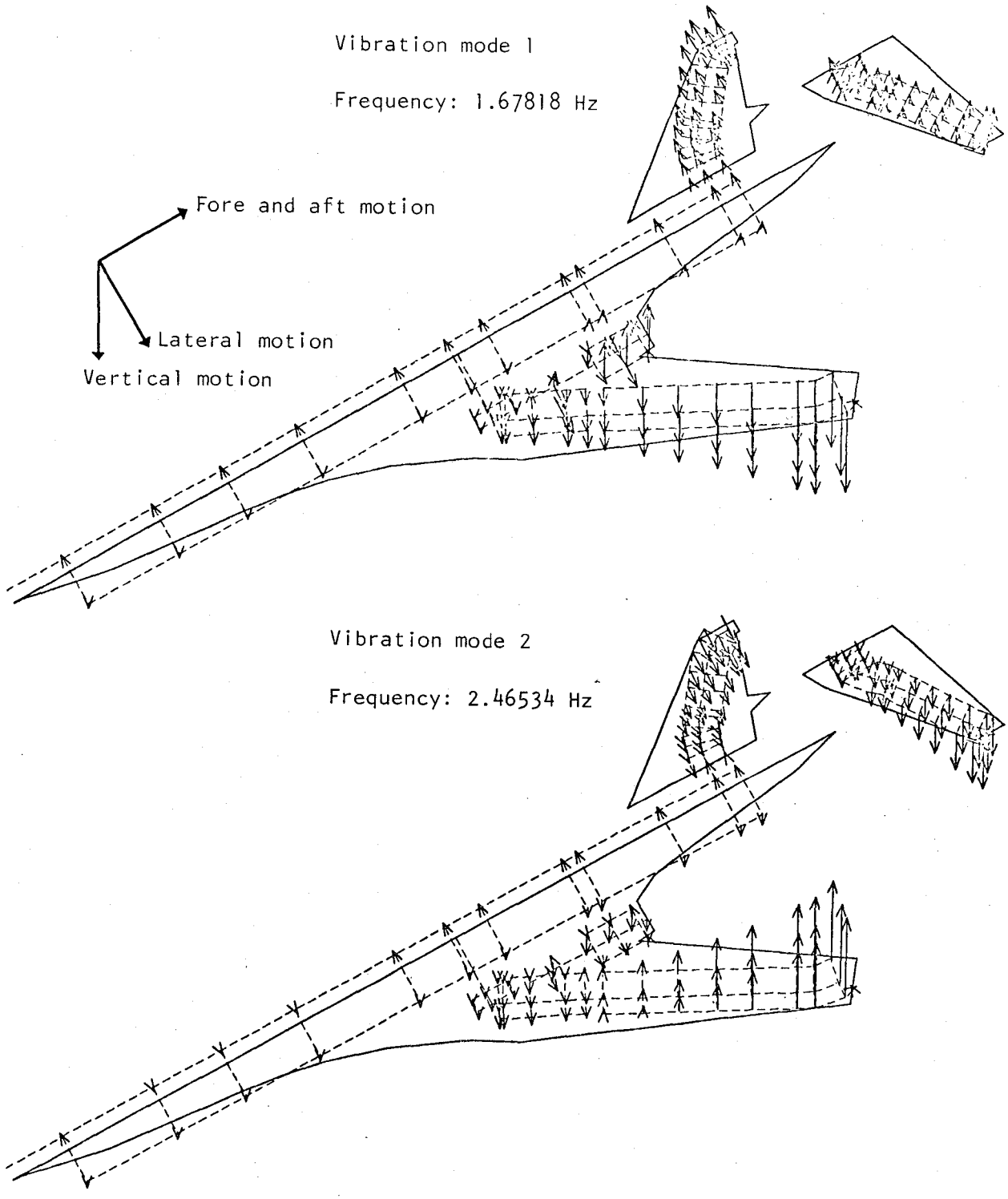

Figure 54. - Antisymmetric modal data for Flight 3-137, weight = 114,156 kg (251,670 lb).

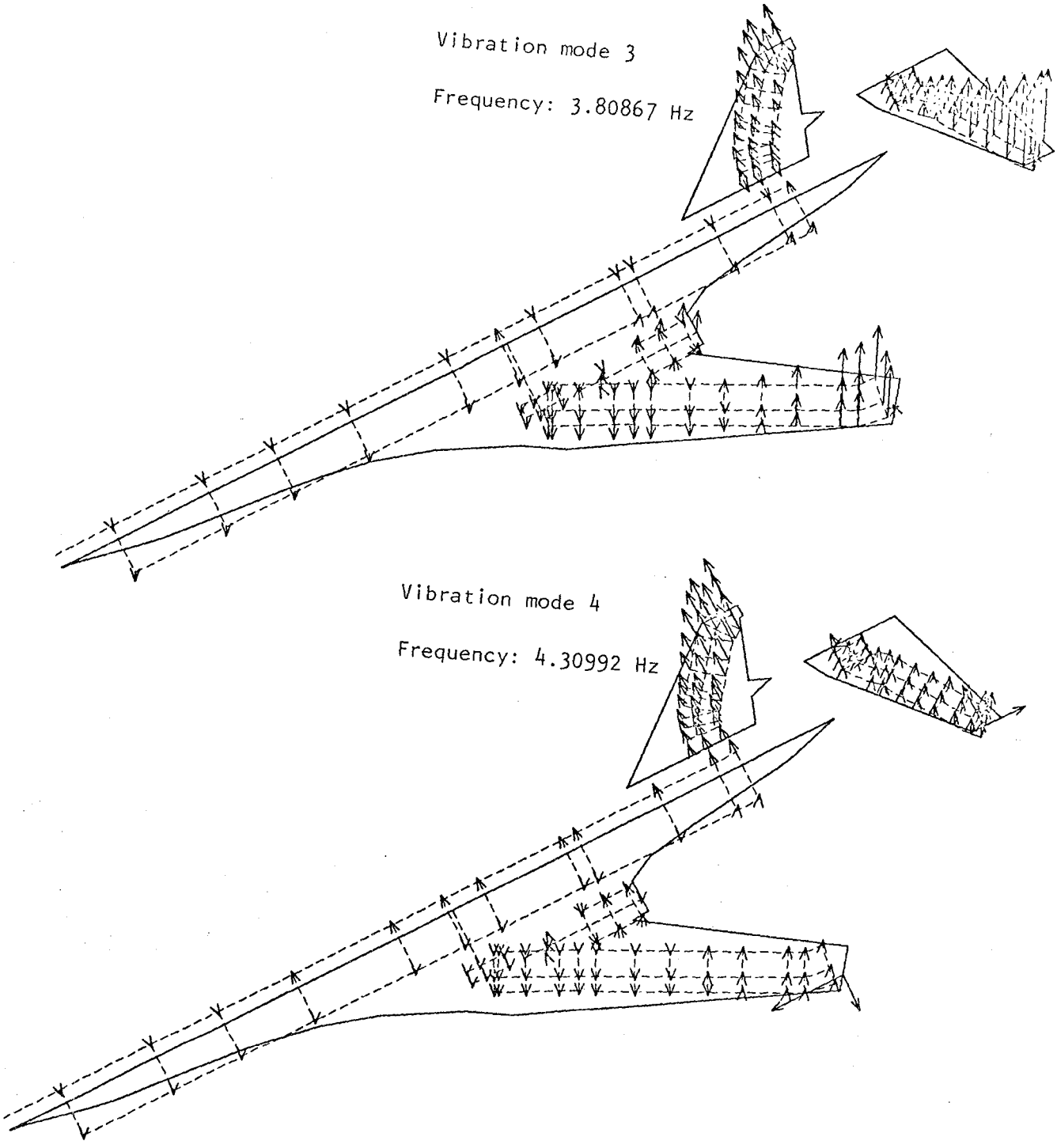

Figure 54. - Continued

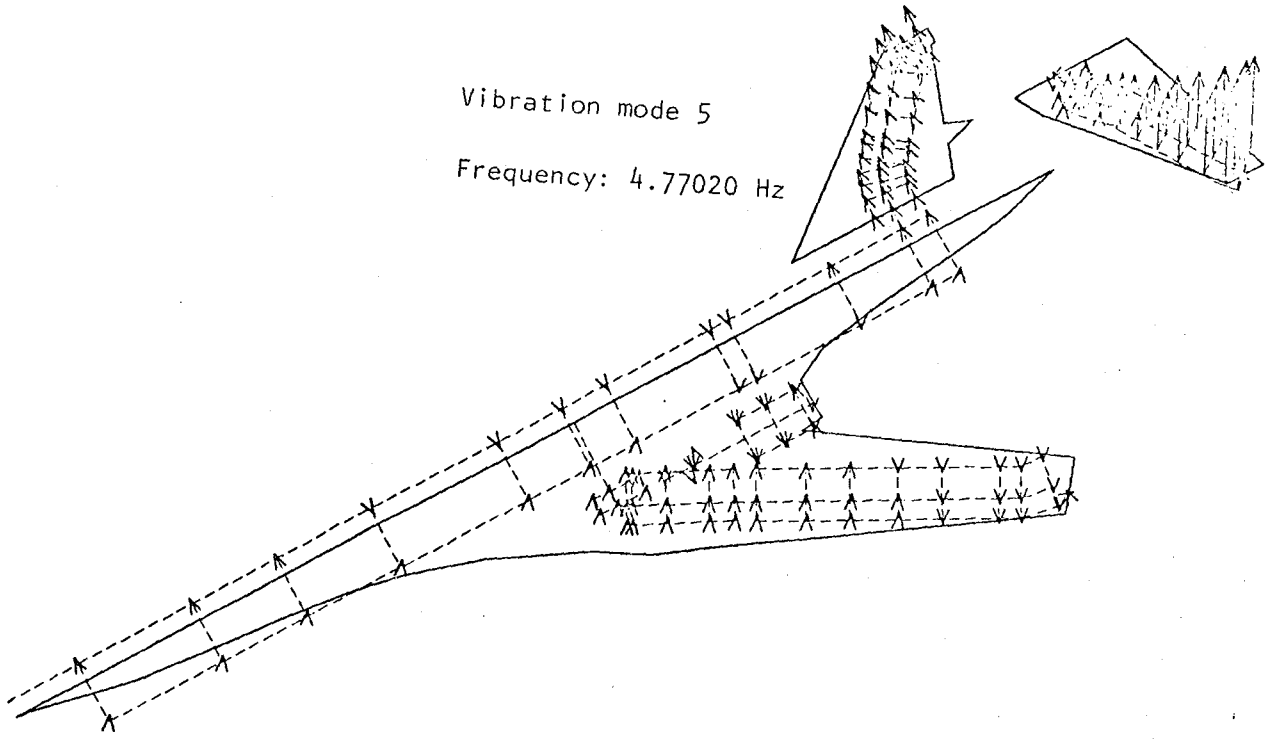

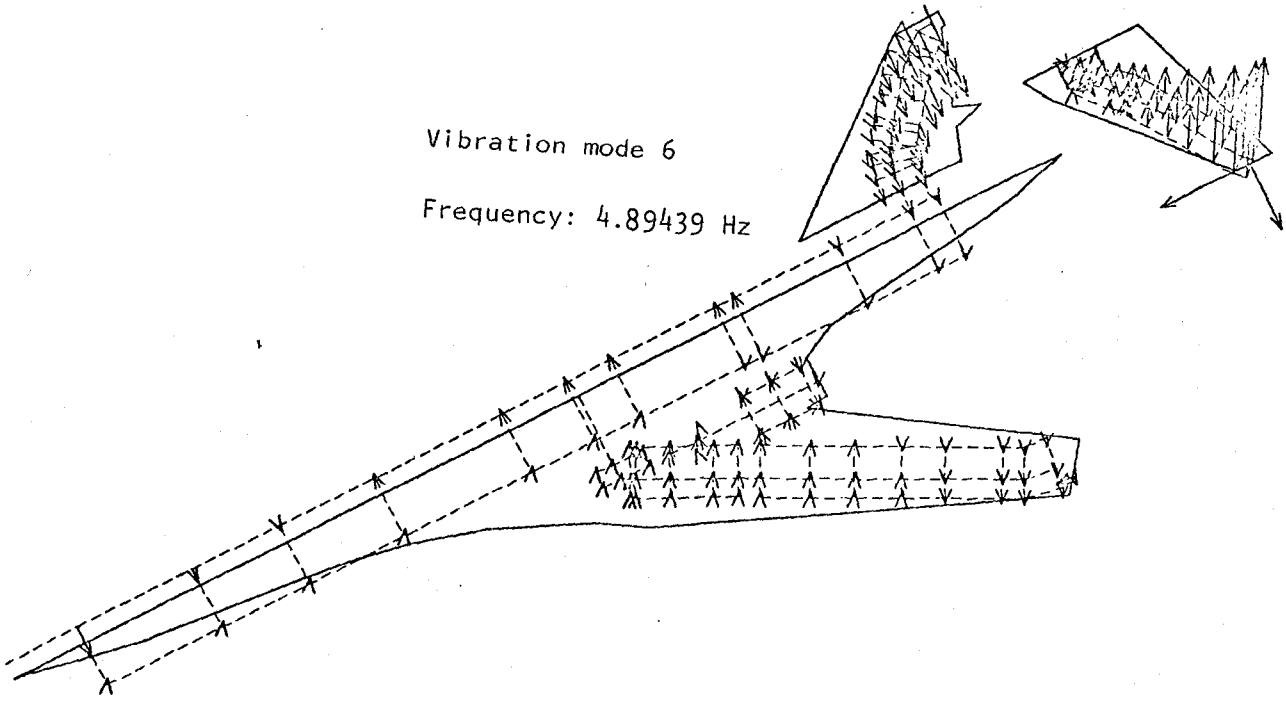

Figure 54. - Continued.

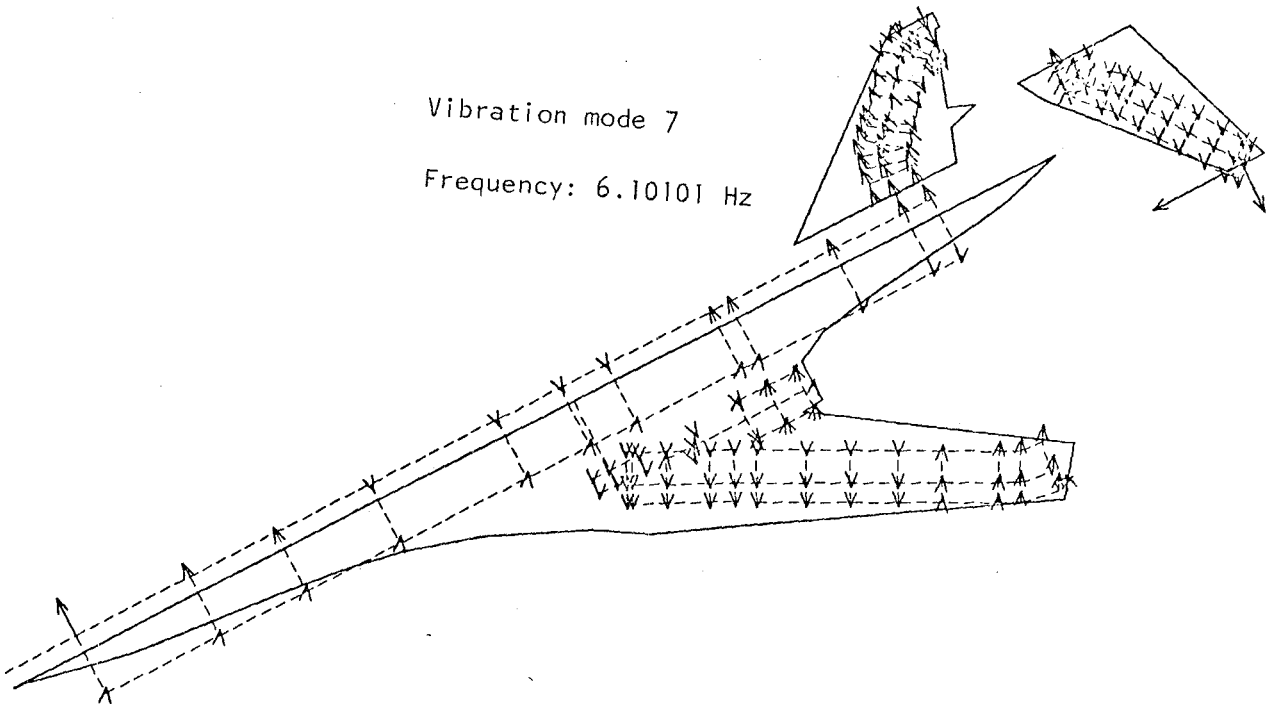

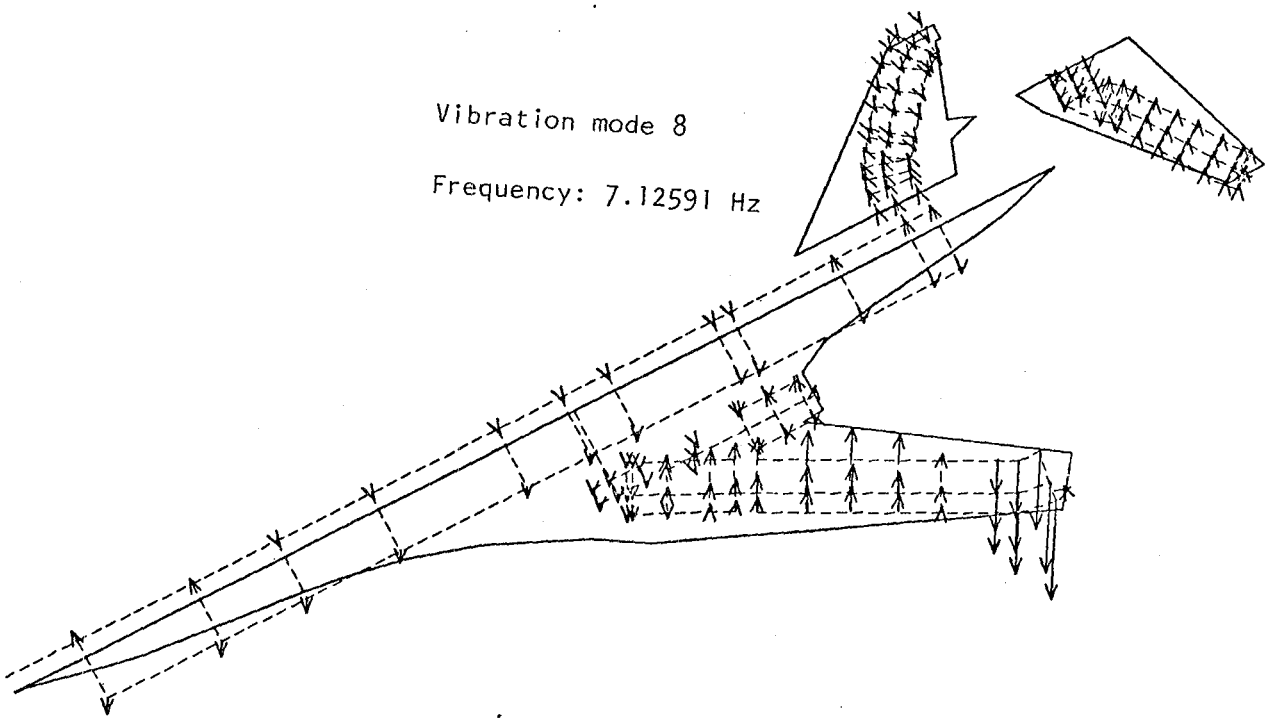

Figure 54. - Continued.

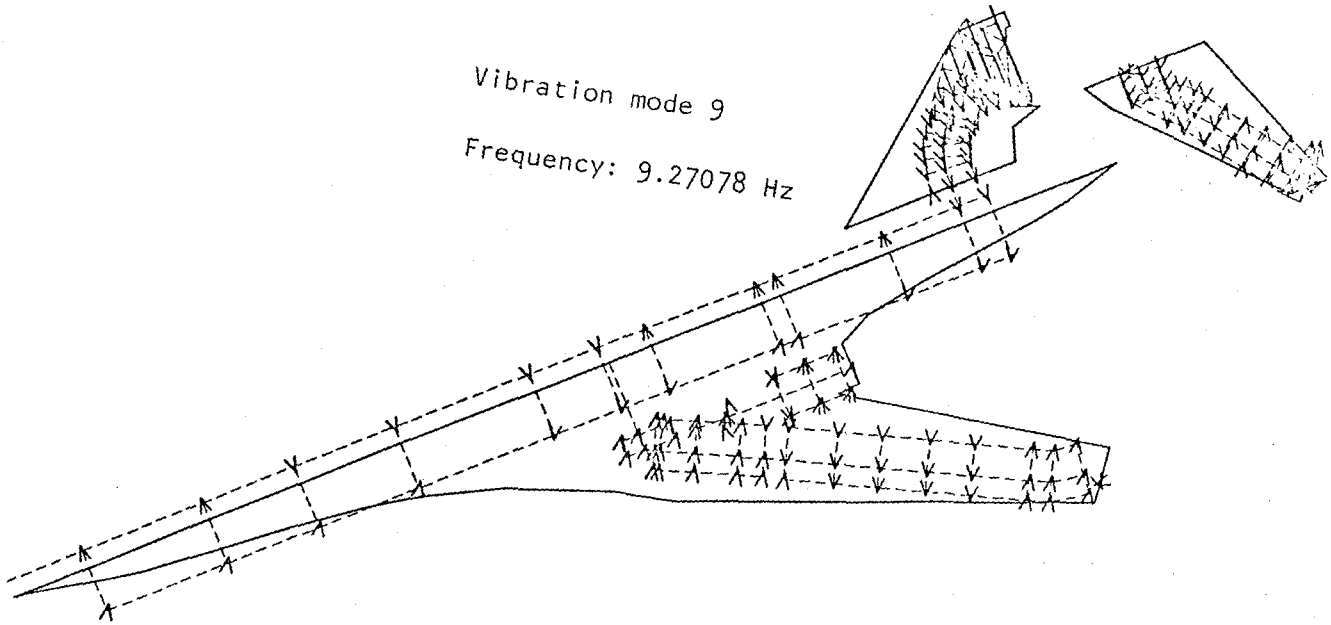

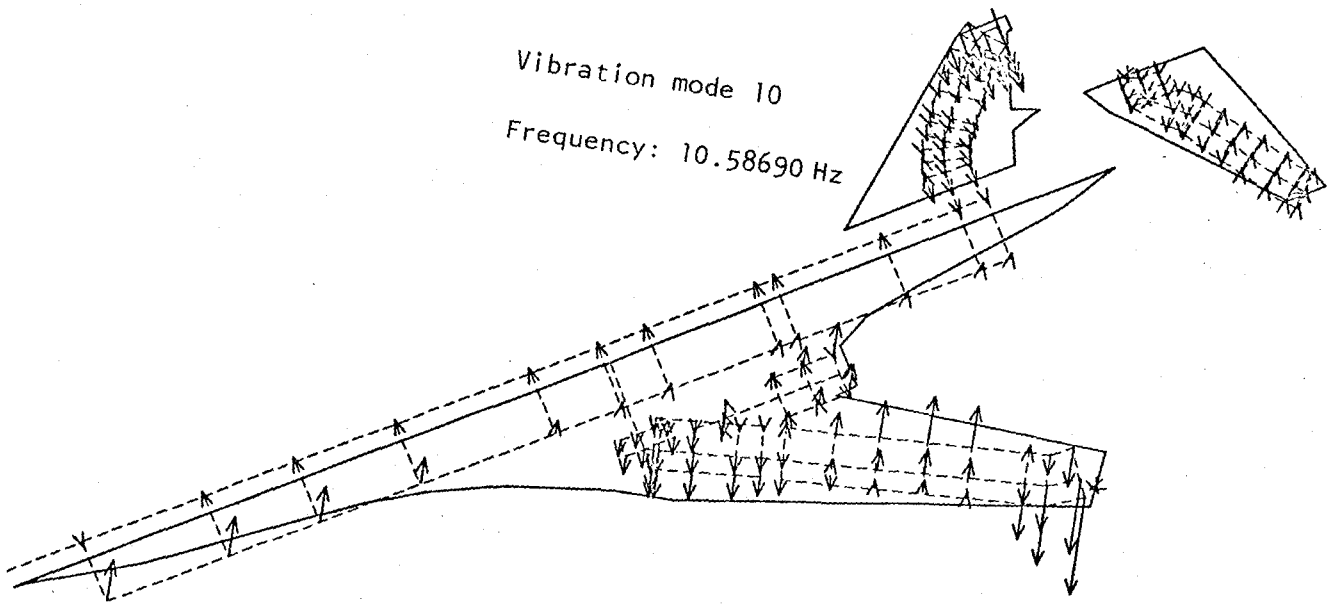

Figure 54. - Continued.

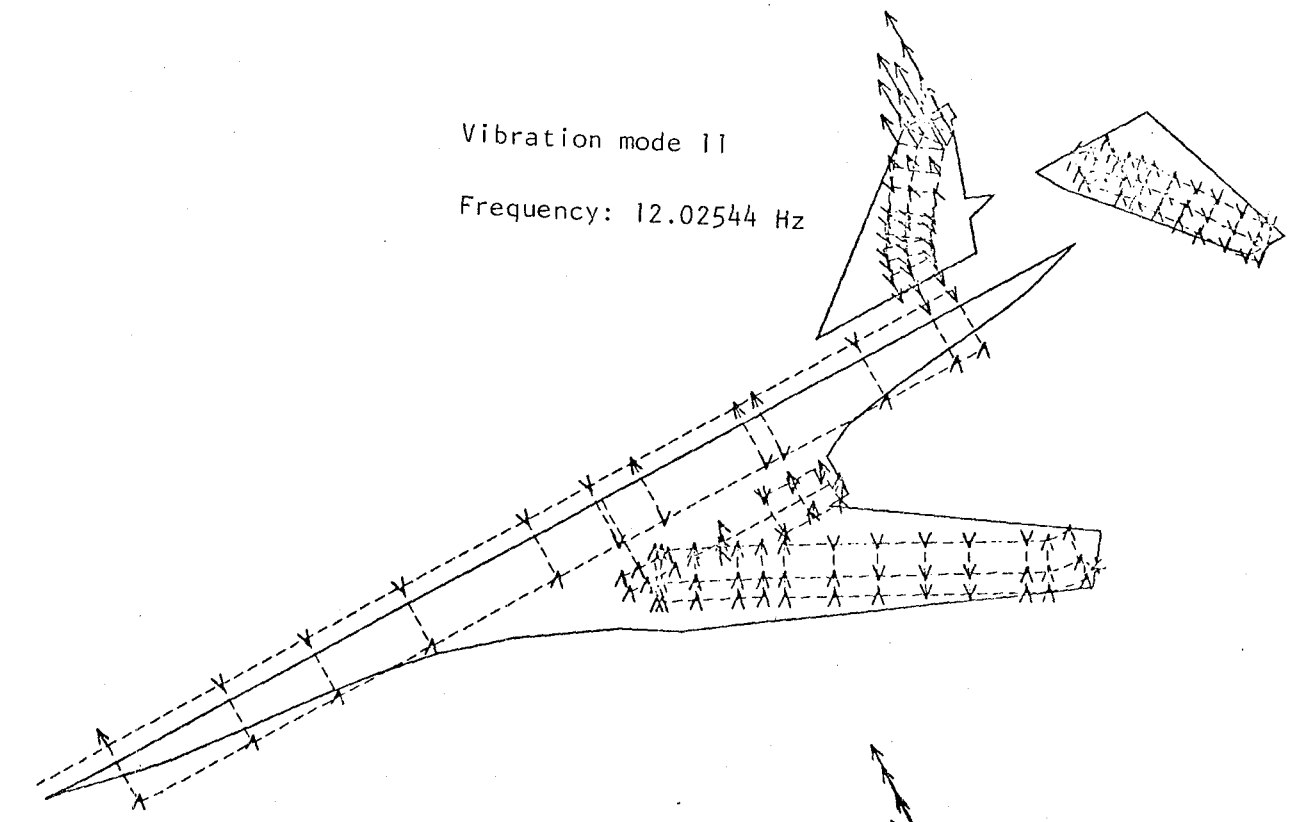

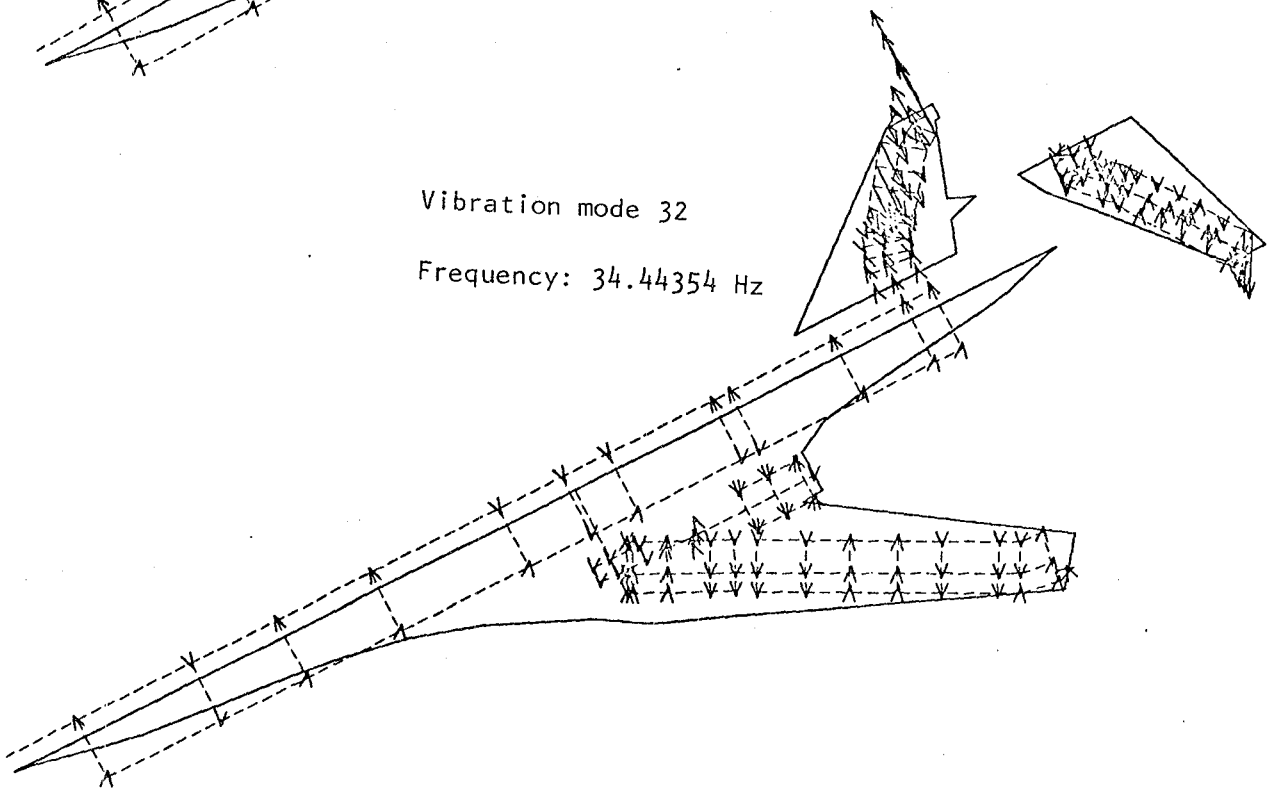

Figure 54. - Concluded.

Appendix C

TIME HISTORIES OF SMCS OPERATION IN TURBULENCE

While the basic intent of flt 3-138 was to fly tests at M = 1.2 at altitude, upon return to base some low-altitude runs were conducted. Light-to-moderate turbulence was present, so some SMCS-off and SMCS-on data were obtained. Since these data represent some of the best time history data obtained to date on the B-1 demonstrating SMCS performance in improving vertical and lateral ride quality, they have been included in this report. The time history data are presented in figure 55. Shown are vertical and lateral load factors at the crew station, and right and left SMCS vane activity.

When the SMCS is not operating, A dominant 3 Hz vertical response is noted at the crew station. Similarly, in the lateral axis, a dominant 5 Hz motion is obtained. These responses are typical of those observed many times when the B-1 has flown in turbulence at low altitudes.

When the SMCS is operated, nearly all of the 3 Hz vertical motion is eliminated; the 5 Hz lateral motion is subdued, but not to the degree that the vertical motion is. The vane deflection activity is shown; because of the superposition of vertical and lateral commands, the left and right vanes appear to be operating independently of each other. In addition to 3 and 5 Hz structural-motion-induced activity, some low-frequency, rigid-body, motion-induced activity may be seen in deflection traces.

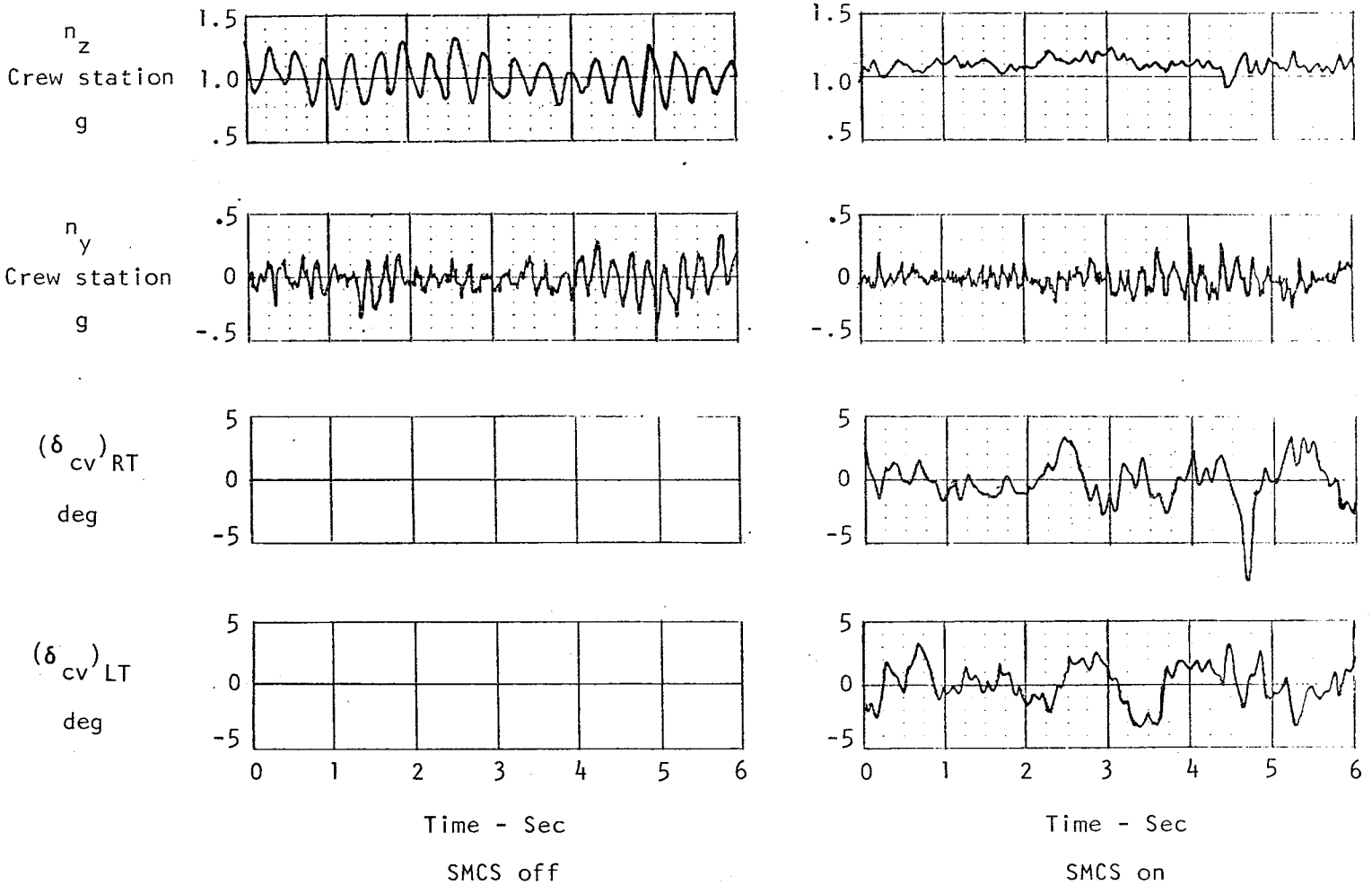

Figure 55. - SMCS performance in improving ride quality at crew station of B-1, flight test data, M = .85, low altitude, Λ = 65°.

REFERENCES

1. Wykes, John H.; Borland, Christopher J.; Klepl, Martin J.; and MacMiller, Cary J.; "Design and Development of a Structural Mode Control System," NASA CR-143846, October 1977.

2. Wykes, John H.; Byar, Thomas R.; MacMiller, Cary J.; and Greek, David C.; "Analyses and Tests of the B-1 Aircraft Structural Mode Control System," NASA CR-144887, January 1980.

3. Ii, Jack M.; Borland, Christopher J.; and Hagley, John R.; "Prediction of Unsteady Aerodynamic Loadings of Non-Planar Wings and Wing-Tail Configurations in Supersonic Flow," AFFDL-TR-71-108, Parts I and II, August 1971.

1. Report No.	2. Government Accession No.	3. Recipient's Catalog No.
NASA CR-170405		

4. Title and Subtitle	5. Report Date
FLIGHT TEST AND ANALYSES OF THE B-1 STRUCTURAL MODE CONTROL SYSTEM AT SUPERSONIC FLIGHT CONDITIONS	December 1983
	6. Performing Organization Code
7. Author(s)	8. Performing Organization Report No.
John H. Wykes, Martin J. Klepl, and Michael J. Brosnan	
	10. Work Unit No.
9. Performing Organization Name and Address	
Rockwell International Corporation Los Angeles, California 90009	11. Contract or Grant No. NAS4-2932
	13. Type of Report and Period Covered
12. Sponsoring Agency Name and Address	Contractor Report - Final
National Aeronautics and Space Administration Washington, D.C. 20546	14. Sponsoring Agency Code RTOP 505-33-54

15. Supplementary Notes

NASA Technical Monitor: Glenn B. Gilyard, Ames Research Center, Dryden Flight Research Facility, Edwards, CA 93523

16. Abstract

The primary objective of demonstrating a practical Structural Mode Control System (SMCS) that could be turned on at takeoff and be left on for the entire flight has been met. The SMCS appears to be more effective in damping the key fuselage bending modes at supersonic speeds than at the design point of Mach 0.85 (for fixed gains). The SMCS has an adverse effect on high-frequency symmetric modes; however, this adverse effect did not make the system unstable and does not appear to affect ride quality performance.

The vertical ride quality analyses indicate that the basic configuration without active systems is satisfactory for long-term exposure. If clear-air turbulence were to be encountered, indications are that the SMCS would be very effective in reducing the adverse accelerations. On the other hand, lateral ride quality analyses indicate that the aircraft with the SMCS on does not quite meet the long-term exposure criteria, but would be satisfactory for short-term exposure at altitude. Again, the lateral SMCS was shown to be very effective in reducing peak lateral accelerations.

A secondary objective of evaluating existing analytical techniques in the supersonic speed range has been accomplished. The Mach Box theory has been shown to provide creditable data for active control systems evaluations even at Mach 1.2, which is approaching the lower speed bounds of the theory. However, the ability of the theory to predict force effectiveness of the small structural mode control vanes on the fuselage appears to be only good to fair.

17. Key Words (Suggested by Author(s))	18. Distribution Statement
Supersonic transport B-1 aircraft Ride control Mode control Ride quality	Unclassified-Unlimited STAR category 08

19. Security Classif. (of this report)	20. Security Classif. (of this page)	21. No. of Pages	22. Price*
Unclassified	Unclassified	109	A06

For sale by the National Technical Information Service, Springfield, Virginia 22161.

End of Document